

**An investigation into pyocyanin-triggered  
carbon monoxide-releasing molecules**

Rachel Rosemary Steen

Masters by Research

University of York  
Chemistry

December 2016

## Abstract

*Pseudomonas aeruginosa* (*P. aeruginosa*) infection is the most common cause of death amongst Cystic Fibrosis patients. Its virulence factor pyocyanin is of interest as a redox-active compound and has been investigated herein.

Carbon-monoxide-releasing molecules have been developed in recent years to deliver carbon monoxide (CO), a known antimicrobial, safely and specifically to where it is required. Pyocyanin has been identified as a potential target to trigger CO-release as it is produced almost exclusively by *P. aeruginosa*.

Pyocyanin was prepared and fully characterised. Electrochemical evidence of a two-step reduction mechanism to leukopyocyanin was observed. And a method to quantify the amount of pyocyanin present in clinical isolates was developed building upon the UV/vis characterisation.

A screen of a range of CO-RMs for activation by pyocyanin activation demonstrated that  $[\text{NEt}_4][\text{MnBr}_2(\text{CO})_4]$ , "pyo-CORM", showed promise. In chlorinated solvents CO is released from pyo-CORM in the presence of pyocyanin. Mass spectrometry evidence indicates that pyocyanin acts as a bidentate ligand causing the loss of CO and bromide ligands. This mechanism is supported through the use of analogues and the release of CO in this system has been demonstrated through gas phase IR spectroscopy. CO is also released from pyo-CORM in aqueous solutions. This is clearly seen through the loss of all solution IR carbonyl bands after 1 hour and the presence of CO in the gas phase IR.

Pyo-CORM shows antimicrobial activity against lab and clinical strains of *P. aeruginosa*, and multiple other bacterial species. Pyo-CORM is also able to reduce the biomass of biofilm after its formation. As biofilms are difficult to treat with traditional antibiotics and common in chronic infections this makes pyo-CORM an important possible therapeutic.

# Table of contents

Abstract .....	2
Table of contents .....	3
Figures .....	6
Schemes .....	10
Tables .....	11
Equations.....	12
Acknowledgements.....	13
Declaration .....	15
1 Introduction .....	17
1.1 Cystic Fibrosis .....	17
1.2 Pseudomonas aeruginosa .....	19
1.3 Pyocyanin.....	20
1.4 Carbon Monoxide.....	22
1.5 CO-RMs.....	23
1.6 Quantifying CO Release.....	25
1.7 Aim.....	26
2 Characterisation of Pyocyanin .....	28
2.1 Introduction.....	28
2.2 Results and Discussion .....	30
2.2.1 Synthesis .....	30
2.2.2 NMR.....	32
2.2.3 UV/vis Analysis .....	32
2.2.4 Electrochemistry .....	33

2.2.5	UV/Vis Spectroelectrochemistry.....	37
2.2.6	IR Analysis.....	39
2.2.7	DFT Calculations.....	41
2.2.8	Cystic Fibrosis Sputum Isolates.....	44
2.3	Conclusion.....	47
3	CO-RM Screening.....	50
3.1	Introduction.....	50
3.2	Results and Discussion.....	52
3.2.1	[NEt <sub>4</sub> ][MnBr <sub>2</sub> (CO) <sub>4</sub> ].....	54
3.3	Conclusion.....	57
4	Pyo-CORM reactions.....	59
4.1	Introduction.....	59
4.2	Analysis of pyo-CORM.....	59
4.2.1	IR Analysis.....	59
4.2.2	Electrochemistry.....	64
4.3	Reactions of pyo-CORM with pyocyanin.....	64
4.3.1	UV/vis Concentration studies.....	65
4.3.2	IR Analysis.....	69
4.3.3	Mass Spectrometry.....	71
4.4	Analogues.....	72
4.4.1	Pyo-CORM analogue.....	72
4.4.2	Pyocyanin analogues.....	73
4.5	Aqueous IR reactions.....	78
4.6	Evolved gas measurements.....	80
4.7	Gas phase IR.....	82
4.8	Biological testing of pyo-CORM.....	85

4.9	Summary and conclusions.....	93
5	Summary, conclusions and future work .....	96
5.1	Conclusions.....	96
5.2	Future work .....	97
6	Experimental .....	100
6.1	Methods .....	100
6.1.1	Solvents and Reagents .....	100
6.1.2	NMR.....	100
6.1.3	ESI-MS .....	100
6.1.4	UV/Vis Spectroscopy .....	100
6.1.5	Electrochemistry .....	101
6.1.6	Spectroelectrochemistry.....	101
6.1.7	IR Spectroscopy.....	101
6.1.8	DFT .....	102
6.2	Pyocyanin synthesis.....	102
6.3	Pyo-CORM synthesis.....	104
6.4	CF sputum isolates preparation .....	104
6.5	CO-RM screening.....	105
6.6	UV/vis concentration studies .....	105
6.7	Gas Phase IR .....	106
6.8	Evolved gas measurements.....	107
6.1	Biological testing of pyo-CORM.....	107
	Abbreviations .....	110
	References.....	115

## Figures

<b>Figure 1.1:</b> Distribution of CFTR mutations into six functional classes according to the primary molecular defect: Class I mutants are no protein synthesis. Class II mutants are impaired trafficking protein. Class III mutants are defective channel gating. Class IV mutants are less functional proteins. Class V mutants are less protein maturation caused by amino acid substitution or alternative splicing. Class VI mutants are less stable protein. wt, wild type; CFTR, cystic fibrosis transmembrane conductance regulator. From Lopes-Pacheco, 2016 <sup>7</sup> under a Creative Commons Attribution License .....	17
<b>Figure 1.2:</b> Typical bacterial cell structure. From Mariana Ruiz Villarreal, 2008 <sup>18</sup> and is in the public domain .....	19
<b>Figure 1.3:</b> Pyocyanin.....	20
<b>Figure 1.4:</b> Chorismic acid, the biological pyocyanin precursor .....	21
<b>Figure 1.5:</b> CORM-2.....	23
<b>Figure 1.6:</b> CORM-3 and Trypto-CORM.....	24
<b>Figure 2.1:</b> Pyocyanin.....	28
<b>Figure 2.2:</b> 1-hydroxyphenazine .....	29
<b>Figure 2.3:</b> Coloured fractions eluted prior to pyocyanin during column chromatography.....	32
<b>Figure 2.4:</b> (Main) UV/Vis absorbance spectra of pyocyanin at different concentrations, as indicated, and (inset) the corresponding molar extinction plot.	33
<b>Figure 2.5:</b> (Main) CVs of pyocyanin and ferrocyanide solution measured over a wide voltage range. (Inset) CVs of pyocyanin (PYO) and PBS-only over a narrower voltage range. Concentration of pyocyanin: 3.33 mM, Concentration of ferrocyanide: excess, atmosphere: air, solvent: PBS, pH: 7.4, temperature: room temperature, scan rate: 0.10 V/s. (Part of dataset A) .....	34
<b>Figure 2.6:</b> CVs of 5.44 mM pyocyanin under an Argon atmosphere. Solvent: PBS, pH 7.4, temperature: room temperature, scan rate: 0.10 V/s. (Dataset B) .....	36
<b>Figure 2.7:</b> UV/Vis spectroelectrochemical spectra of pyocyanin 0.13 mM, -0.5 V vs Ag/AgCl.....	37
<b>Figure 2.8:</b> Pyocyanin (0.13 mM) A) before and B) after electrochemical reduction	38

<b>Figure 2.9:</b> UV/Vis spectra of pyocyanin (PYO) and leukopyocyanin (LPYO) at similar concentrations .....	39
<b>Figure 2.10:</b> IR spectra of pyocyanin A) in chloroform B) as a KBr disk.....	40
<b>Figure 2.11:</b> Pyocyanin zwitterion .....	41
<b>Figure 2.12:</b> 55a-HOMO and 56a-LUMO electron density distribution diagrams.....	43
<b>Figure 2.13:</b> 54a-HOMO -1 and 57a-LUMO +1 electron density distribution diagrams .....	43
<b>Figure 2.14:</b> 53a-HOMO -2 and 58a-LUMO +2 electron density distribution diagram .....	43
<b>Figure 2.15:</b> Examples of CF supernatant UV/vis spectra.....	46
<b>Figure 2.16:</b> Comparison of concentrations from single point absorbance scans at 691 nm using a plate reader and from UV/Vis scans using the absorbance at 692 nm .....	47
<b>Figure 3.1:</b> Pyocyanin and leukopyocyanin .....	50
<b>Figure 3.2:</b> UV/vis spectra of thermal CO-releasing molecule [NEt <sub>4</sub> ][MoBr(CO) <sub>5</sub> ] every 4 minutes for 49 minutes A) 24 μM CO-RM, and B) 24 μM CO-RM and 24 μM PYO in PBS solution .....	52
<b>Figure 3.3:</b> UV/vis spectra measured over 66 minutes, A) 24 μM [NEt <sub>4</sub> ][MnBr <sub>2</sub> (CO) <sub>4</sub> ] and 24 μM PYO in PBS solution, B) 24 μM [NEt <sub>4</sub> ][MnBr <sub>2</sub> (CO) <sub>4</sub> ] in PBS solution.....	54
<b>Figure 3.4:</b> UV/vis spectra measured over 128 minutes, A) 48 μM [NEt <sub>4</sub> ][MnBr <sub>2</sub> (CO) <sub>4</sub> ] and 24 μM PYO in PBS solution, B) 48 μM [NEt <sub>4</sub> ][MnBr <sub>2</sub> (CO) <sub>4</sub> ] in PBS solution.....	55
<b>Figure 3.5:</b> UV/vis difference spectrum after 88 minutes of 48 μM [NEt <sub>4</sub> ][MnBr <sub>2</sub> (CO) <sub>4</sub> ] and 24 μM PYO in PBS solution.....	55
<b>Figure 3.6:</b> UV/Vis spectra at 1 and 36 minutes and the difference spectra for 48 μM [NEt <sub>4</sub> ][MnBr <sub>2</sub> (CO) <sub>4</sub> ] and 48 μM PYO in PBS.....	56
<b>Figure 3.7:</b> UV/vis spectra measured over 74 minutes, A) 30 μM [Mn(CO) <sub>4</sub> Br <sub>2</sub> ][NEt <sub>4</sub> ] and 30 μM LPYO in PBS B) 30 μM [Mn(CO) <sub>4</sub> Br <sub>2</sub> ][NEt <sub>4</sub> ] in PBS .....	57
<b>Figure 4.1:</b> [NEt <sub>4</sub> ][MnBr <sub>2</sub> (CO) <sub>4</sub> ], pyo-CORM.....	59
<b>Figure 4.2:</b> IR spectra of pyo-CORM as a KBr disk .....	60
<b>Figure 4.3:</b> IR spectra of pyo-CORM in A) chloroform and B) water .....	61
<b>Figure 4.4:</b> IR spectra of pyo-CORM in chloroform after being dissolved in water ..	62

<b>Figure 4.5:</b> IR spectra of pyo-CORM upon heating to 50 °C .....	63
<b>Figure 4.6:</b> IR spectra of pyo-CORM in chloroform A) after being in solution for 1 min and B) after being in solution for 60 min.....	64
<b>Figure 4.7:</b> Percentage change in the absorbance with an exponential growth fit at A) 692 nm ( $R^2=0.786$ ) and B) 312 nm ( $R^2=0.829$ ) for the reaction of pyo-CORM and pyocyanin after 36 minutes .....	67
<b>Figure 4.8:</b> A) Zero, B) First and C) Second order rate plots for the corrected absorbance at 312 nm over 24 minutes for experiment H, 1:1 ratio.....	68
<b>Figure 4.9:</b> $k_{obs}$ for all ratios of pyo-CORM to pyocyanin with a non-weighted polynomial fit .....	69
<b>Figure 4.10:</b> IR spectra of the reaction of 5 mM of pyo-CORM and 2.5 mM of pyocyanin over 35 mins .....	70
<b>Figure 4.11:</b> Product of pyo-CORM and pyocyanin .....	71
<b>Figure 4.12:</b> UV/vis spectra over 30 minutes of 24 $\mu$ M pyocyanin and 48 $\mu$ M tetraethyl ammonium bromide in DI water.....	73
<b>Figure 4.13:</b> 2-keto-N-methyl phenazine.....	74
<b>Figure 4.14:</b> UV/vis absorbance spectra of pyocyanin synthesis pink fraction (2-keto-N-methyl phenazine) at different the concentrations indicated and the molar extinction plot .....	75
<b>Figure 4.15:</b> IR spectra of CO region for pyo-CORM and pyo-CORM with 2-keto-N-methyl phenazine over time in DI water .....	76
<b>Figure 4.16:</b> 8-hydroxyquinoline.....	76
<b>Figure 4.17:</b> IR spectra of 8 mM of pyo-CORM before the addition of 8 mM of 8-HOQ and after 20 mins reaction. ....	77
<b>Figure 4.18:</b> Product of pyo-CORM and 8-HOQ.....	78
<b>Figure 4.19:</b> IR spectra of 10 mM of pyo-CORM and 5 mM of pyocyanin in DI water. ....	79
<b>Figure 4.20:</b> IR spectra of pyo-CORM only in DI water after A) 1 min and B) 90 mins. ....	80
<b>Figure 4.21:</b> Change in pressure in the headspace of a flask containing pyo-CORM in chlorobenzene, pyo-CORM in chlorobenzene with water and chlorobenzene only (secondary axis).....	81

<b>Figure 4.22:</b> Change in pressure in the headspace of a flask containing only water and pyo-CORM in water.....	82
<b>Figure 4.23:</b> Gas phase IR spectra of 12 mg of pyo-CORM in 4 mL of chlorinated solvent after 1 hour A) chloroform, B) dry DCM, C) chloroform and 0.5 mL of water, D) chloroform with 12 mg of pyocyanin, * chloroform band, ** DCM band.....	83
<b>Figure 4.24:</b> Gas phase IR spectra after 1 hour of A) 12 mg of Pyo-CORM with 12 mg of pyocyanin in PBS solution and B) 12 mg of pyo-CORM only in PBS solution. ....	84
<b>Figure 4.25:</b> Gas phase IR spectra of 12 mg of pyo-CORM in 4 mL of aqueous solvent after 1 hour A) water, B) DMSO, C) 100 vol% LB, D) 2 molar NaCl, *unknown band	85
<b>Figure 4.26:</b> Corrected optical density at 600 nm of PA01 <i>P. aeruginosa</i> strain when grown with different concentrations of pyo-CORM for 24 hours at 37 °C in media as indicated.....	86
<b>Figure 4.27:</b> Optical density measurements at 600 nm of PA01 <i>P. aeruginosa</i> strain when grown with different concentrations of pyo-CORM for 24 hours at 37 °C in M9 glucose medium.....	88
<b>Figure 4.28:</b> Optical density at 600 nm of PA01 <i>P. aeruginosa</i> strain and a phenazine knockout strain (PCN) when grown with different concentrations of pyo-CORM for 8 hours at 37 °C in 10 vol% LB.....	89
<b>Figure 4.29:</b> Crystal violet absorbance of different <i>P. aeruginosa</i> strains and mutants, grown at 37 °C in 10% LB media with the addition of pyo-CORM A) before 24 hours of biofilm formation and B) after 24 hours of biofilm formation. – to +++: no pyo-CORM and increasing pyo-CORM concentration, exact concentrations unknown.....	90
<b>Figure 4.30:</b> A) optical density at 600 nm, B) crystal violet absorbance of the addition of pyo-CORM before biofilm formation and C) crystal violet absorbance of the addition of pyo-CORM after biofilm formation, for different clinical and lab <i>P. aeruginosa</i> strains grown at 37 °C in 10% LB media.....	91
<b>Figure 4.31:</b> Corrected optical density at 600 nm of PA01 <i>P. aeruginosa</i> strain, PA01-phenazine knockout strain (PCN), <i>Ralstonia spp</i> , <i>S. aureus</i> and <i>S. maltophilia</i> when grown with different concentrations of pyo-CORM for 8 hours at 37 °C in 10 vol% LB .....	93
<b>Figure 6.1:</b> Gas phase IR experimental set up .....	106

## Schemes

<b>Scheme 1.1:</b> Conversion of haem to bilirubin including the loss of CO. Catalysed by A) Haem oxygenase 1 and B) biliverdin reductase .....	22
<b>Scheme 2.1:</b> Redox cycling of pyocyanin. Modified from Jacob et al <sup>31</sup> .....	30
<b>Scheme 2.2:</b> Synthesis of pyocyanin from phenazine methosulfate.....	31

## Tables

<b>Table 2.1:</b> Ferrocyanide redox couple internal reference data.....	34
<b>Table 2.2:</b> CV potentials for pyocyanin in air, dataset A.....	35
<b>Table 2.3:</b> CV potentials for pyocyanin in Argon, dataset B .....	36
<b>Table 2.4:</b> DFT derived electronic transitions.....	42
<b>Table 2.5:</b> CF isolates and their absorbances and corresponding pyocyanin concentration, *: from UV/vis spectroscopy, **: from well plate spectrophotometer measurements .....	45
<b>Table 3.1:</b> CO-RMs selected for screening for pyocyanin activation.....	51
<b>Table 3.2:</b> Results of testing CO-RMs for activation by pyocyanin (PYO) or leukopyocyanin (LPYO). Yes: A significant change in the UV/vis spectrum occurred in the presence of the pyocyanin species. No: No significant changes were observed. ....	53
<b>Table 4.1:</b> Table showing pyo-CORM and PYO concentrations, ratios and observed rate constant .....	66

## Equations

<b>Equation 2.1:</b> Voltage separation equation.....	35
---	----

## Acknowledgements

There are many people that have helped, guided me and made this project possible and enjoyable. I couldn't have asked to be surrounded by a better group of people.

First and foremost I would like to thank my supervisors Dr Jason Lynam, Dr Alison Parkin and Prof. Ian Fairlamb who have helped and supported me both scientifically and personally over the last year. I apologise for the tears. And also thanks to Prof. Robin Perutz for the use of your IR spectrometer and Dr Naser Jasim for fixing it when it broke.

A huge thanks to both Karinna Saxby and Dr Lindsey Flanagan for being kind enough to tackle the practical biological aspects of this thesis, it really wouldn't be the same without your input. And thanks to Ben Aucott for being endlessly patient with my multitude of questions about everything from CO-RMs to electrochemistry. And I never got to do a Myoglobin assay, maybe one day...

To Lewis, Lucy and Meghan for helping me find my way around the lab and keeping me company during the hours spent sitting at the UV/vis spectrometer. And Nina, Maddi and the rest of the Lynam and Slattery groups for making me laugh when I needed it most.

Thanks to the Fairlamb group for the endless morning coffee breaks and to Alice for being my travel buddy and making me leave York at the weekends. To the lunch crew; Luisa, Ben, Martin, Tom, Ellis, Chris and Dan for the endless laughter and odd conversations... you know which ones I'm talking about. And of course the Parkin group for your multitude of amusing emails keeping me entertained from a distance.

Thank you all for making me feel so welcome in this new University.

Most of all I wish to thank my whole family for being so supportive during the whole process. Charlotte we both managed it! Mum it is wonderful to see you so much better, we will be able to celebrate this one together. Finally, I would like to express my love and gratitude to my Dad for just being amazing and encouraging me follow my ambitions, words cannot describe my admiration for you. This accomplishment would not have been possible without you.

And yes Ollie I will get to graduate again!

Rachel Steen

## Declaration

I declare that this thesis is a presentation of original work and I am the sole author. This work has not previously been presented for an award at this, or any other, University. All sources are acknowledged as References.

All work is my own except for the following:

- ESI-MS experiments were carried out by Dr Ed Bergstrom and Mr Karl Heaton.
- Density functional theory calculations were carried out by Dr Jason Lynam.
- Biological testing was carried out by Miss Karinna Saxby and Dr Lindsey Flanagan in the Department of Biology at the University of York.
- Synthesis of CO-RMs were performed by Mr James Pitts, Dr Ciara O'Brien, Dr Wei-Qiang Zhang and Dr Jonathan Ward.

These contributions are highlighted in the text.

# Introduction

## Chapter 1

# 1 Introduction

## 1.1 Cystic Fibrosis

Cystic Fibrosis (CF) is the most prevalent life-limiting genetic condition amongst the Caucasian population, affecting 1 in 2500 births in the UK, with 1 in 25 people being a carrier<sup>1</sup>. It is mainly diagnosed through neonatal screening from a blood sample taken at birth. The disorder is caused by a mutation in the gene for the Cystic Fibrosis transmembrane conductance regulator (CFTR) membrane bound protein<sup>1</sup>. The CFTR is a cyclic-AMP dependent epithelial ion channel that transports chloride ions out of the epithelial cells to the lumen<sup>2</sup> and was first described in Science in 1989<sup>3-5</sup> (**Figure 1.1**). Because the CFTR transporter is present in all epithelial cell membranes, reduced function is responsible for abnormal electrolyte transport in epithelial cells throughout the body. The organs most affected by this defect are the lungs, pancreas, liver, intestines and reproductive organs. Most men with CF are infertile and fertility is reduced in women<sup>6</sup>.

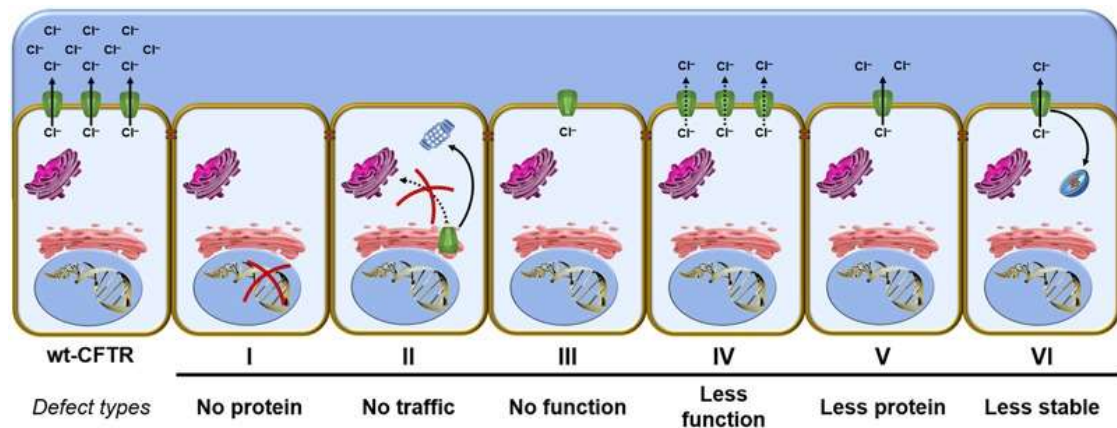


**Figure 1.1:** Distribution of CFTR mutations into six functional classes according to the primary molecular defect: Class I mutants are no protein synthesis. Class II mutants are impaired trafficking protein. Class III mutants are defective channel gating. Class IV mutants are less functional proteins. Class V mutants are less protein maturation caused by amino acid substitution or alternative splicing. Class VI mutants are less stable protein. wt, wild type; CFTR, cystic fibrosis transmembrane conductance regulator. From Lopes-Pacheco, 2016<sup>7</sup> under a Creative Commons

Attribution License

Over 2000 mutations to the CFTR gene have been described, however, only 127 of these are known to cause CF<sup>8</sup>. The mutations are categorised by the molecular defect they cause, as shown below in **Figure 1.1**. The many different mutations that cause CF means that the severity of the disorder changes from patient to patient, depending on how the CFTR protein function is limited, but generally this is a condition associated with impaired lung function. This is because in the lungs the reduction in chloride ion transport increases the viscosity of the mucus close to the epithelial membrane. As the mucus becomes thicker it is harder for the cilia to clear it from the lungs<sup>9</sup>. As mucus is used to trap and clear pathogens and particulate matter from the lung tissue, this leaves the CF lung vulnerable to infection and scarring. As a result of chronic lung infections and the associated inflammation, respiratory failure is the biggest cause of death amongst CF patients (80-95%<sup>10</sup>).

The three bacterial species most associated with the CF lung are *Staphylococcus aureus* (*S. aureus*), *Haemophilus influenzae* (*H. influenzae*) and *Pseudomonas aeruginosa* (*P. aeruginosa*). *S. aureus* is often the first pathogen to colonise the CF lung,<sup>11</sup> but the most common infection is from *P. aeruginosa*, which affects 70-80% of CF patients by the time they reach their teens<sup>10</sup>. It is believed that earlier infections by *S. aureus* and *H. influenzae* play a role in priming the lungs for *P. aeruginosa* infection,<sup>12</sup> since although *S. aureus* can easily be treated with antibiotics, this suppression may increase the risk of infection by *P. aeruginosa*, this causing a long-term decrease in life expectancy<sup>13</sup>.

The use of chest physiotherapy can help with the clearance of mucus and the trapped bacteria, reducing the infection risk. In extreme cases, lung transplants can be performed to increase life expectancy and quality of life, although there is a risk of rejection associated with organ transplants. However, the most important medical tool for dealing with serious chest infections in CF patients remains the use of antibiotics and this project aims to expand the chemical toolkit of molecules we can use to eradicate *P. aeruginosa* infections.

## 1.2 *Pseudomonas aeruginosa*

*P. aeruginosa* is an opportunistic gram-negative bacterium that is present in a large number of natural and clinical environments. The typical eukaryotic cell structure is shown in **Figure 1.2**. Gram-negative bacteria have more complex cell wall structures than gram-positive bacteria, giving them greater natural resistance to antibiotics.

*P. aeruginosa* was first isolated in 1882 by Gessard<sup>14,15</sup> from the blue and green coloured patches found on used bandages. Although infections of *P. aeruginosa* are rare in healthy people they are extremely common in immunocompromised patients, e.g. CF patients, and those with a natural or surgical break in their epithelium, particularly burns victims. For patients with chronic infections of leg ulcers or burns, 52% of these will be due to *P. aeruginosa*<sup>16</sup>. *P. aeruginosa* also has the second biggest incidence of infection in intensive care wards worldwide after *S. aureus*<sup>17</sup>.

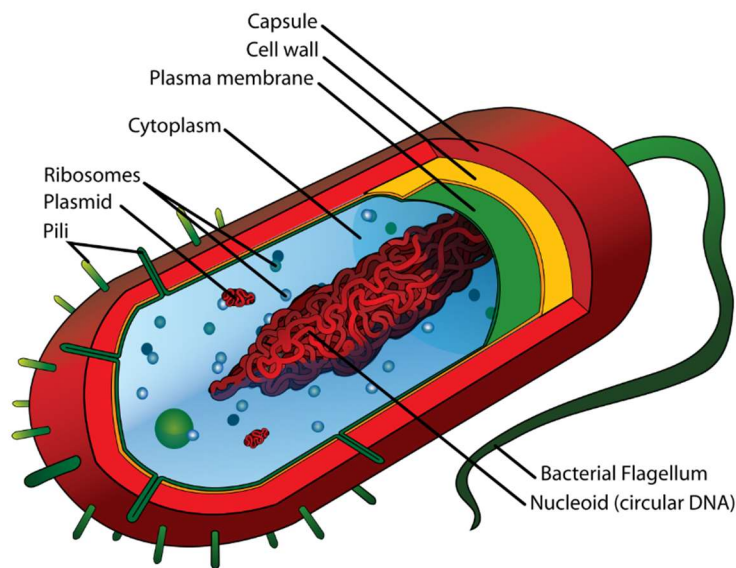


**Figure 1.2:** Typical bacterial cell structure. From Mariana Ruiz Villarreal, 2008<sup>18</sup> and is in the public domain

Current treatment for *P. aeruginosa* infection is limited to antibiotic cocktails, normally including one or more aminoglycoside derived antibiotic<sup>19</sup>, which are chosen for each patient based on the strain involved in infection; however,

antibiotic resistance is becoming a problem. A 2003 UK survey found that in *P. aeruginosa* isolates from CF patients, 62% were resistant to between one and six of the antibiotics tested<sup>20</sup>. The prevalence of *P. aeruginosa* antibiotic resistance has resulted from a combination of factors including the inherent extra drug-resistance arising from the gram-negative cell wall; the ability of *P. aeruginosa* to easily acquire and transfer resistance genes<sup>21</sup>; and the fact that the mucoid form of *P. aeruginosa* that is always present during chronic infection forms biofilms, making it more resistant to both drugs and the natural immune response<sup>19</sup>. Specifically, the presence of a biofilm increases bacterial resistance to antibiotics by between 10 and 1000 times<sup>22</sup>. Very recently a review was published about the state of *P. aeruginosa* vaccines<sup>17</sup>. Although there have been many promising preliminary trials, a vaccine has yet to be licensed, emphasising the continued requirement for new classes of effective antibiotic drugs.

### 1.3 Pyocyanin

Pyocyanin (**Figure 1.3**) is a very important redox-active, phenazine-derived compound that is produced and secreted by 90-95% of all *P. aeruginosa* strains<sup>23</sup>. Pyocyanin was identified prior to the association with a bacteria through extraction with chloroform from wound dressings in 1859 by Fordos<sup>24</sup>, who gave the molecule its name from the Greek for 'Pus' and 'Blue'. The blue colouration pyocyanin gives skin and bandages is still be used by clinicians today as a diagnostic indicator of *Pseudomonas* infection, although it is now known that the molecule turns red under acidic conditions.

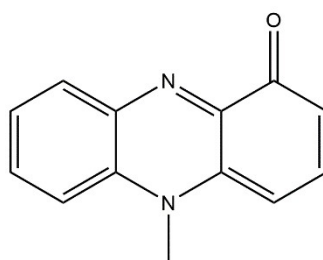


**Figure 1.3:** Pyocyanin

Although *Pseudomonas spp.* are the sole gram-negative nonfermenting bacteria that produce pyocyanin<sup>23</sup>, other phenazines are produced by both gram-positive and gram-negative bacterial species as well as the archaea *Methanosarcina*<sup>25</sup>. Over 100 naturally derived phenazines have been discovered so far<sup>26</sup>.

Pyocyanin is biosynthetically derived from two molecules of chorismic acid (**Figure 1.4**). Although an increased understanding of the synthesis has been achieved in recent years, partially due to the identification of the genes involved, details of some aspects of the core pathway still require further investigation<sup>25,26</sup>.

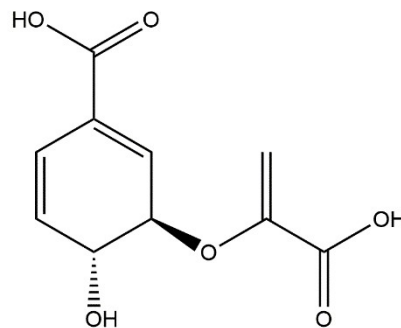


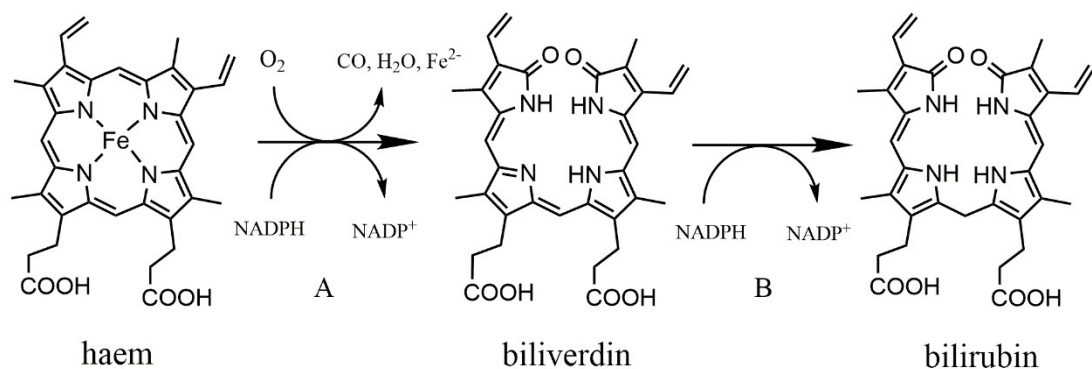
**Figure 1.4:** Chorismic acid, the biological pyocyanin precursor

The production of pyocyanin is beneficial to *Pseudomonas* in many ways. It can act as both an antibiotic<sup>27</sup> and as an antifungal<sup>23</sup>, protecting the bacterium from organisms present in natural environments and decreasing resource competition. When *Pseudomonas* bacteria are present in the soil, around the roots of plants, it is thought pyocyanin promotes the growth of the plant due to the protection it offers from other pathogenic bacteria<sup>23</sup>. In human infections, pyocyanin is an important virulence factor because it interferes with the growth and function of mammalian cells<sup>28</sup> and reduces the efficiency of host immune responses<sup>23</sup>. When *Pseudomonas* enters the mucoid phenotype pyocyanin acts as a quorum sensing molecule<sup>29</sup>. Quorum sensing molecules are small compounds used by bacteria to coordinate certain behaviours, such as biofilm production<sup>30</sup>. The redox properties of pyocyanin mean that it is an important modulator of cellular redox cycling, and can cause the production of reactive oxygen species<sup>31</sup>. The redox properties of pyocyanin also

help to release iron from transferrin into a form the bacteria can use for growth<sup>32</sup>. This project aims to test the hypothesis that because of the importance of pyocyanin in *P. aeruginosa* biochemistry, a drug which is activated by pyocyanin should be a very promising candidate for a new antimicrobial therapy.

## 1.4 Carbon Monoxide

In animals, carbon monoxide (CO) is produced endogenously. This was first described in 1951 when it was noted that the concentration of CO in expired air was greater than in inhaled air<sup>33</sup>. Carbon monoxide is produced as a by-product of the breakdown of haemoglobin by haem oxygenase 1 (and sometimes haem oxygenase 2) into bilirubin via biliverdin (**Scheme 1.1**)<sup>34</sup>.



**Scheme 1.1:** Conversion of haem to bilirubin including the loss of CO. Catalysed by A) Haem oxygenase 1 and B) biliverdin reductase

In addition to the well-known poisonous effects of CO as an irreversible binder to the oxygen-carrier proteins haemoglobin and myoglobin, it has also been discovered to play a life-sustaining role as an endogenous cell signalling molecule in humans, known as a gasotransmitter. In this signalling behaviour, CO has a similar biological function to nitric oxide and hydrogen sulphide<sup>35</sup>. Indeed, low-level doses of CO have been shown to have therapeutic value, including as an anti-inflammatory<sup>36</sup> and in organ transplantation surgery. By bathing an organ in CO it is both better preserved prior to transplantation, and the chance of rejection is

diminished after transplantation has occurred<sup>37</sup>. Gaseous CO for use as an inhaled anti-inflammatory medicine has passed Phase I clinical trials, which ascertained its biological safety and pharmacokinetics in healthy human subjects<sup>36</sup>. However, this is not a very specific method of CO delivery so higher doses are likely to be required to have the desired effect and may cause side effects. Also the poor public image of CO means that a non-gaseous delivery method is required in order to give patients confidence in their treatment. So molecular methods of CO-delivery are needed to overcome these difficulties. Development of such CO-releasing drug molecules presents an opportunity for the invention of new antimicrobials, since the positive impact of low-level CO doses on human tissue are not generally observed in bacterial colonies, meaning there is a potential therapeutic window in which CO-releasing drug will kill bacteria but not damage human cells.

## 1.5 CO-RMs

In response to the search for therapeutic CO-delivery drugs, CO-releasing molecules (CO-RMs) have become an important class of compounds. A publication outlining the possible therapeutic applications was first published in 2002<sup>38</sup>. The first generation of CO-RMs was a series of very simple ruthenium carbonyl compounds<sup>38-40</sup>, some of which are now commercially available (CORM-2, **Figure 1.5**, CAS: 22594-69-0<sup>41</sup>). Most CO-RMs are organometallic compounds although a series of boron-based CO-RM have been discovered (e.g. CORM-A1)<sup>42,43</sup>. More recently very elaborate ligands have been developed for specific biological applications.

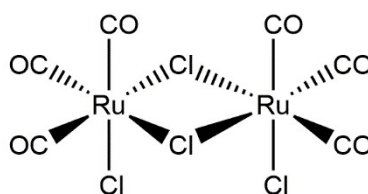


**Figure 1.5:** CORM-2

CO-RMs which simply release CO over time are referred to as “thermally activated”, e.g. CORM-2 and CORM-3, and such CO-RMs have been shown to have antibacterial properties against a range of bacterial species. As CORM-2 (**Figure 1.5**) and CORM-3 (**Figure 1.6**) are commercially available most previous bacterial testing has been performed using these CO-RMs. Both CORM-2 and CORM-3 at concentrations of between 10-500  $\mu\text{M}$  inhibit the bacterial growth of *P. aeruginosa* over a 20 hour period<sup>40,44</sup>. CORM-2 is also completely bactericidal to *Escherichia coli* (*E. Coli*) grown in aerobic and anaerobic conditions and *S. aureus* in aerobic and microaerobic conditions at concentrations of 250  $\mu\text{M}$  over a 4 hour period<sup>45</sup>. The same paper showed similar effects for CORM-3 although it was less effective against *S. aureus*. The light-activated CORM, Trypto-CORM (**Figure 1.6**), has also been shown to completely inhibit the growth of *E. coli* cells at a concentration of 100  $\mu\text{M}$  upon irradiation with light at 400 nm wavelength over 3 hours. Without irradiation there it caused no change in the growth of the bacteria<sup>46</sup>. The antimicrobial effects of these CO-RMs are greater than for CO alone, possibly due to the toxicity of the metal which is released after the CO-RM has lost its CO<sup>47</sup> and that it is released close to or inside the bacterial cells.

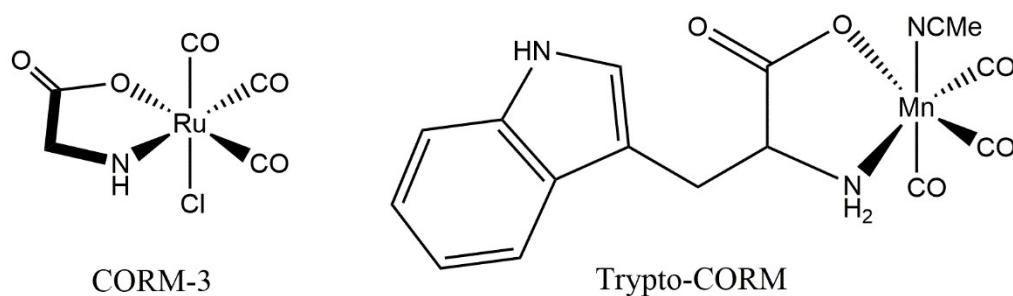


**Figure 1.6:** CORM-3 and Trypto-CORM

The focus of most recent CO-RM synthesis publications has been the design of activated CO-releasing molecules, which should promote more precise targeting of CO release *in vivo*. There are currently three main classifications of such activated CO-RMs, defined by the mechanism of CO release as light-induced, enzyme triggered, or ligand-exchanged CO-RMs<sup>48</sup>.

For light-induced CORMs, the light can either be in the visible or UV region of the electromagnetic spectrum<sup>49</sup> and causes the breakdown of the molecule and the dissociation of CO from the metal centre. This is a reliable way to induce CO release, and recent research at York has focused on this class of CO-RM. There are practical limitations in the treatment of disease using light-activated CO-RMs, namely (1) not many wavelengths can penetrate deep into the body, and (2) the compounds will degrade if exposed to stray light, therefore careful handling and storage are required. The use of light-induced CORMs for the eradication of lung-based *P. aeruginosa* infections seems particularly impractical.

Enzyme-triggered CO-RMs are the most recent development. These structures contain specific enzyme-cleavable groups, the degradation of which triggers CO-release. Such molecules have been designed with the intention of releasing CO in specific organs where there is a high concentration of a particular enzyme<sup>50</sup>. These CO-RMs are, however, hard to design as they require complex and specific ligands.

Finally, ligand-exchange CO-RMs are designed to release CO upon interaction with a compound that will displace the CO ligand at the metal centre. The advantages of such CO-RMs are that the design doesn't have to be as complex as for enzyme-triggered CO-RMs, and such molecules should have less specific storage requirements than light-activated CO-RMs. A disadvantage is the potential lack of specificity since molecules with a similar structure to the target activation ligand could activate CO release. This project will explore if pyocyanin is a good choice for a ligand that can activate CO-RMs in order to try and develop a *P. aeruginosa* antibiotic.

## 1.6 Quantifying CO Release

It is essential to relate the capacity for CO release to the biological activity of a therapeutic CO-RM, and there are two different methods available. Most commonly, the amount of CO that is released is determined by a myoglobin assay, as was first reported in 2002<sup>38</sup>. This technique utilises the fact that a strong bond

can be formed between CO and the haem iron in myoglobin. Initially, myoglobin is reduced with sodium dithionite to generate deoxymyoglobin and then exposed to the CO-RM. The CO released from the CO-RM then binds to the deoxymyoglobin, forming carboxymyoglobin. The deoxy- and carboxy- forms of myoglobin have distinct UV/vis spectra between 500 and 600 nm wavelength, enabling the indirect measurement of CO release. A more recent and direct method of monitoring CO release, free from the requirement of reducing agent, uses in-line gas phase infrared to directly track the appearance of CO in the gaseous phase<sup>51</sup>.

## 1.7 Aim

It is hypothesized that the structural and electrical properties of pyocyanin, and the fact it is produced almost exclusively by *Pseudomonas spp.*, make it a promising target for triggering CO release from a CO-RM, and this might be a method for developing a new class of antibiotic compounds that would be particularly effective in treating CF patients. The aims of this project are therefore to find a CO-RM that is water soluble, thermally and light stable and test if CO release can be triggered by the presence of pyocyanin. Any compound with these properties will then be investigated as a potential candidate for the therapeutic treatment of *P. aeruginosa* infections.

# Characterisation of Pyocyanin

Chapter 2

## 2 Characterisation of Pyocyanin

### 2.1 Introduction

When looking for a CO-RM activated by pyocyanin, the first challenge is to generate pure pyocyanin against which screening experiments can be conducted (**Figure 2.1**). As already introduced, the first purification of pyocyanin, previously known as pyocyanine, was achieved via the extraction of the bacterially generated molecule<sup>24</sup>.

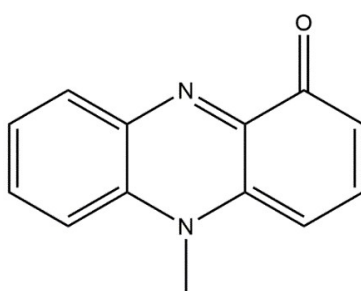


**Figure 2.1:** Pyocyanin

Pyocyanin is still commercially produced for research purposes (CAS: 85-66-5<sup>52</sup>) by extraction from *Pseudomonas* bacterial cultures, using a method unchanged since the 1800s<sup>24</sup>. As this is a costly and time consuming process, considerable research has been conducted to choose the highest pyocyanin-yielding *Pseudomonas* species, and optimise the molecular extraction<sup>53</sup>. On a smaller scale, it is possible to obtain pyocyanin via chemical synthesis. A simple photochemical method which uses commercially available phenazine methosulfate as the starting material was described by McIlwain in 1937,<sup>54</sup> with a modified work up procedure published by Borrero et al.<sup>55</sup>.

The chemical characterisation of pyocyanin using modern techniques has been sporadic. As the most commonly used identifying feature of pyocyanin is its distinctive blue colour, UV/vis spectroscopy has often been used in the analysis of this molecule<sup>53,56,57</sup>. The spectra is pH- and solvent-dependant; at low pH the

solution changes to an orange/red colour, reflected by the development of a peak at 520 nm and shifts in the UV region of the UV/Vis spectrum<sup>53</sup>.

No Infra-red (IR) analysis of pyocyanin has been found in the literature, but the related compound 1-hydroxyphenazine (**Figure 2.2**) has been analysed as a potassium bromide (KBr) disk<sup>58</sup>, indicating that phenazines can be analysed by IR.

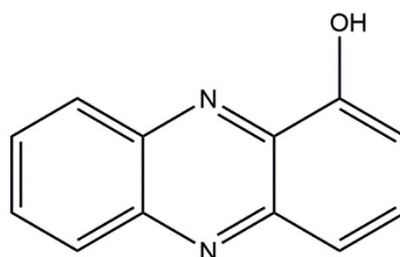
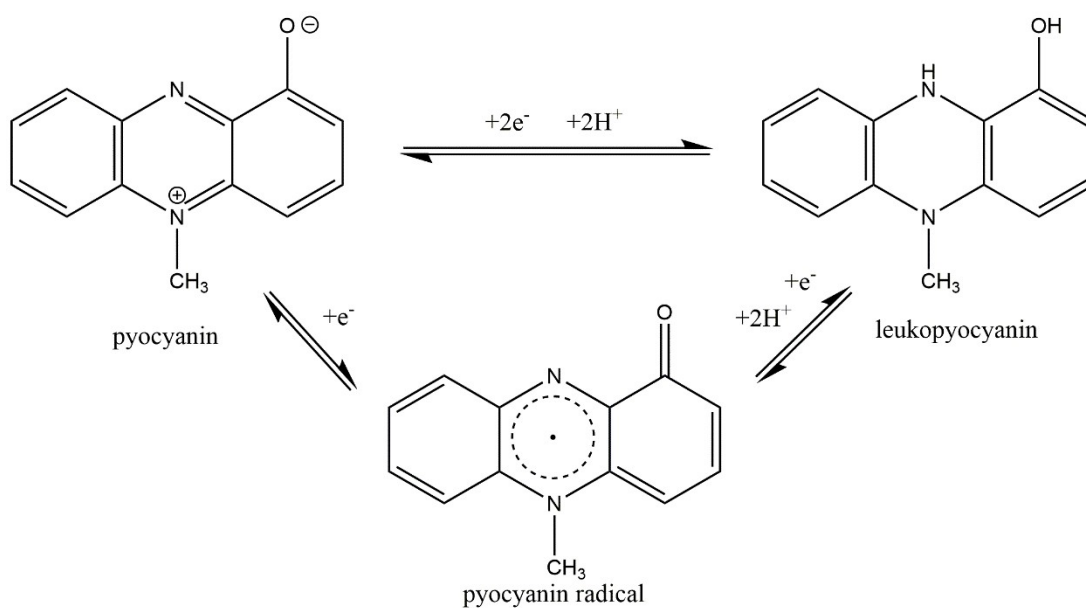


**Figure 2.2:** 1-hydroxyphenazine

The two-electron, two-proton reduction of pyocyanin to leukopyocyanin (**Scheme 2.1**) was first described by Elema in 1931<sup>59</sup>. The redox activity has been linked to the many different postulated biological roles of pyocyanin (virulence factor<sup>60</sup>, iron scavenger<sup>32</sup> and quorum sensor<sup>29</sup>) since pyocyanin can easily be reduced by the physiological reducing agents of NAD(P)H<sup>61</sup> and thiols<sup>31</sup>. Jacob et al.<sup>31</sup> postulated that this reaction proceeds via a radical intermediate (**Scheme 2.1**), and all three oxidation states take part in the catalytic cycle of reactive oxygen species generation in *P. aeruginosa*<sup>57</sup>.



**Scheme 2.1:** Redox cycling of pyocyanin. Modified from Jacob et al<sup>31</sup>

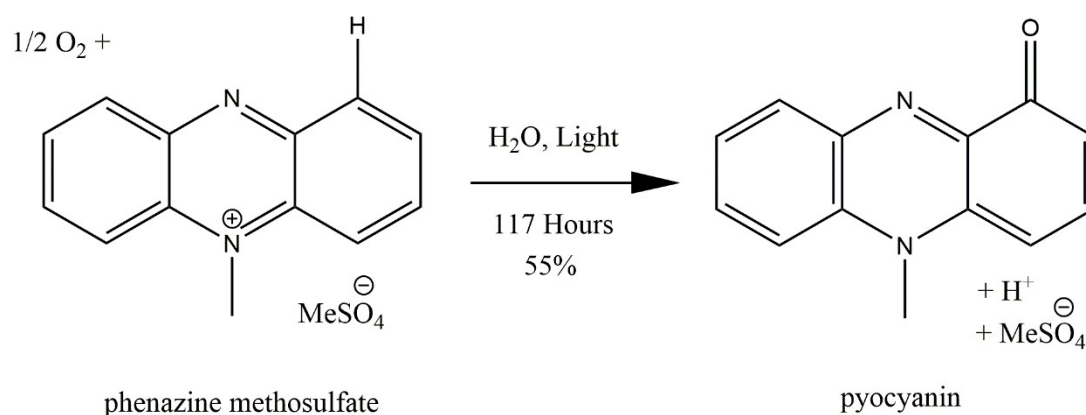
Leukopyocyanin is colourless, and therefore has a substantially different UV/Vis spectra to pyocyanin<sup>61</sup>, with the main difference being the loss of the broad peak around 698 nm and some slight shifting of the other peaks. These differences permit spectral monitoring of the redox reaction, and the induction of the chemical oxidation of leukopyocyanin to pyocyanin using ferrihydrite particles was tracked by UV/Vis spectroscopy, revealing the growth of three peaks at 310 nm, 390 nm and 700 nm as a function of time<sup>62</sup>.

The redox activity of pyocyanin could play a role in the activation of a CO-RM, and this Chapter describes the electrochemical investigation of this reactivity along with the laboratory preparation and full characterisation of pyocyanin.

## 2.2 Results and Discussion

### 2.2.1 Synthesis

The literature method of photochemical synthesis of pyocyanin was repeated but using an artificial light rather than sunlight and over a longer period of time (literature procedure used 8 hours), as shown in **Scheme 2.2**.



**Scheme 2.2:** Synthesis of pyocyanin from phenazine methosulfate

When initially dissolved, the phenazine methosulfate gave a clear green aqueous solution which turned very dark red while exposed to light. After quenching with aqueous sodium carbonate the solution turned green again. A blue fraction was extracted into chloroform and purified using column chromatography. Three different fractions were eluted before the blue, pyocyanin fraction, in an array of colours – yellow, green and red/pink (**Figure 2.3**). As described in the experimental, pyocyanin was returned in good yields as dark blue/black pyocyanin crystals. It was then analysed for purity using NMR and ESI mass spectrometry (**Chapter 6**).



**Figure 2.3:** Coloured fractions eluted prior to pyocyanin during column chromatography

### 2.2.2 NMR

The proton NMR was run in a solution of  $d_4$ -methanol and confirmed that the pyocyanin sample was pure and suitable for use in further characterisation experiments. This conclusion was reached because six separate peaks related to pyocyanin were observed in the spectrum, five peaks in the aromatic region (6.4 to 8.3 ppm), which integrated to 7 protons, and a single peak at 4.6 ppm which integrated to 3 protons and is characteristic of the N-methyl group. The only additional two peaks in the spectrum related to the methanol solvent.

### 2.2.3 UV/vis Analysis

The **Figure 2.4** shows the UV/Vis spectra for pH 7.4, Phosphate Buffer Saline (PBS) solutions of pyocyanin. This pH was chosen because the pKa of pyocyanin is

between 4.6 and 4.9<sup>63</sup>, and therefore the population of molecules are all in the same protonation state.

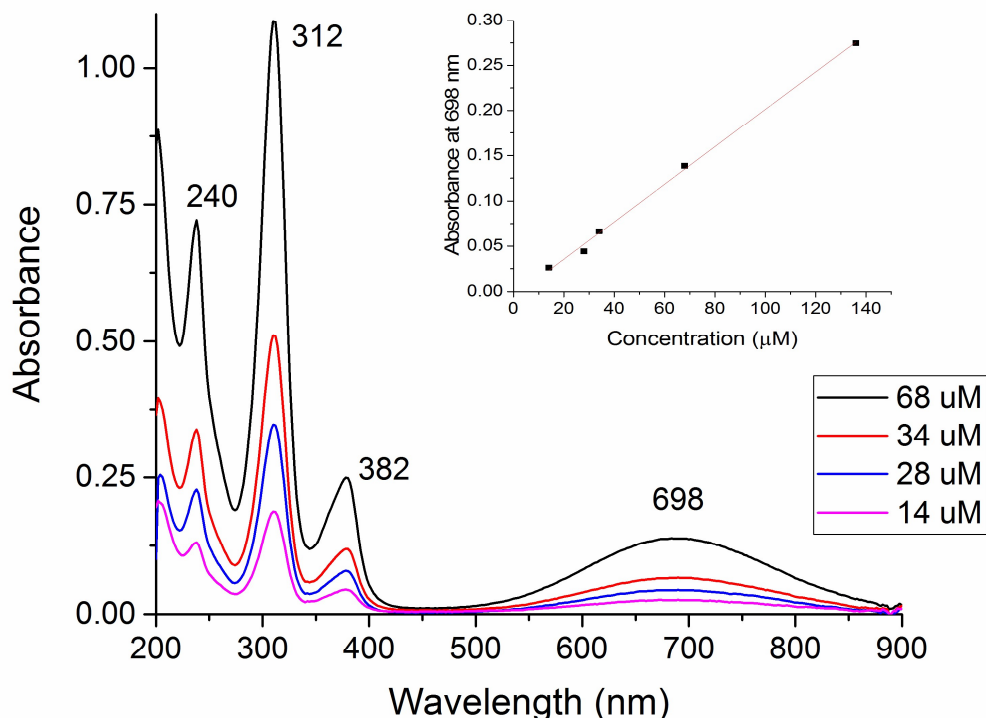


**Figure 2.4:** (Main) UV/Vis absorbance spectra of pyocyanin at different concentrations, as indicated, and (inset) the corresponding molar extinction plot

The spectra are all consistent with the literature data<sup>56</sup>. The broad peak centred at 698 nm is responsible for the vivid blue colour of the solution, while the other three bands are in the UV region. The absorbance at 698 nm is concentration dependant in a linear fashion, giving an extinction coefficient of  $2070 \pm 60 \text{ M}^{-1} \text{ cm}^{-1}$  (**Figure 2.4 Insert**).

#### 2.2.4 Electrochemistry

In order to probe the redox reactivity of pyocyanin, cyclic voltammograms (CVs) were run using a 0.5 mL glass electrochemical cell with a platinum disk working electrode, silver wire pseudo-reference electrode and a platinum wire counter electrode. Because a pseudo-reference electrode is used an internal reference is

required and the ferrocyanide-ferricyanide redox couple (redox potential +0.361 V vs SHE<sup>64</sup>) was added to the pyocyanin solution, yielding CVs such as that shown in **Figure 2.5**. Analysis of the high potential ferricyanide redox couple enables extraction of the correction data shown in **Table 2.1**, with a different dataset for each day of experiments.

	$E_{\text{ox}}$ (V vs Ref)	$E_{\text{red}}$ (V vs Ref)	$E_{\text{avg}}$ (V vs Ref)	Reference electrode correction
Dataset A	0.310	0.125	0.2175	+ 0.1435
Dataset B	0.195	0.07	0.1325	+ 0.2285

**Table 2.1:** Ferrocyanide redox couple internal reference data

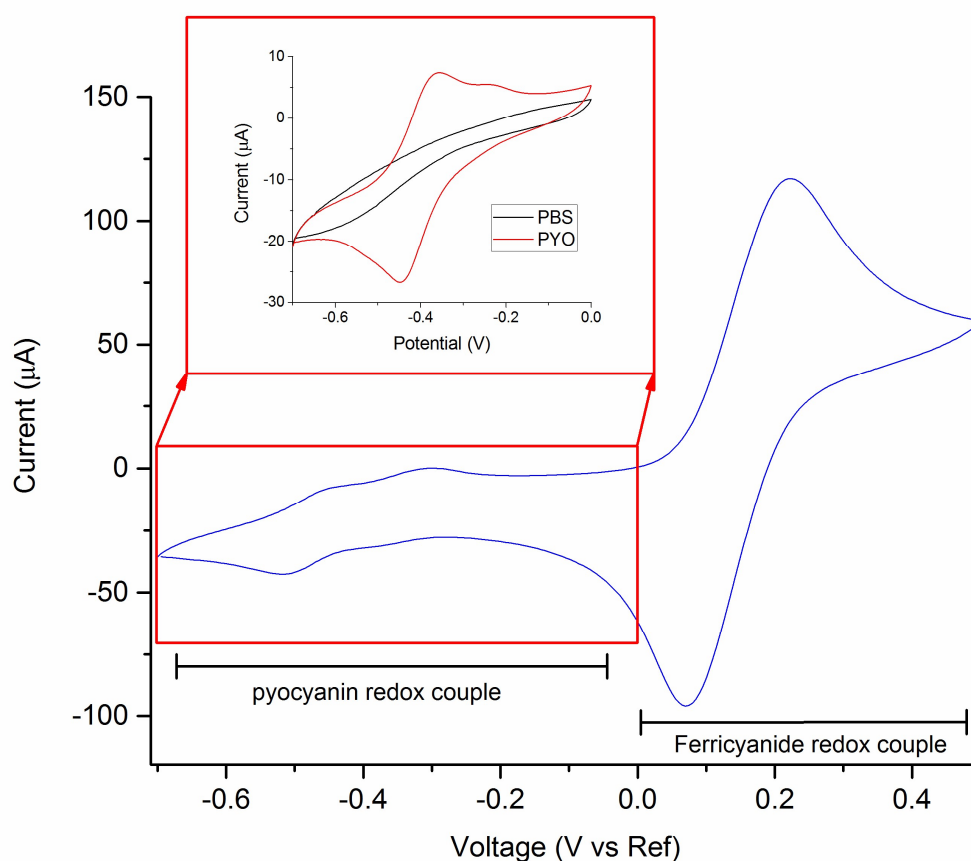


**Figure 2.5:** (Main) CVs of pyocyanin and ferrocyanide solution measured over a wide voltage range. (Inset) CVs of pyocyanin (PYO) and PBS-only over a narrower voltage range. Concentration of pyocyanin: 3.33 mM, Concentration of ferrocyanide: excess, atmosphere: air, solvent: PBS, pH: 7.4, temperature: room temperature, scan rate: 0.10 V/s. (Part of dataset A)

The first pyocyanin electrochemistry experiments were conducted in air, and typical data is displayed in **Figure 2.5**. Upon confining measurements to a negative voltage range (**Figure 2.5 Inset**), a well-defined redox event attributable to pyocyanin was clearly observed, centred at -0.40 V vs Ref, or -0.26 V vs SHE (**Table 2.2**, and **Figure 2.5**). The number of electrons,  $n$ , involved in the electrochemically detected redox event can be calculated using the voltage separation,  $\Delta E$ , of the peak current potentials (**Equation 2.1**), where  $E_{ox}$  indicates the potential of the oxidative current peak, and  $E_{red}$  indicates the potential of the reductive current peak<sup>65</sup>.

$$\Delta E = E_{ox} - E_{red} = \frac{59 \text{ mV}}{n}$$

**Equation 2.1:** Voltage separation equation

For pyocyanin in air,  $\Delta E$  was a scan rate independent parameter of +75 mV, equating to an  $n$  value of 0.79 (**Table 2.2**). Since it is impossible to have fractions of an electron, this indicates that a single electron redox reaction is observed, instead of the expected two electron redox reaction. As is clear in the main part of **Figure 2.5**, a second redox process can be partially seen between -0.4 and -0.2 V, suggesting further investigation is needed. The buffer-only control experiment (**Figure 2.5 Inset**) indicated that substantial oxygen reduction currents could be perturbing the measurements, and that more accurate analysis would be possible in the absence of this process.

Scan rate (V/s)	$E_{ox}$ (V vs SHE)	$E_{red}$ (V vs SHE)	$E_{avg}$ (V vs SHE)	$\Delta E$ (V)
0.02	-0.2215	-0.2965	-0.259	0.075
0.05	-0.2315	-0.3065	-0.269	0.075
0.10	-0.2165	-0.3015	-0.259	0.075

**Table 2.2:** CV potentials for pyocyanin in air, dataset A

In order to improve the resolution of the electrochemical experiments the conditions were therefore changed so that a higher concentration of pyocyanin (5.44 mM rather than 3.33 mM) was used, as well as an inert argon atmosphere. As shown in **Figure 2.6** this permitted clear resolution of two separate one-electron redox events, with one centred at -0.117 V vs SHE and the other at -0.252 V vs SHE (**Table 2.3**).

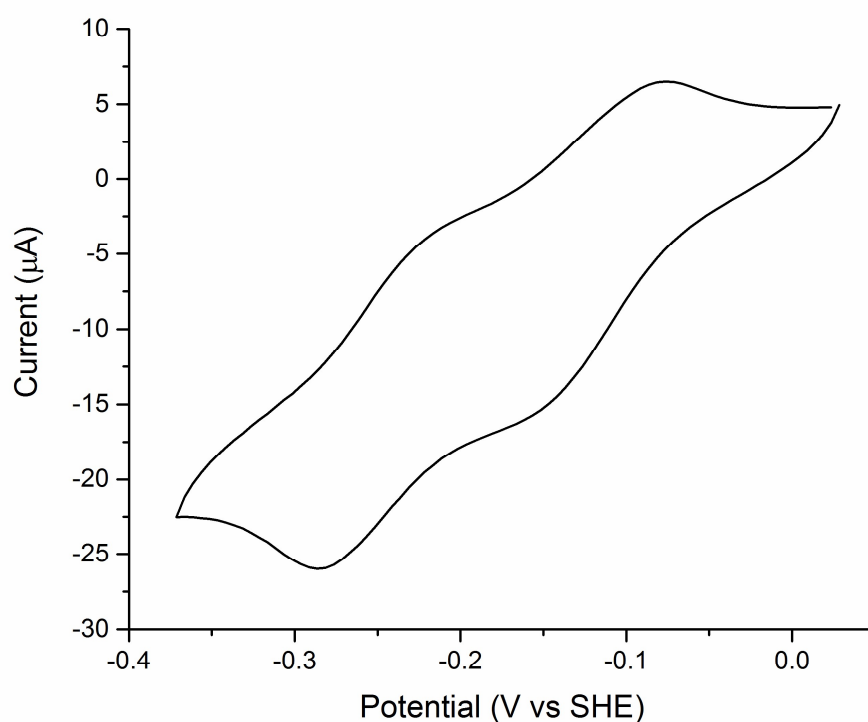


**Figure 2.6:** CVs of 5.44 mM pyocyanin under an Argon atmosphere. Solvent: PBS, pH 7.4, temperature: room temperature, scan rate: 0.10 V/s. (Dataset B)

	$E_{\text{ox}}$ (V vs SHE)	$E_{\text{red}}$ (V vs SHE)	$E_{\text{avg}}$ (V vs SHE)	$\Delta E$ (V)
Peak 1	-0.0765	-0.1565	-0.1165	0.075
Peak 2	-0.2215	-0.2815	-0.2515	0.070

**Table 2.3:** CV potentials for pyocyanin in Argon, dataset B

This data therefore supports the mechanism that pyocyanin is reduced to leukopyocyanin via formation of the pyocyanin radical, as shown in **Scheme 2.1**.

### 2.2.5 UV/Vis Spectroelectrochemistry

Spectroelectrochemistry was used to relate the change in pyocyanin UV/Vis spectra to the change in redox state. A voltage of -0.5 V vs Ag/AgCl (equivalent to -0.270 V vs SHE) was applied to the sample in order to ensure complete reduction to leukopyocyanin.

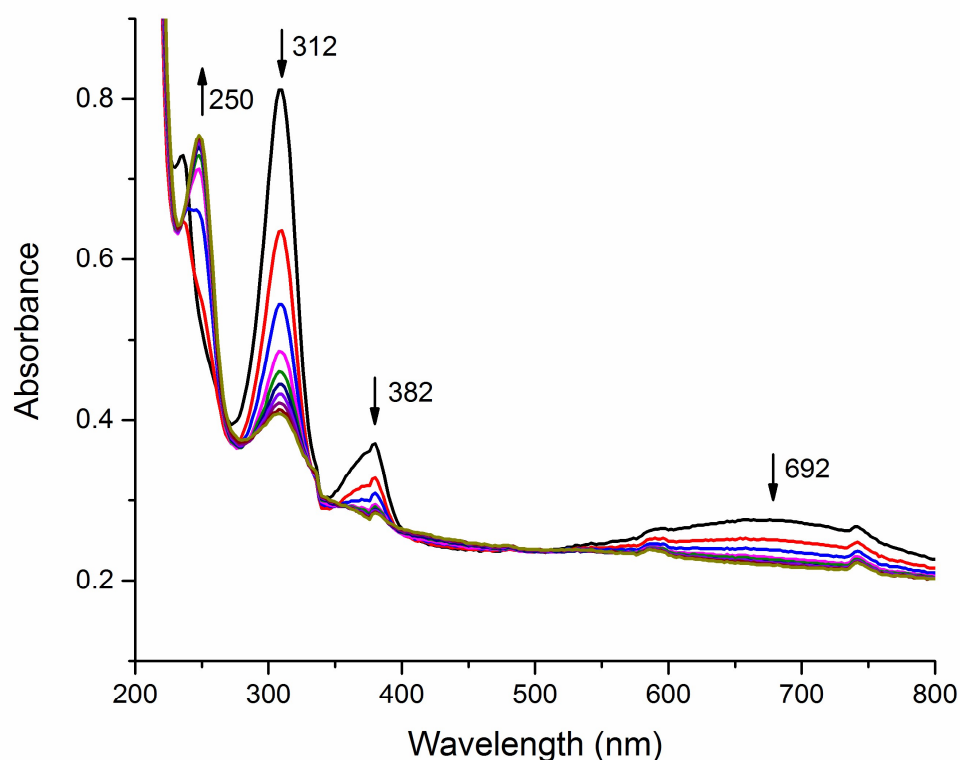


**Figure 2.7:** UV/Vis spectroelectrochemical spectra of pyocyanin 0.13 mM, -0.5 V vs Ag/AgCl

Four distinct change in the UV spectra were observed (**Figure 2.7**). The peak at 250 nm was the only peak to increase in intensity, and three peaks reduced in intensity; at 310 nm, 382 nm and 692 nm. The disappearance of the peak at 692 nm was seen visually as the solution in the cuvette changed from blue to colourless upon reduction. These are the same changes seen in the literature. The colour is

presumably lost due to the disruption of the conjugated system across the three rings. Once reduced the solution of leukopyocyanin remained colourless upon storage (**Figure 2.8**).

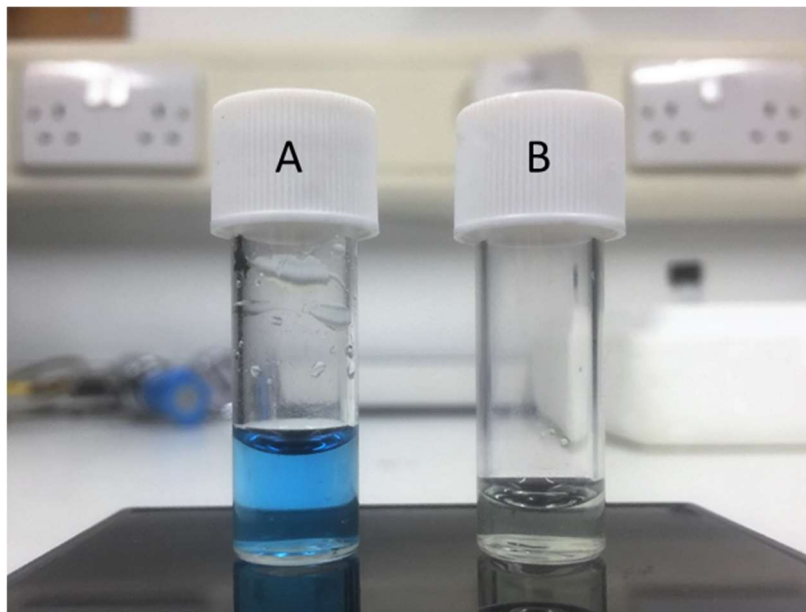


**Figure 2.8:** Pyocyanin (0.13 mM) A) before and B) after electrochemical reduction

Having identified the UV/Vis fingerprint of leukopyocyanin (**Figure 2.7**) it was confirmed that this state can be reached by chemical means, as could occur in a redox triggered CO release mechanism. **Figure 2.9** shows the UV/Vis spectra of blue, oxidised pyocyanin (PYO) and pyocyanin that has been partially chemically reduced to leukopyocyanin (LPYO). The reduction was purposefully incomplete, as it was important to determine conditions in which excess sodium dithionite would not persist.

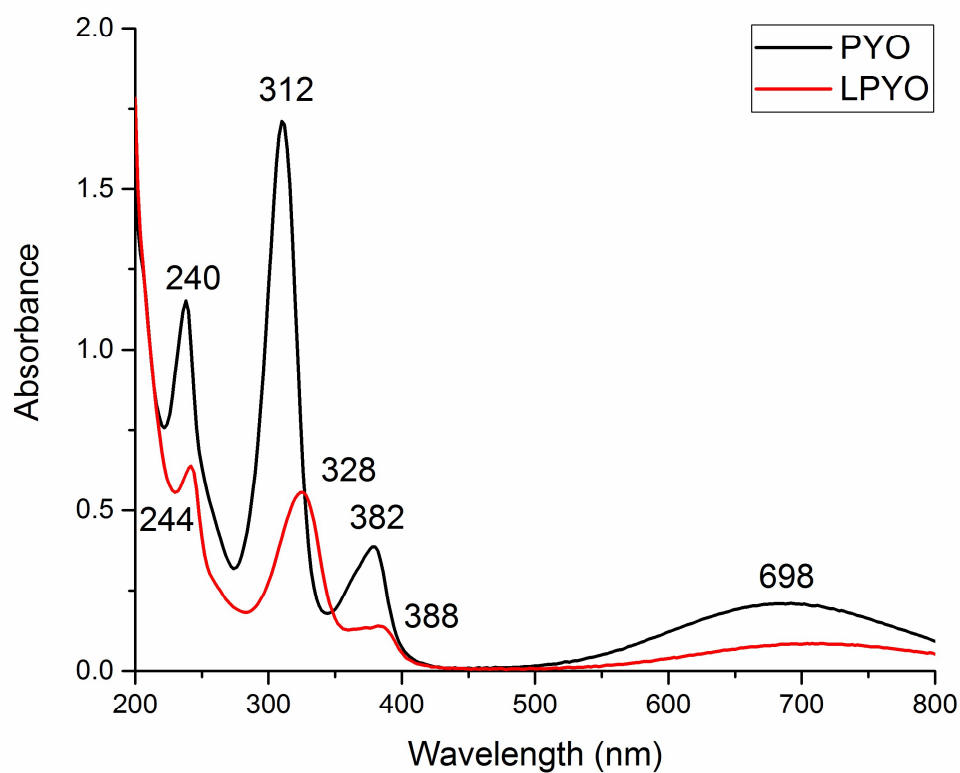


**Figure 2.9:** UV/Vis spectra of pyocyanin (PYO) and leukopyocyanin (LPYO) at similar concentrations

### 2.2.6 IR Analysis

The IR spectrum of pyocyanin was recorded as a solid in a KBr disk and as a solution of chloroform (**Figure 2.10**). In order for the IR bands to be seen such high concentrations of pyocyanin were required that a saturated chloroform solution had to be used.

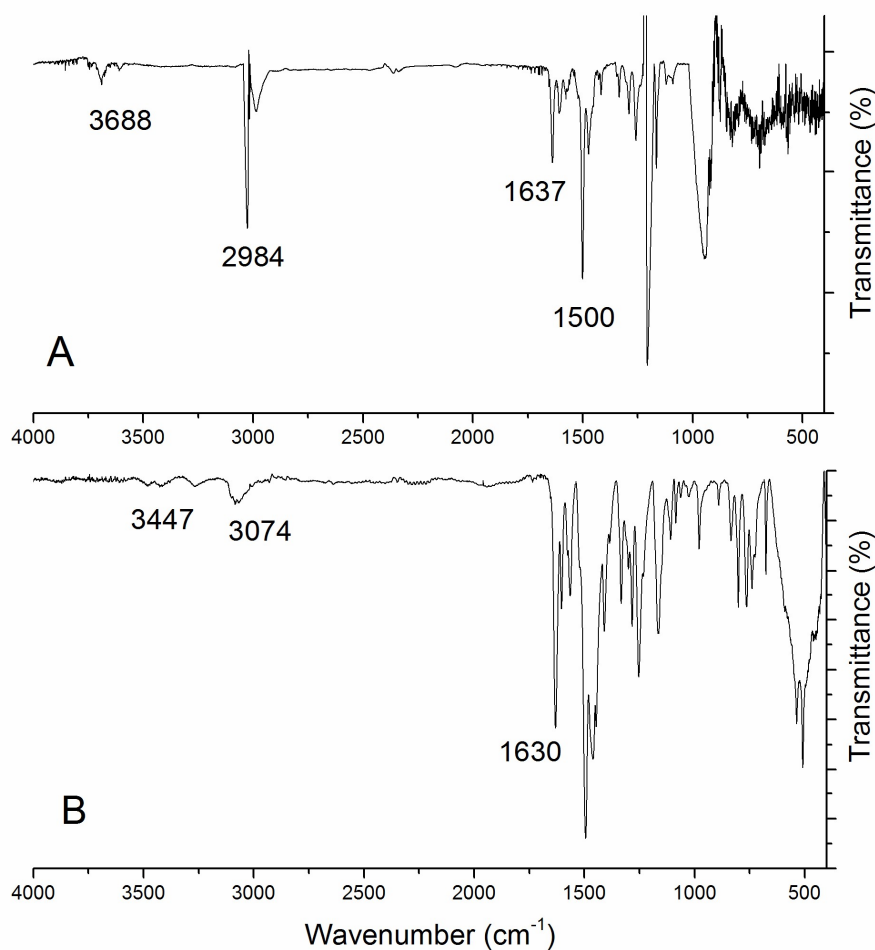


**Figure 2.10:** IR spectra of pyocyanin A) in chloroform B) as a KBr disk

In both IR spectra a very small peak was seen in the O-H ( $3688 \text{ cm}^{-1}$  and  $3447 \text{ cm}^{-1}$ ) region, showing that there is a small amount of leukopyocyanin present in both states. The peaks in the C=O region ( $1630$  and  $1637 \text{ cm}^{-1}$ ) are larger, with it being more significant in the solid state, this band is linked to the neutral state of pyocyanin (**Figure 2.1**). Because of the difference in intensity of these peaks it shows that the leukopyocyanin is more likely to be found in the solution phase than the solid phase.

According to the literature the zwitterionic form of pyocyanin (**Figure 2.11**) is the most predominant form of pyocyanin in neutral environments<sup>66</sup>. As the zwitterion has neither a hydroxyl nor a carboxyl group, it doesn't contribute to the spectra in

these regions. This proves that the zwitterion is common in both the solid and solution state because the observed bands are less intense than expected.

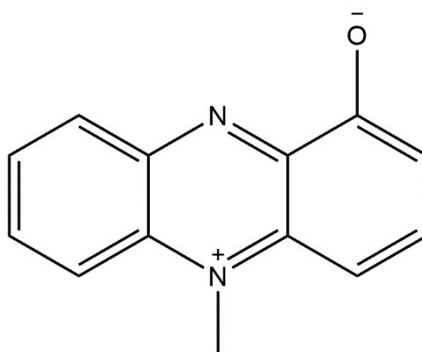


**Figure 2.11:** Pyocyanin zwitterion

### 2.2.7 DFT Calculations

Density functional theory (DFT) calculations were carried out by Dr Jason Lynam in the Department of Chemistry at the University of York.

Density functional theory can be used to determine the electronic energy transitions that occur when a molecule is excited. The six lowest energies transitions are shown in **Table 2.4**. The lowest predicted energy transition at 591 nm is related to the broad band in the UV/vis spectra for pyocyanin centred at 698 nm (**Figure 2.4**). This is a simple electronic HOMO to LUMO-type transition (**Figure 2.12**). The second lowest energy transition at 509 nm (a simple 54a to 56a-LUMO transition) is likely to be a transition unseen in the solution phase UV/vis due to its small oscillator strength and the broadness of the peak at 698 nm.

Due to the large oscillator strength of the calculated transition at 303 nm this therefore corresponds to the large experimental transition at 312 nm. This transition is not a simple transition and instead involves contributions from four molecular orbitals, which each contribute different amounts to the overall transition.

The three predicted electronic transitions at 359 nm, 332 nm, and 321 nm each have a small oscillator strength. Due to the fact these transitions have similar wavelengths it is possible that in the experimental data the three transitions are seen as a single one in the peak at 382 nm (**Figure 2.4**). The peak with the lowest energy, 359 nm, is also a pure transition from orbital 51a to 56a but the other two have contributions from multiple molecular orbitals.

Transition	Excitation energy / nm	Oscillator Strength	Occupied Orbitals (energy /eV)	Virtual Orbitals (energy /eV)	%age
1	591	0.110	55 a (-5.69)	56 a (-2.92)	96.1
2	509	0.335 E-02	54 a (-6.81)	56 a (-2.92)	96.0
3	359	0.149 E-02	51 a (-7.95)	56 a (-2.92)	93.7
4	332	0.455 E-02	53 a (-7.48)	56 a (-2.92)	57.1
			55 a (-5.69)	57 a (-1.03)	36.2
5	321	0.708E-02	52 a (-7.67)	56 a (-2.92)	45.7
			55 a (-5.69)	57 a (-1.03)	30.8
			53 a (-7.48)	56 a (-2.92)	19.4
6	303	0.376	52 a (-7.67)	56 a (-2.92)	45.7
			55 a (-5.69)	57 a (-1.03)	28.0
			55 a (-5.69)	58 a (-0.62)	11.0
			53 a (-7.48)	56 a (-2.92)	10.3

**Table 2.4:** DFT derived electronic transitions

Molecular orbital 54a (**Figure 2.13**) consists mostly of a carbonyl type antibonding orbital. Orbitals 55a and 56a have electron density focused on the carbonyl aromatic ring, whereas the electron density for 53a and 58a (**Figure 2.14**) is mainly on the other aromatic ring. 57a-LUMO +1 (**Figure 2.13**) is different in that the potential electron density is completely delocalised over the whole aromatic region rather than being dominant in one region.

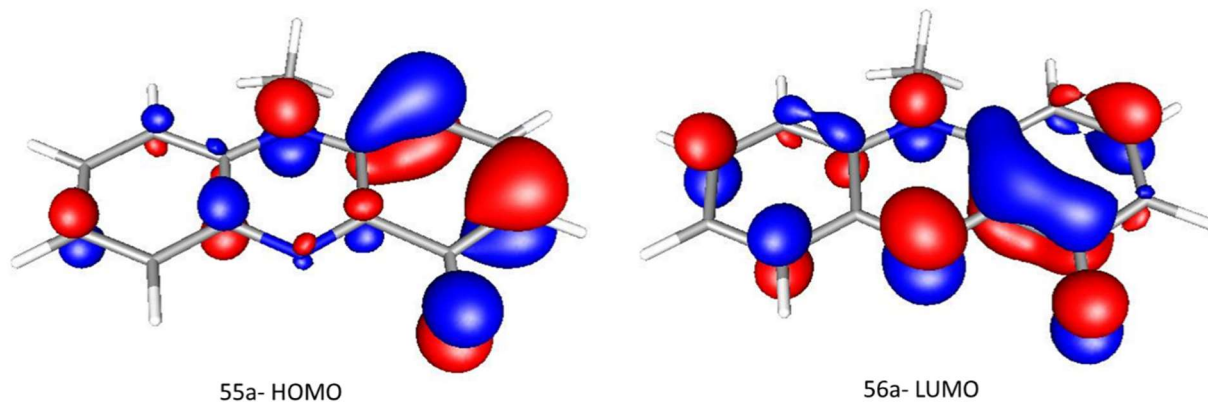


**Figure 2.12:** 55a-HOMO and 56a-LUMO electron density distribution diagrams

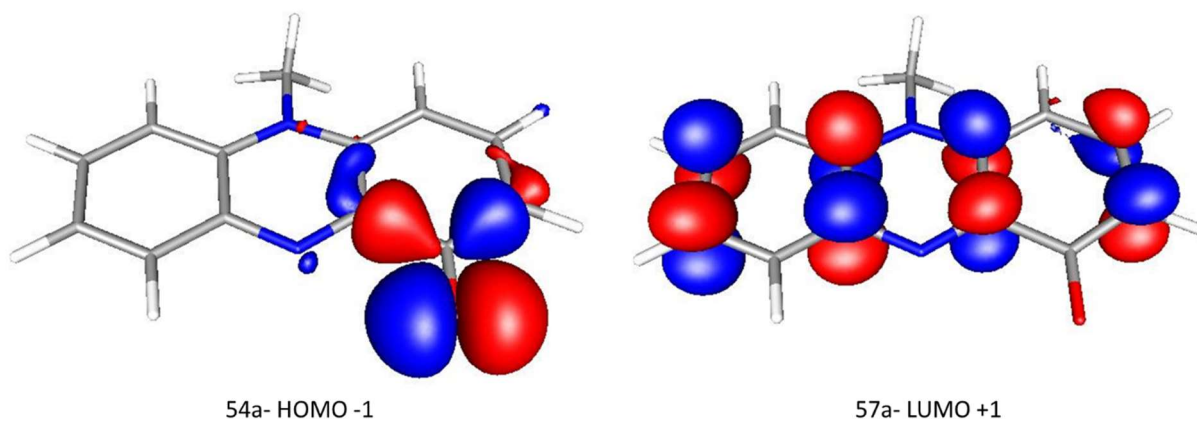


**Figure 2.13:** 54a-HOMO -1 and 57a-LUMO +1 electron density distribution diagrams

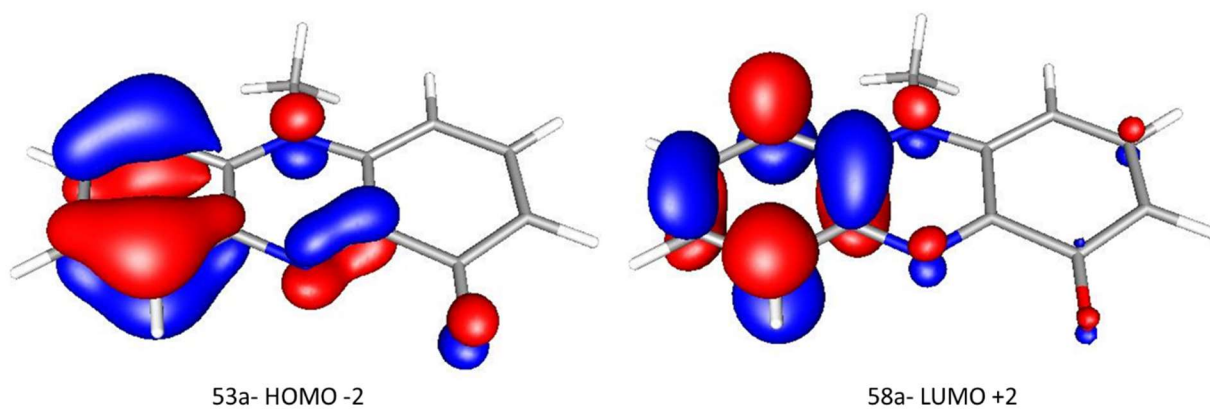


**Figure 2.14:** 53a-HOMO -2 and 58a-LUMO +2 electron density distribution diagram

### 2.2.8 Cystic Fibrosis Sputum Isolates

Since pure pyocyanin has been isolated it was possible to determine the extinction coefficient for pyocyanin in Lysogeny broth (LB), the media used to culture *P. aeruginosa*. Clinical isolates of *P. aeruginosa* from CF sputum collected from a Liverpool hospital could then be cultured in LB in York, and UV/vis analysis of the supernatant could be used to quantify the different pyocyanin production levels of different bacterial strains. It is important to know the concentration range of pyocyanin in medically relevant samples because this indicates the binding affinity any potential pyocyanin-activated drug may need to display in order for pyocyanin to be an effective *in vivo* activator.

The extinction coefficient of pyocyanin was measured in two different solvent systems, 100% LB broth, the media in which the bacterial samples were grown, and a 1 in 6 dilution of LB in distilled water. This yielded extinction coefficient values at 692 nm of  $4710 \pm 250 \text{ M}^{-1}\text{cm}^{-1}$  and  $5670 \pm 100 \text{ M}^{-1}\text{cm}^{-1}$  respectively. The LB had a slight yellow colour and contains many types of proteins and growth nutrients needed by the bacteria.

A series of 40 *P. aeruginosa* strains were isolated from the sputum of CF patients. The samples were prepared and provided by Dr Siobhan O'Brien (Brockhurst lab, Department of Biology, York). They were cultured in LB broth overnight, centrifuged to pellet bacteria and the supernatant removed. The supernatant was stored at -20°C before the measurements were run on the spectrophotometer, measurements using the well plate were taken immediately. No live bacteria were present in the supernatant solution. Thirteen of the supplied CF isolate supernatant samples were randomly selected, along with three different lab strains (PA01, LESB58 and PA01-PVD-PCH), diluted and analysed by UV/Vis spectroscopy (**Table 2.5**). The UV/Vis spectra of three of these samples, representative of all the types of spectra observed, are seen in **Figure 2.15**.

Isolate ID	Absorbance at 692 nm*	Conc. mM	Absorbance at 691 nm**	Conc. mM
1	0.05203	0.05507	0.3246	0.06885
3	0.01059	0.01121	0.0726	0.01540
12	0.02573	0.02723	0.1364	0.02893
17	0.06619	0.07006	0.4114	0.08727
18	0.00512	0.00542	0.0597	0.01266
19	0.00972	0.01029	0.0648	0.01375
20	0.06583	0.06967	0.4169	0.08843
24	0.01795	0.01810	0.0967	0.02051
27	0.06076	0.06431	0.4552	0.09656
29	0.08546	0.09050	0.6184	0.13117
33	0.03971	0.04203	0.2009	0.04261
36	0.05502	0.05823	0.2698	0.05723
39	0.05323	0.05634	0.2786	0.05910
LESB58	0.08578	0.09200	0.3246	0.06885
PA01	0.01478	0.01580	0.0726	0.01540
PA01-PVD- PCH	0.01811	0.01940	0.1364	0.02893

**Table 2.5:** CF isolates and their absorbances and corresponding pyocyanin concentration, \*: from UV/vis spectroscopy, \*\*: from well plate spectrophotometer measurements

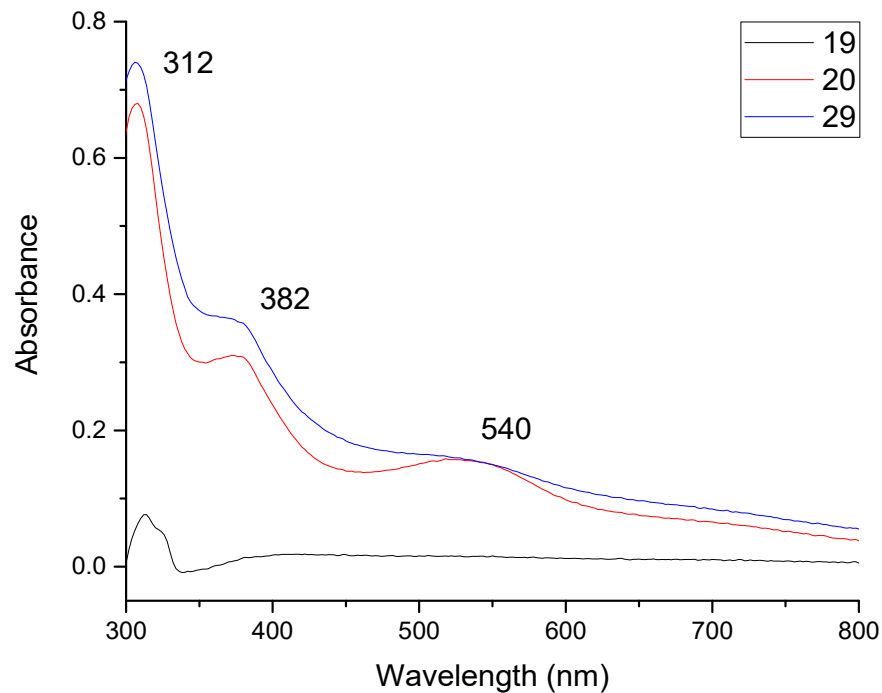


**Figure 2.15:** Examples of CF supernatant UV/vis spectra

Due to the proteins and other nutrients present in the broth the spectra were uninformative at wavelengths shorter than 300 nm. All samples showed the characteristic pyocyanin peak at 312 nm, although for some this was the only visible peak. Some of the samples had a slight purple colour indicating that other metabolites were present, this was reflected in peaks visible at about 540 nm. Other samples had more of the characteristic pyocyanin spectra and were often blue/green in colour.

The concentration of pyocyanin in each of the samples was found using the extinction coefficients at 692 nm for the relevant percentage of LB (**Figure 2.16**). The absorbance measurements from the plate reader were at 691 nm however the UV/Vis spectra only measured even wavelengths so the correlation coefficient was calculated using 692 nm. Because the peak here is broad it was determined that the extinction coefficient is still accurate for 691 nm.

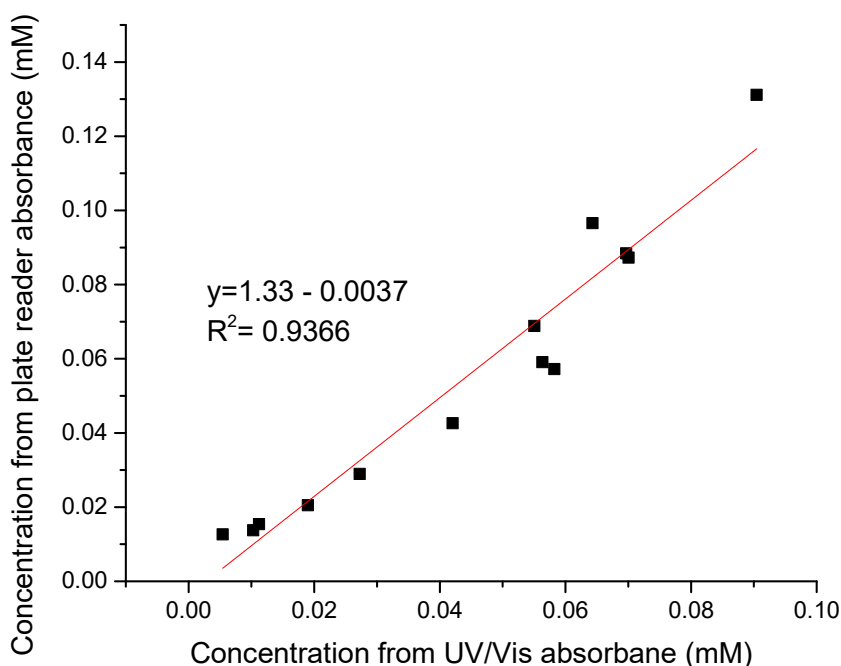


**Figure 2.16:** Comparison of concentrations from single point absorbance scans at 691 nm using a plate reader and from UV/Vis scans using the absorbance at 692 nm

A significant correlation was seen between the concentrations found in pure LB and in the 1 in 6 dilution. The concentrations given are not exact due to the nature of the media and other phenazines that are produced by *P. aeruginosa*.

### 2.3 Conclusion

A simple inexpensive method of producing pyocyanin has been utilised, and simplified, as an alternative to extraction from *Pseudomonas aeruginosa*. A complete characterisation of synthetically made pyocyanin was undertaken with the results matching with the literature values where they were available. Spectroelectrochemistry, IR and DFT have been used for the first time in the analysis of pyocyanin. Understanding the properties of pyocyanin, particularly its UV/vis and IR spectra, is important for observing changes to pyocyanin that should occur during reaction with a CO-RM.

The extinction coefficient found for pyocyanin in 100% LB means that the concentration of pyocyanin in biological samples can be measured for the first time, giving further insight into *P. aeruginosa* infection in the CF lung.

# CO-RM Screening

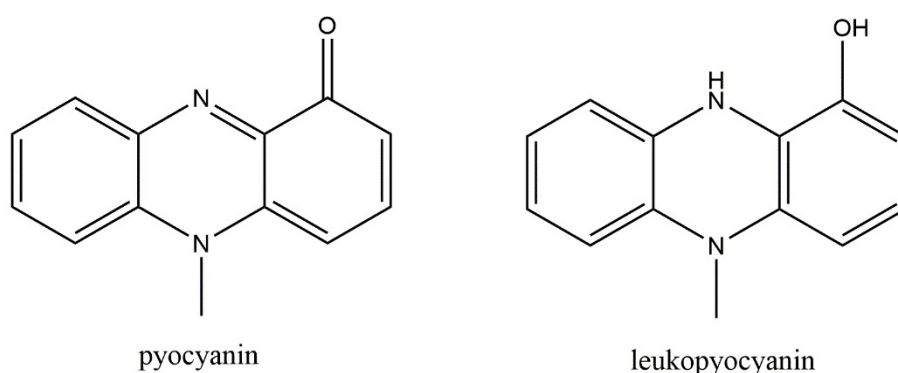
## Chapter 3

### 3 CO-RM Screening

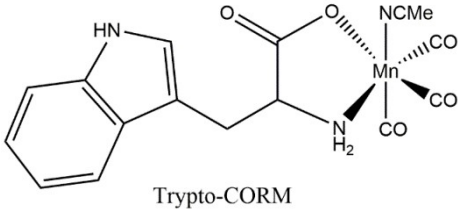
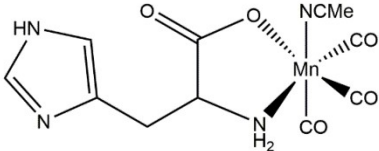
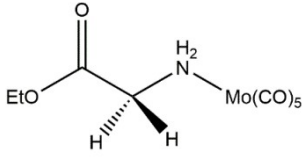
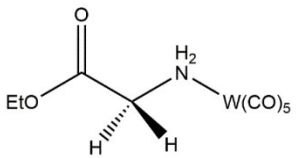
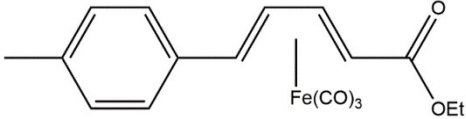
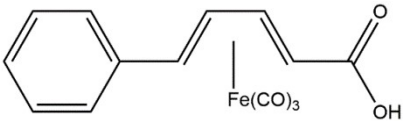
#### 3.1 Introduction

A large number of CO-RMs have been synthesised previously in the Lynam and Fairlamb groups<sup>46,67–71</sup>. A selection of compounds from this CO-RM “library” was chosen to test for potential pyocyanin-induced CO release, as summarised in **Table 3.1**. The CO-RMs listed were chosen for their probable water solubility, biological suitability, and known CO-releasing properties. Water solubility is a particularly important feature in drug molecule design since it may promote the bioavailability of the compound *in vivo*. In the CO-RM field, “biological suitability” refers to the fact that the central metal ion in the CO-RM is not toxic, e.g. Mn rather than Pt.

Since pyocyanin can be reduced under biological conditions, CO-RM reactivity was tested with both blue, oxidised pyocyanin and the colourless, reduced “leukopyocyanin” form (**Figure 3.1**). Pyocyanin has a characteristic UV/vis spectrum arising from the conjugation in the molecule (see **Chapter 2**). UV/vis spectroscopy was therefore used to detect structural changes to pyocyanin in response to exposure to a CO-RM. Many CO-RMs also have characteristic bands in the UV/vis spectra which can be monitored to follow the progress of a reaction.



**Figure 3.1:** Pyocyanin and leukopyocyanin

CO-RM	Synthesis reference
$\text{MnBr}(\text{CO})_5$	CAS: 14516-54-2 <sup>72</sup>
$[\text{NEt}_4][\text{MoBr}(\text{CO})_5]$	W-Q Zhang et al, 2009 <sup>67</sup>
$[\text{NEt}_4][\text{WBr}(\text{CO})_5]$	W-Q Zhang et al, 2009 <sup>67</sup>
$[\text{NEt}_4][\text{MnBr}_2(\text{CO})_4]$	Angelici, 1964 <sup>73</sup>
 <p>Trypto-CORM</p>	J Ward et al, 2014 <sup>46</sup>
 <p>His-CORM</p>	Mohr et al, 2012 <sup>74</sup>
 <p>Mo-1</p>	W-Q Zhang et al, 2010 <sup>69</sup>
 <p>W-1-a</p>	W-Q Zhang et al, 2010 <sup>69</sup>
 <p>Chalcone CORM 1</p>	Synthesized by Dr Ciara O'Brien (unpublished)
 <p>Chalcone CORM 2</p>	Synthesized by Dr Ciara O'Brien (unpublished)

**Table 3.1:** CO-RMs selected for screening for pyocyanin activation

## 3.2 Results and Discussion

Of the CO-RMs selected for pyocyanin-activation screening (**Table 3.1**), the compounds  $\text{MnBr}(\text{CO})_5$  was immediately rejected from the trial because it was not soluble in water or PBS solution. The remaining CO-RMs were then screened for spontaneous CO release in PBS by monitoring the UV/Vis spectra of  $24 \mu\text{M}$  solutions as a function of time for up to 300 min. CO-RMs which spontaneously degrade at a rapid rate under these conditions are classified as “thermally activated”, and **Figure 3.2** shows sample data for one such compound,  $[\text{NEt}_4][\text{MoBr}(\text{CO})_5]$ . This thermal release mechanism was also observed for the CO-RMs  $[\text{NEt}_4][\text{MoBr}(\text{CO})_5]$  and  $[\text{NEt}_4][\text{WBr}(\text{CO})_5]$ . These were subsequently all rejected because the rate of degradation in the absence of pyocyanin was so fast that it was impossible to detect any further pyocyanin-dependent activation reaction.

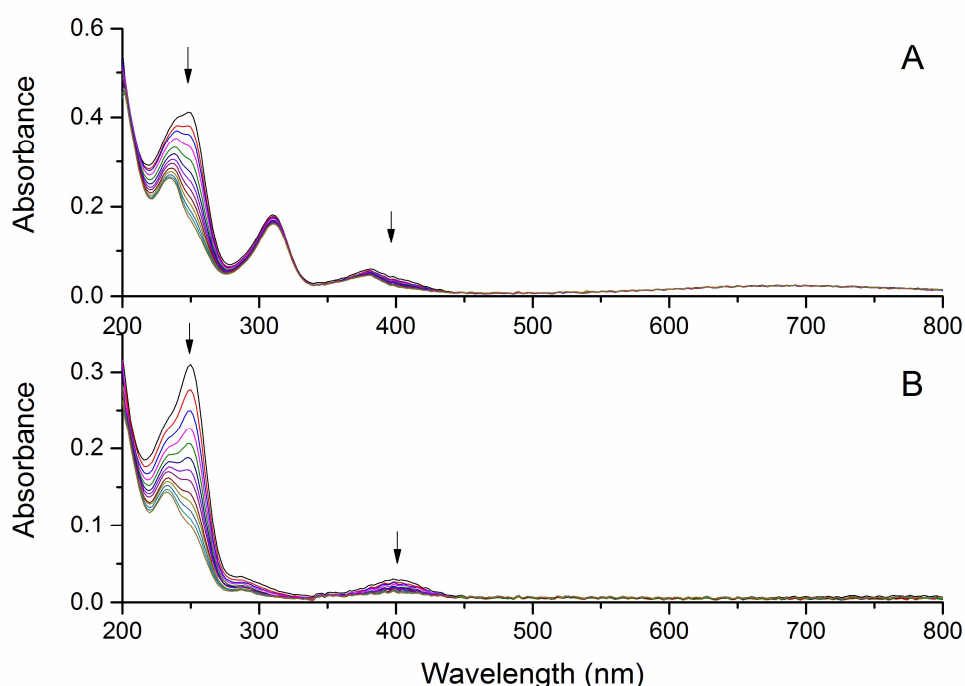


**Figure 3.2:** UV/vis spectra of thermal CO-releasing molecule  $[\text{NEt}_4][\text{MoBr}(\text{CO})_5]$  every 4 minutes for 49 minutes A)  $24 \mu\text{M}$  CO-RM, and B)  $24 \mu\text{M}$  CO-RM and  $24 \mu\text{M}$  PYO in PBS solution

Having eliminated any unsuitable CO-RMs from the selection, the remaining PBS-soluble, non-thermal releasing molecules were each dissolved separately in PBS solution and then added to cuvettes containing either pyocyanin or leukopyocyanin. **Table 3.2** lists the results of these screening tests.

CO-RM	With PYO	With LPYO
[NEt <sub>4</sub> ] [MnBr <sub>2</sub> (CO) <sub>4</sub> ]	Yes	No
Trypto-CORM	No	No
His-CORM	No	-
Mo-1 <sup>d</sup>	No	No
W-1-a <sup>d</sup>	No	-
Chalcone CORM 1	-	No
Chalcone CORM 2	No	No

**Table 3.2:** Results of testing CO-RMs for activation by pyocyanin (PYO) or leukopyocyanin (LPYO).  
 Yes: A significant change in the UV/vis spectrum occurred in the presence of the pyocyanin species.  
 No: No significant changes were observed.

The leukopyocyanin was generated from pyocyanin via chemical reduction using sodium dithionite since electrochemical reduction is hard to achieve on a milligram scale. Since the reduction of pyocyanin to leukopyocyanin requires two-electrons, two-equivalents of sodium dithionite would be necessary for complete reduction. However, as some CO-RMs have shown activation by sodium dithionite<sup>51</sup>, it was important to ensure that no excess reduced sodium dithionite remained in solution, so the molar ratio of sodium dithionite to pyocyanin was always slightly less than 2:1. It was impossible to spectroscopically detect the redox state of the dithionite because the reduced state has a single peak in the UV at 314 nm which is masked by the strong pyocyanin absorbance at 310 nm, and oxidised sodium dithionite does not absorb UV/vis radiation<sup>75</sup>.

### 3.2.1 [NEt<sub>4</sub>][MnBr<sub>2</sub>(CO)<sub>4</sub>]

Of all the CO-RMs screened, [NEt<sub>4</sub>][MnBr<sub>2</sub>(CO)<sub>4</sub>] was the only one that showed reactivity with either oxidation state of pyocyanin. At concentrations of 24 μM CO-RM and 24 μM pyocyanin, a small but significant decrease in absorbance at 312 nm is observed, attributed to a change in the pyocyanin structure (**Figure 3.3A**). **Figure 3.3B** shows a control experiment confirming there is no change in the UV/Vis spectrum of the CO-RM in the absence of pyocyanin.

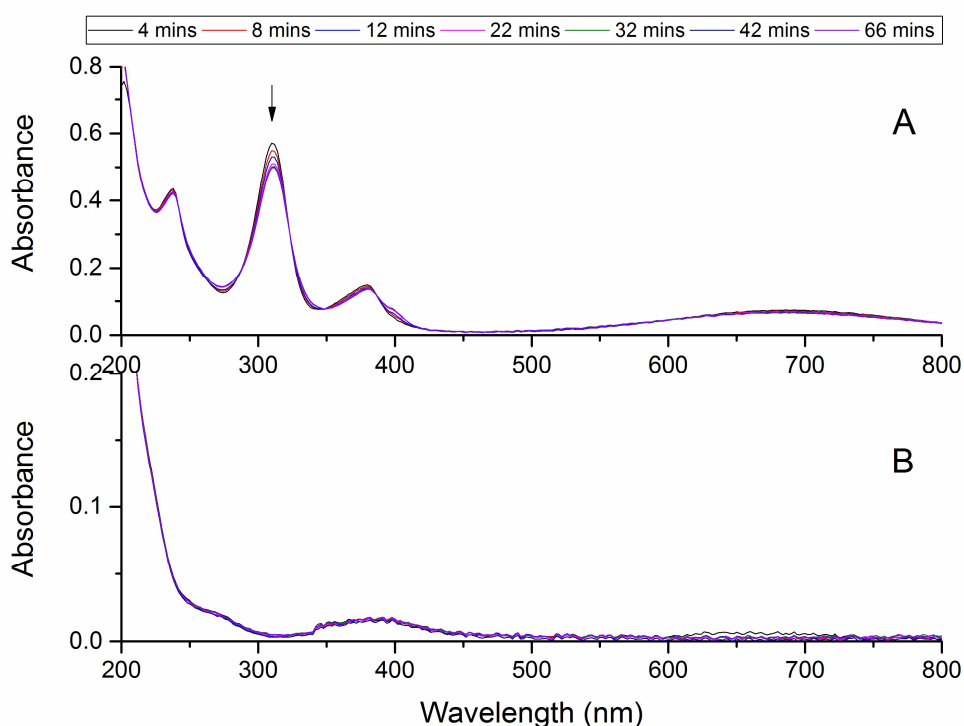


**Figure 3.3:** UV/vis spectra measured over 66 minutes, A) 24 μM [NEt<sub>4</sub>][MnBr<sub>2</sub>(CO)<sub>4</sub>] and 24 μM PYO in PBS solution, B) 24 μM [NEt<sub>4</sub>][MnBr<sub>2</sub>(CO)<sub>4</sub>] in PBS solution

In order to further explore the reaction between pyocyanin and [NEt<sub>4</sub>][MnBr<sub>2</sub>(CO)<sub>4</sub>], UV/Vis experiments were performed at a higher concentration of CO-RM. When the concentration of CO-RM was doubled to 48 μM, but the concentration of pyocyanin was maintained at 24 μM, larger changes in the UV/Vis spectrum were seen, with a reduction in the absorbance at 312 nm, 382 nm and 698 nm (**Figure 3.4A**). Again, no change was seen in the absorbance spectra of [NEt<sub>4</sub>][MnBr<sub>2</sub>(CO)<sub>4</sub>] on its own (**Figure 3.4B**). The difference spectrum for the same reaction (**Figure 3.5**) gives a clearer indicator of the changes that occur over 88 minutes of reaction.

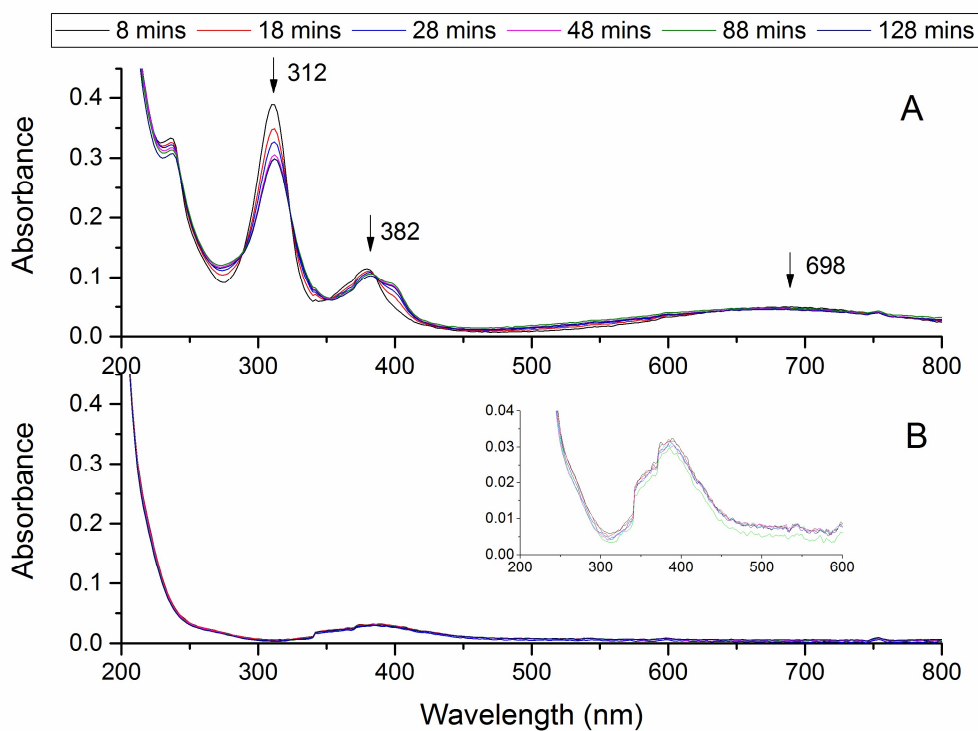


**Figure 3.4:** UV/vis spectra measured over 128 minutes, A) 48  $\mu\text{M}$   $[\text{NEt}_4][\text{MnBr}_2(\text{CO})_4]$  and 24  $\mu\text{M}$  PYO in PBS solution, B) 48  $\mu\text{M}$   $[\text{NEt}_4][\text{MnBr}_2(\text{CO})_4]$  in PBS solution

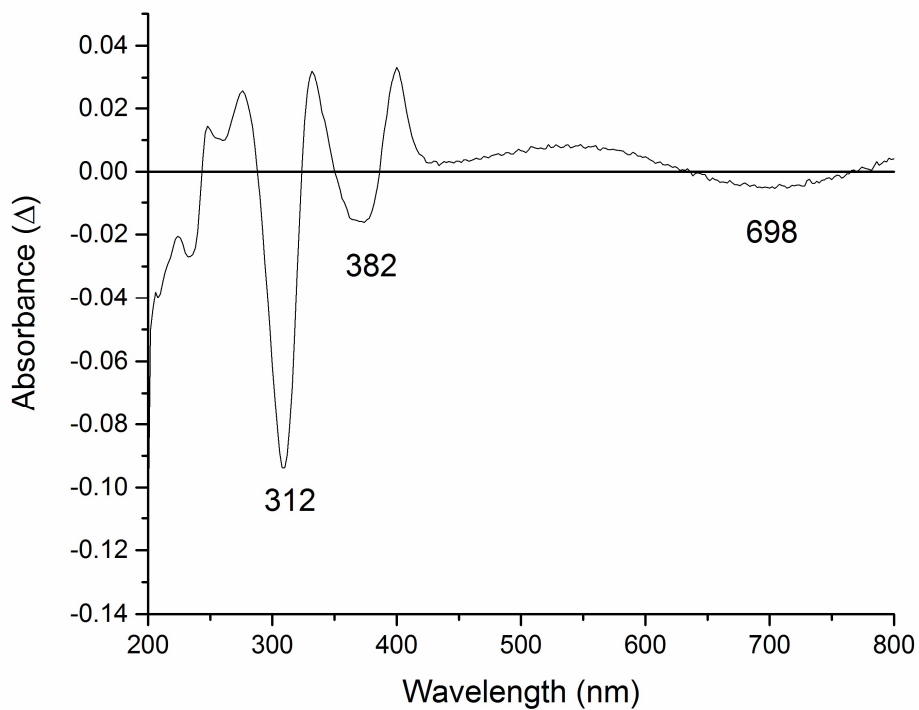


**Figure 3.5:** UV/vis difference spectrum after 88 minutes of 48  $\mu\text{M}$   $[\text{NEt}_4][\text{MnBr}_2(\text{CO})_4]$  and 24  $\mu\text{M}$  PYO in PBS solution

Raising the concentration of pyocyanin so that both reagents are present at  $48 \mu\text{M}$  appears to increase the rate of reaction (**Figure 3.6**).

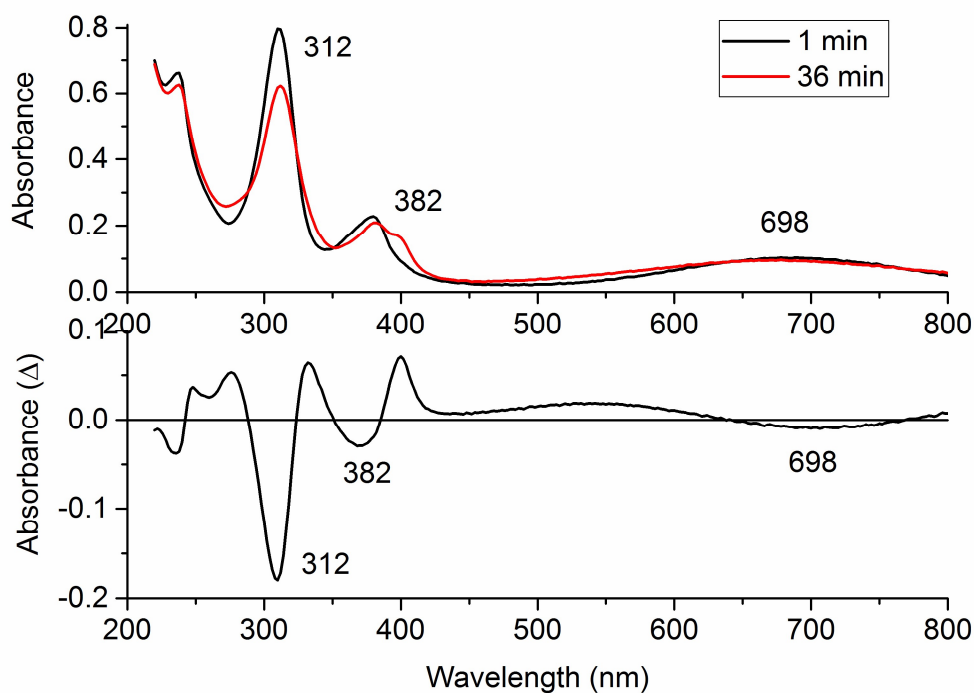


**Figure 3.6:** UV/Vis spectra at 1 and 36 minutes and the difference spectra for  $48 \mu\text{M}$   $[\text{NEt}_4][\text{MnBr}_2(\text{CO})_4]$  and  $48 \mu\text{M}$  PYO in PBS

Experiments at higher concentration of  $[\text{NEt}_4][\text{MnBr}_2(\text{CO})_4]$  and leukopyocyanin continue to show no apparent reactivity (**Figure 3.7**), indicating that a structural property of pyocyanin but not in leukopyocyanin is important for reactivity.

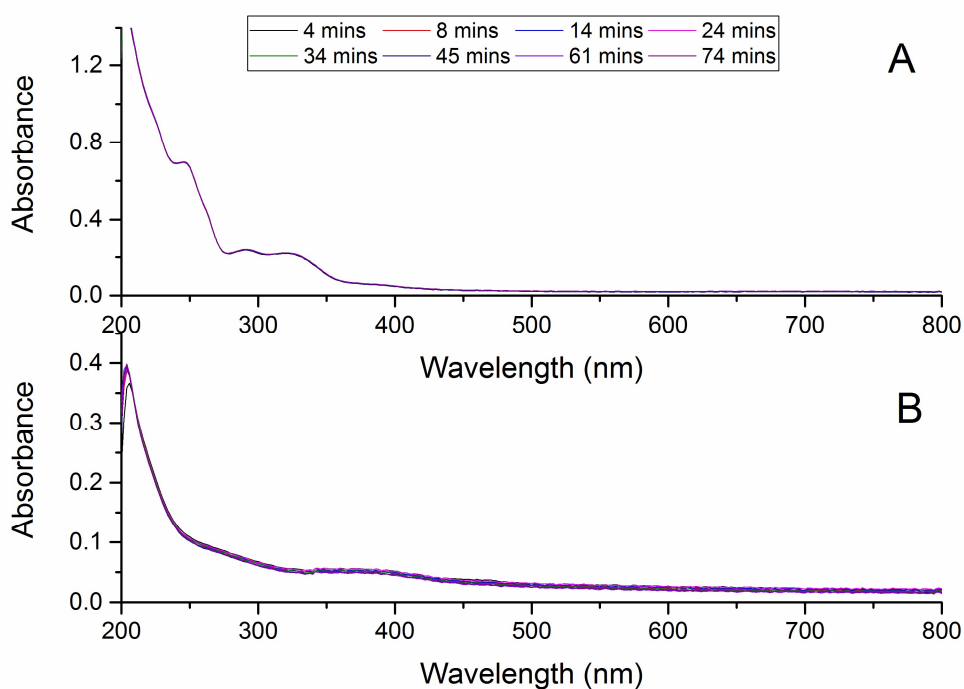


**Figure 3.7:** UV/vis spectra measured over 74 minutes, A)  $30\ \mu\text{M}$   $[\text{Mn}(\text{CO})_4\text{Br}_2][\text{NEt}_4]$  and  $30\ \mu\text{M}$  LPYO in PBS B)  $30\ \mu\text{M}$   $[\text{Mn}(\text{CO})_4\text{Br}_2][\text{NEt}_4]$  in PBS

### 3.3 Conclusion

The CO-RM  $[\text{NEt}_4][\text{MnBr}_2(\text{CO})_4]$  was found to cause changes to the pyocyanin UV/vis spectra that indicate a reaction has occurred which has induced a structural change in the pyocyanin. Due to the nature of pyocyanin, it is postulated that it could either coordinate to the Mn centre or participate in a redox reaction. Both of these mechanisms would likely induce carbon monoxide loss in the CO-RM. If pyocyanin acts as a ligand to the Mn then it is likely to bind in a bidentate manner through the oxygen and close nitrogen, and for this to happen two of the existing ligands need to be removed, implying CO release. An electrochemical activation mechanism would change the oxidation state of the manganese centre, which would affect the binding of the ligands, and CO could be evolved. Understanding this reaction is the focus of the following work.

# Pyo-CORM reactions

Chapter 4

## 4 Pyo-CORM reactions

### 4.1 Introduction

Due to the pyocyanin reactivity described in **Chapter 3**, the simple organometallic salt  $[\text{NEt}_4][\text{MnBr}_2(\text{CO})_4]$  was re-named “pyo-CORM” (**Figure 4.1**). This compound was synthesised by Angelici<sup>73</sup> and also by Abel and Butler<sup>76</sup> in 1964 via reaction of  $\text{MnBr}(\text{CO})_5$  with  $\text{NEt}_4\text{Br}$ . The four carbonyl stretching bands in the solution IR spectrum<sup>73,76</sup> of pyo-CORM are consistent with a  $C_{2v}$  symmetry *cis* conformation of the bromide ligands<sup>77</sup>. Despite being first synthesised over 50 years ago, very little characterisation has been performed on pyo-CORM.

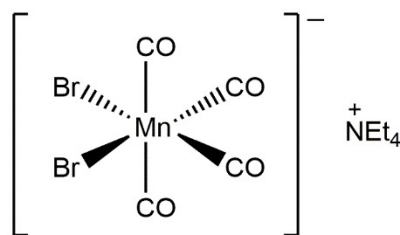


**Figure 4.1:**  $[\text{NEt}_4][\text{MnBr}_2(\text{CO})_4]$ , pyo-CORM

The aim of the work described in this Chapter was to prove if CO release is triggered in the reaction between pyocyanin and pyo-CORM.<sup>67</sup> In particular, two possible activation mechanisms for reaction between pyo-CORM by pyocyanin will be explored, namely if the pyo-CORM manganese centre is oxidised by pyocyanin, or if there is direct coordination of pyocyanin to the manganese centre.

### 4.2 Analysis of pyo-CORM

#### 4.2.1 IR Analysis

The infrared analysis of pyo-CORM is of particular interest due to the presence of the four carbonyl ligands. The number of carbonyl bands relates to the symmetry of the molecule and usually the number of carbonyls at the metal centre.

The solid state IR spectra were recorded using a KBr disk. The carbonyl region of this spectrum is shown in **Figure 4.2**. Four main bands were seen at 2090, 2001, 1984 and 1942  $\text{cm}^{-1}$  and a small shoulder was seen at 1897  $\text{cm}^{-1}$ . The four main bands correspond to the  $A_1^a$ ,  $B_1$ ,  $A_1^b$  and  $B_2$  IR vibrational modes respectively. This is relatively consistent with the solid state literature values (2095, 2007, 1990, 1932, and 1912  $\text{cm}^{-1}$ )<sup>73</sup>.

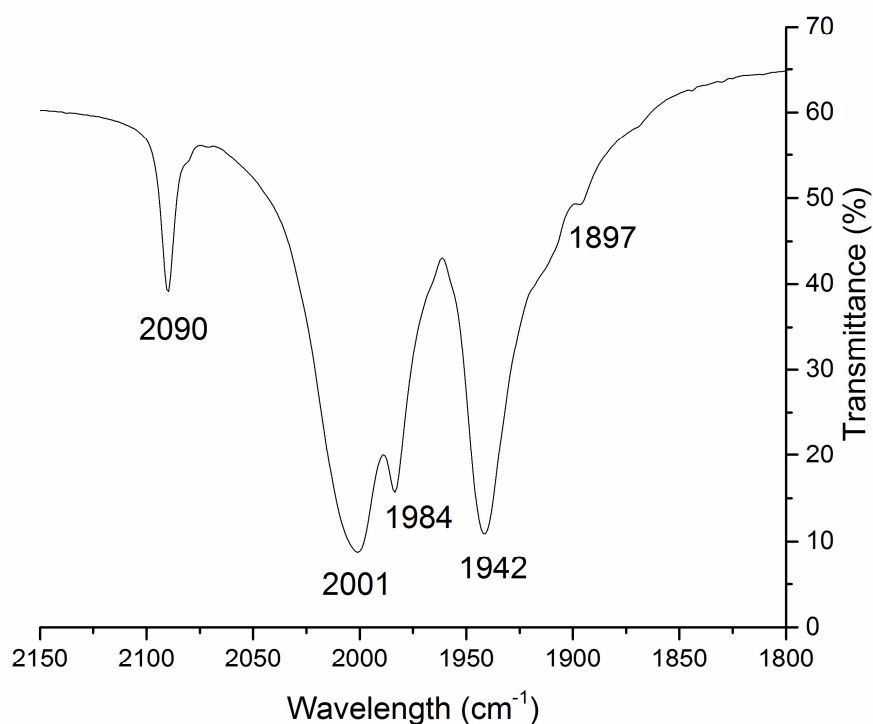


**Figure 4.2:** IR spectra of pyo-CORM as a KBr disk

In a chloroform solution of pyo-CORM four distinct bands were observed at 2092, 2015, 1987 and 1943  $\text{cm}^{-1}$  (**Figure 4.3A**), again this was similar to the literature despite a different solvent being used (2098, 2026, 1990 and 1937  $\text{cm}^{-1}$  in dichloroethane)<sup>73</sup>. The solid and solution phases show a different number of carbonyl bands indicating that there is a change in the symmetry of the two states. In contrast, when pyo-CORM was dissolved in water only two main bands were observed at 2050 and 1943  $\text{cm}^{-1}$  (**Figure 4.3B**).

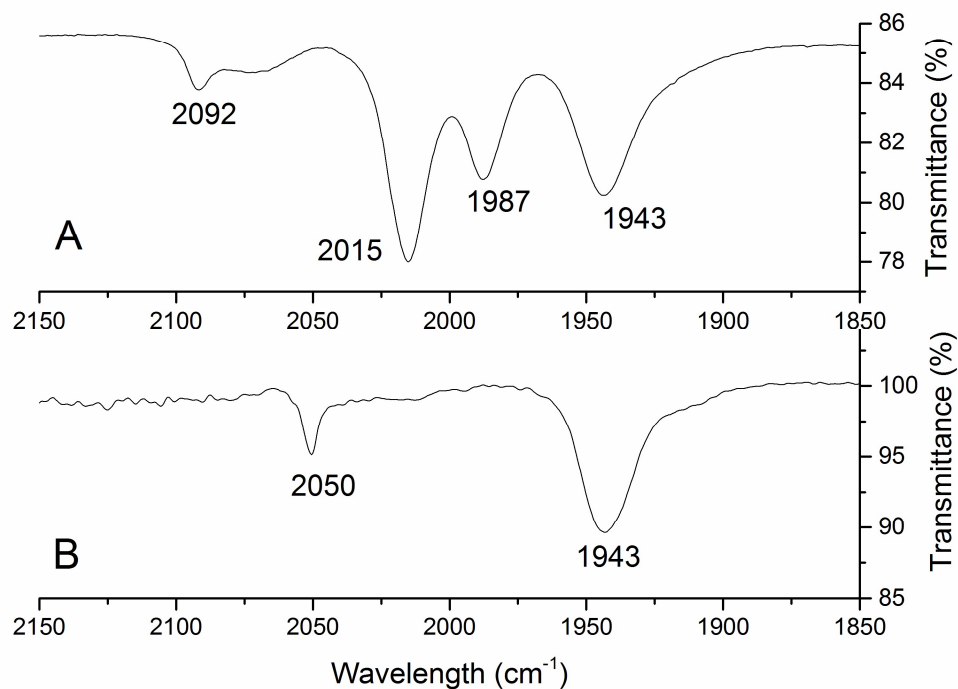


**Figure 4.3:** IR spectra of pyo-CORM in A) chloroform and B) water

In order to show that there is no reaction with water over short periods of time, pyo-CORM was dissolved in water and immediately dried. The resulting solid was then dissolved in chloroform and a solution IR recorded (**Figure 4.4**). This spectrum proved to be practically identical to the spectrum recorded following direct dissolution in chloroform (**Figure 4.3A**). Therefore the observation of only two IR bands in a pyo-CORM spectrum in water simply reflects a change in molecular symmetry, and is not evidence of loss of CO immediately following aqueous dissolution.

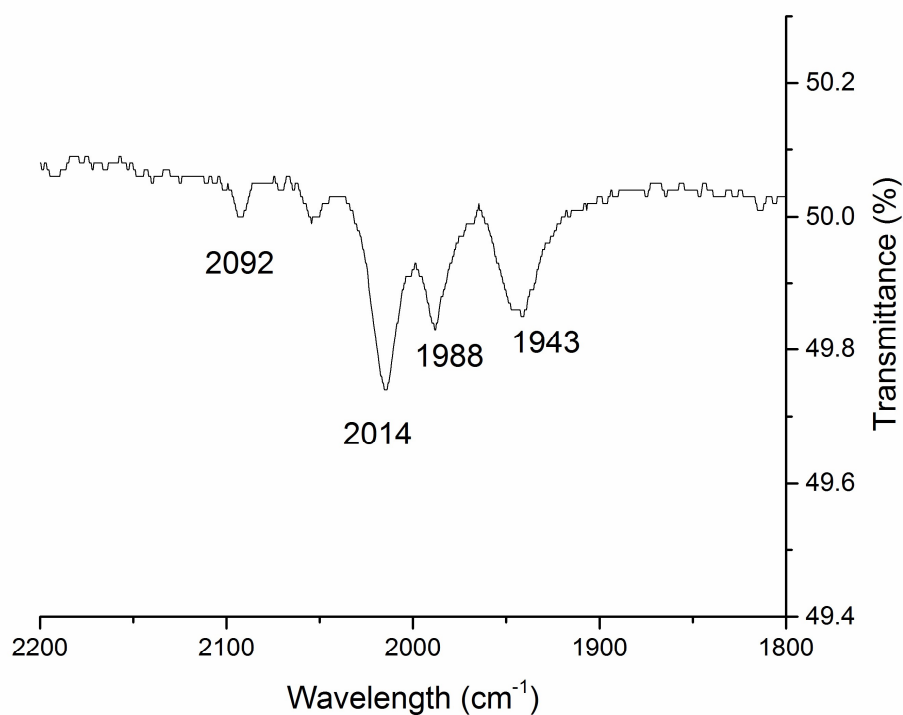


**Figure 4.4:** IR spectra of pyo-CORM in chloroform after being dissolved in water

Compound stability is an important factor for a potentially therapeutic molecule. If decomposition occurs upon storage then its effectiveness can be reduced, meaning that the treatment could be ineffective. The stability of pyo-CORM in the solid state was confirmed by heating a sample of solid pyo-CORM to 50 °C and running ATR IR spectra at 1 hour intervals. **Figure 4.5** shows the carbonyl region of the spectra for this stability test. The spectra indicates that there is very little difference in the carbonyl bands observed so we can conclude that pyo-CORM is stable to air when in the solid state as reported<sup>73</sup>.

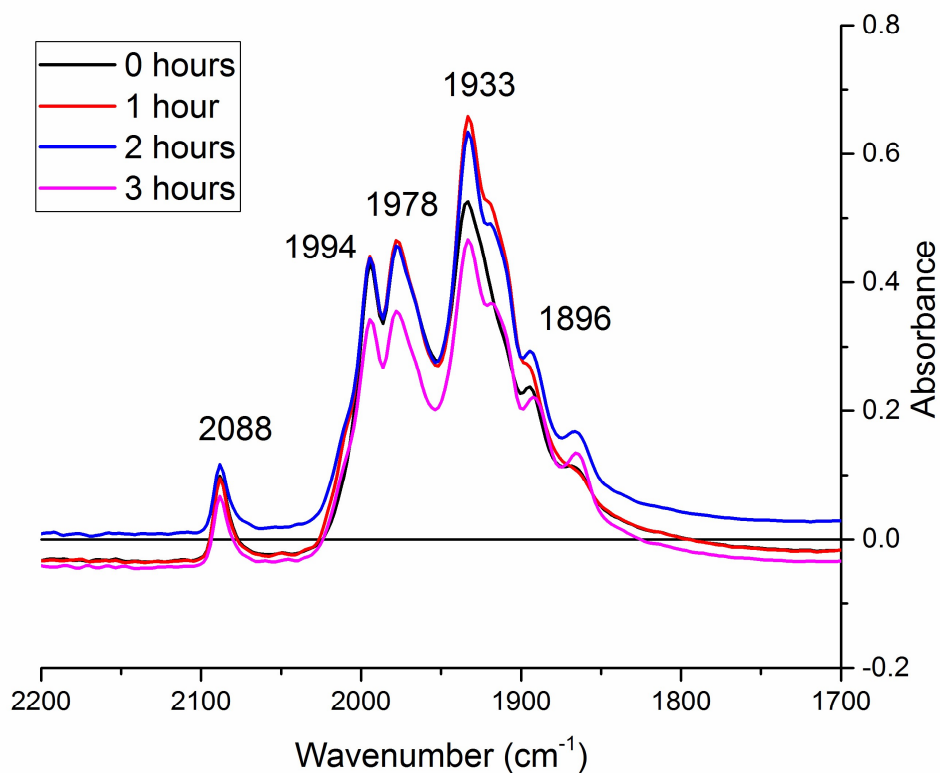


**Figure 4.5:** IR spectra of pyo-CORM upon heating to 50 °C

The stability of pyo-CORM as a 10 mM solution in chloroform and stored in air was also tested. Solution IR of the carbonyl region showed no difference between the spectra run directly after dissolution and after one hour (**Figure 4.6**); indicating chloroform is a good solvent for use in further reactions.

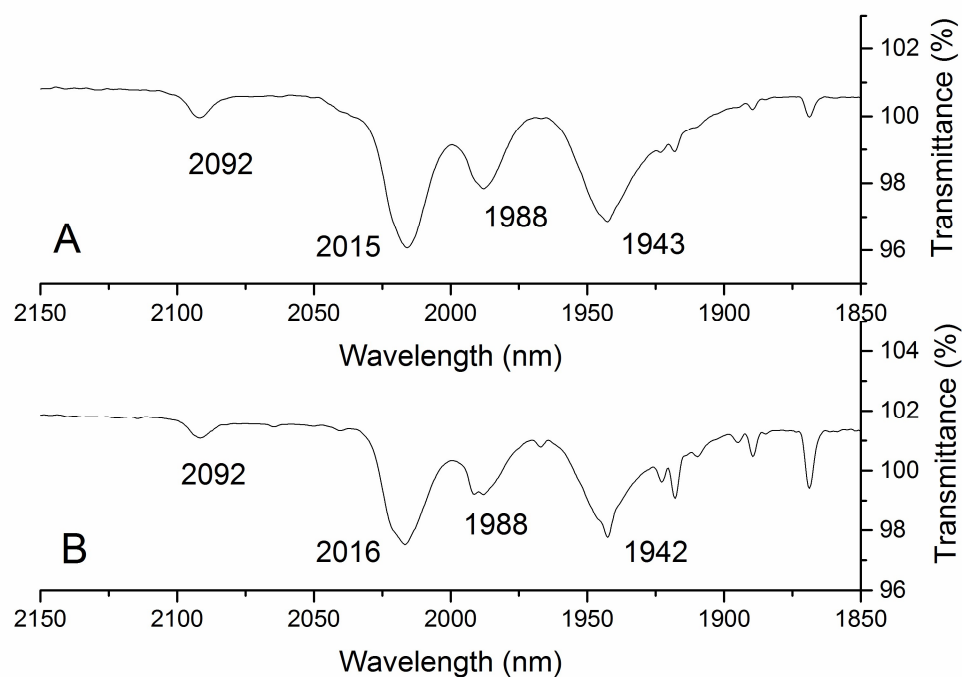


**Figure 4.6:** IR spectra of pyo-CORM in chloroform A) after being in solution for 1 min and B) after being in solution for 60 min

#### 4.2.2 Electrochemistry

A cyclic voltammetry experiment was carried out on a 2 mM solution of pyo-CORM in PBS solution to determine if there was a reduction potential that could be contributing to the reactivity with pyocyanin. However, no reversible redox event was seen when scanned across the wide range from 0 to 2 V vs Ref (about 0.2 to 2.2 V vs SHE). Therefore pyo-CORM appears to be redox-inactive, making it is unlikely that the reaction with pyocyanin described in **Chapter 3** is an electrochemically driven reaction.

#### 4.3 Reactions of pyo-CORM with pyocyanin

The reactions of pyo-CORM with pyocyanin were monitored further through UV/vis spectroscopy, solution IR spectroscopy and mass spectrometry. The methods of UV/vis and IR spectroscopy are particularly complementary since UV/vis provides a

clear indication of changes to the pyocyanin structure (see **Chapter 2**), while IR spectroscopy shows changes to the carbonyl ligands of pyo-CORM.

As described in **Chapter 1**, a myoglobin assay<sup>78</sup> is most commonly used to quantify the amount of CO released by a CO-RM, using a protocol that requires the use of an excess of sodium dithionite to reduce oxymyoglobin to deoxymyoglobin. Since sodium dithionite will reduce pyocyanin (**Chapters 2 and 3**), this method cannot be used here, and therefore a headspace analysis is developed.

#### 4.3.1 UV/vis Concentration studies

UV/vis spectroscopy was used to determine which ratio of pyo-CORM to pyocyanin gives the fastest reaction in PBS. **Table 4.1** summarises all the different concentrations used and the ratio of pyo-CORM to pyocyanin.

Experiment	Pyo-CORM conc ( $\mu\text{M}$ )	PYO conc ( $\mu\text{M}$ )	Ratio pyo-CORM:PYO	$k_{\text{obs}} \text{ s}^{-1}$
A	24	24	1	$0.077 \pm 0.004$
B	24	36	0.67	$0.080 \pm 0.001$
C	24	48	0.5	$0.087 \pm 0.001$
D	24	60	0.4	$0.116 \pm 0.006$
E	48	12	4	$0.077 \pm 0.003$
F	48	24	2	$0.082 \pm 0.002$
G	48	36	1.33	$0.094 \pm 0.005$
H	48	48	1	$0.093 \pm 0.002$
I	48	60	0.8	$0.123 \pm 0.009$
J	48	72	0.67	$0.094 \pm 0.019$
K	24	24	1	$0.112 \pm 0.004$
L	48	24	2	$0.134 \pm 0.005$
M	72	24	3	$0.110 \pm 0.003$
N	96	24	4	$0.123 \pm 0.002$
O	120	24	5	$0.244 \pm 0.011$
P	144	24	6	$0.306 \pm 0.062$
Q	24	24	1	$0.095 \pm 0.004$
R	48	24	2	$0.101 \pm 0.003$
S	72	24	3	$0.117 \pm 0.002$
T	96	24	4	$0.158 \pm 0.007$

**Table 4.1:** Table showing pyo-CORM and PYO concentrations, ratios and observed rate constant

Because varying the concentration of pyocyanin in solution changes the intensity of the absorbance peaks, it is impossible to compare the rates of reaction by just analysing the change in absorbance. Instead, the percentage change in the peak intensity after a fixed amount of time can be quantified in order to make the data comparable. Pyocyanin absorbance at two different wavelengths was analysed; the sharp peak in the UV region at 312 nm, and the broad peak in the visible region centred around 692 nm. These results are shown in **Figure 4.7**.

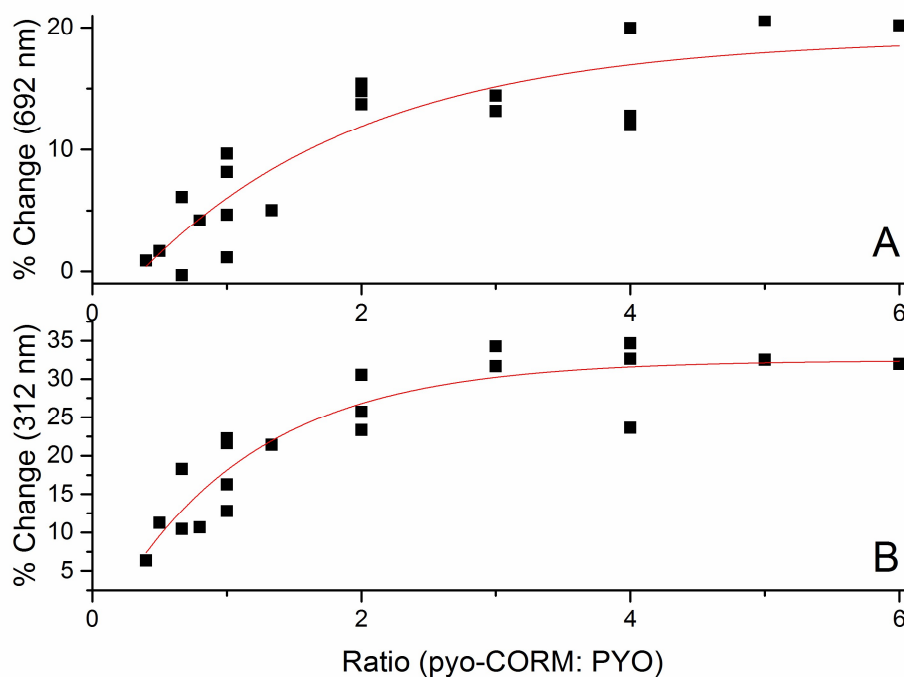


**Figure 4.7:** Percentage change in the absorbance with an exponential growth fit at A) 692 nm ( $R^2=0.786$ ) and B) 312 nm ( $R^2=0.829$ ) for the reaction of pyo-CORM and pyocyanin after 36 minutes

At higher concentrations of pyocyanin a larger change in the absorbance was seen, however at high concentrations the spectrometer becomes less accurate so the results need to be considered carefully, as when the absorbance is above 1.0 the Beer-Lambert law is no longer obeyed, and this is particularly relevant for experiment J as it had a very high pyocyanin concentration. Both **Figure 4.7A** and **B** show exponential growth curves for the percentage change in absorbance. Following the peak at 312 nm gave the better fit as the peak is sharp, whereas 692 nm is at the top of a very broad peak. This data shows that above a 3:1 ratio of pyo-CORM to pyocyanin the increase in the percentage change is only very small, so it can be assumed that the reaction has reached completion over the time period observed.

The data obtained in these experiments was also used to examine the rate of reaction. Following the absorbance at 312 nm, data points were recorded every 4

mins between 0 and 24 mins, then corrected to the final absorbance at 36 minutes. Zero, first and second order rate graphs were plotted for experiment H, a 1:1 ratio (**Figure 4.8**). The data shows a linear fit to first order kinetics, the natural logarithm of the absorbance is a straight line with the equation  $y = -0.092x - 1.748$  and an  $R^2$  of 0.997.

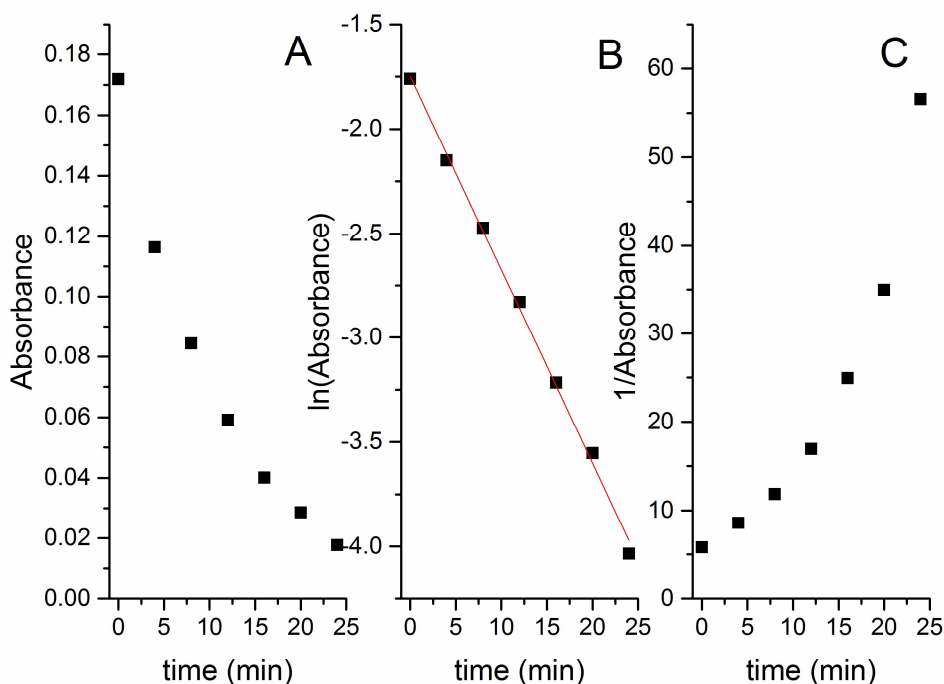


**Figure 4.8:** A) Zero, B) First and C) Second order rate plots for the corrected absorbance at 312 nm over 24 minutes for experiment H, 1:1 ratio

The change in absorbance was extracted and corrected in the same way for all the reactions, and the first order rate equation found for each. However **Table 4.1** and **Figure 4.9** shows that when the concentration of either pyocyanin or pyo-CORM is doubled there isn't the corresponding doubling of the observed rate constant expected for a true first order reaction. In fact, there is such a small change in rate that below a 5:1 ratio that they can be assumed to be the same. This means that the relative amounts of pyocyanin and pyo-CORM have very little impact on the overall rate of reaction, however, when the concentration of one of the reactants is significantly greater than the other it starts to have an effect.

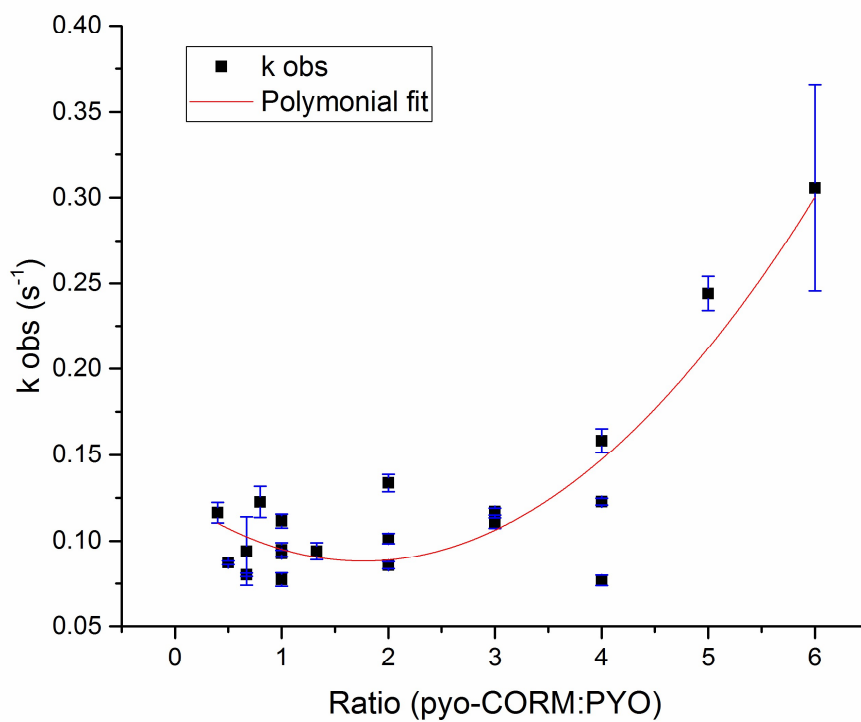


**Figure 4.9:**  $k_{\text{obs}}$  for all ratios of pyo-CORM to pyocyanin with a non-weighted polynomial fit

### 4.3.2 IR Analysis

Infrared spectroscopy was used to follow the changes in carbonyl bands during the reaction. The number of carbonyl bands can be used to determine the number of CO ligands at a metal centre. A reduction in the number of carbonyl bands is to be expected following the loss of CO.

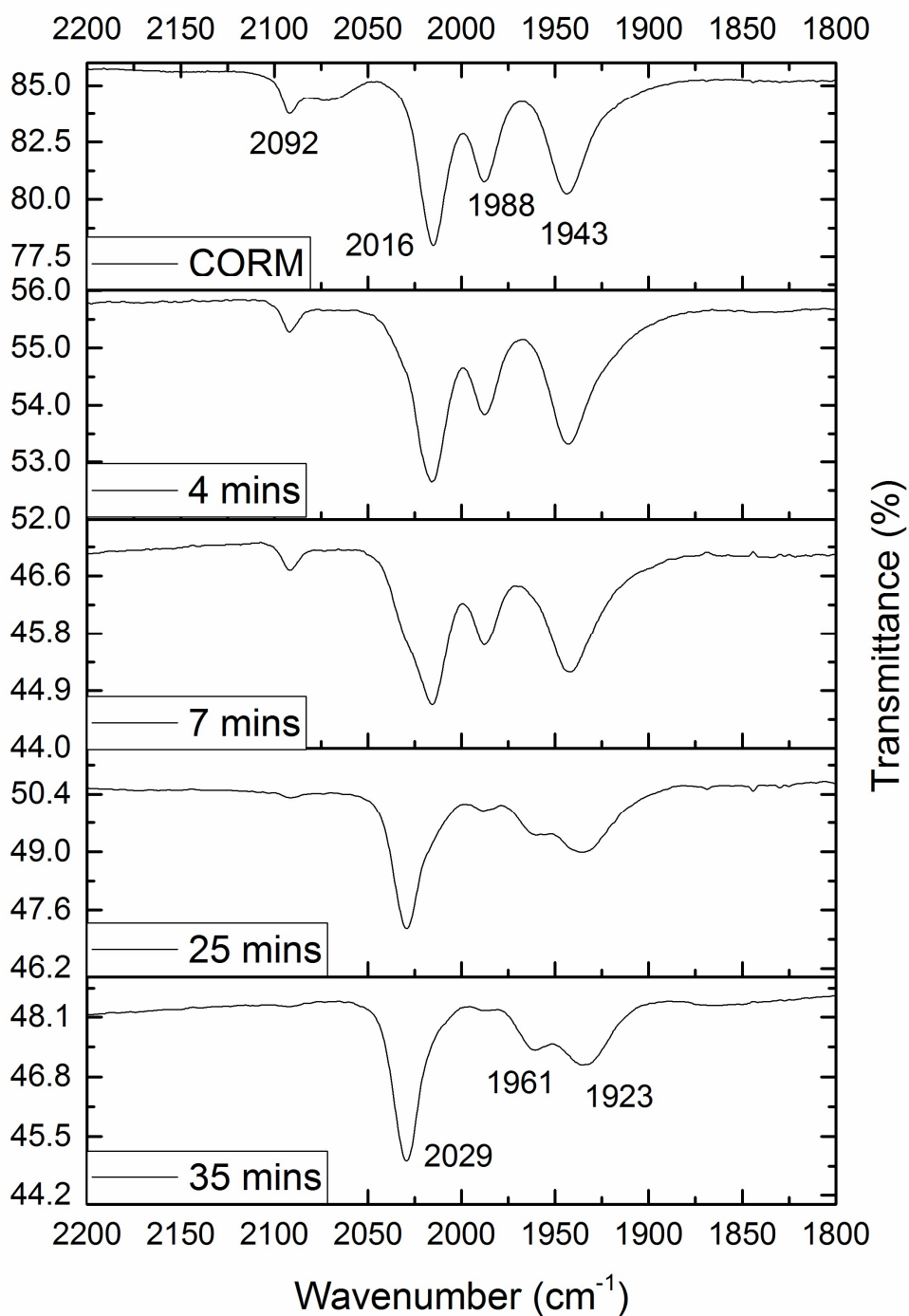


**Figure 4.10:** IR spectra of the reaction of 5 mM of pyo-CORM and 2.5 mM of pyocyanin over 35 mins

The reaction of pyo-CORM and pyocyanin shows the gradual loss of the IR band at 2092  $\text{cm}^{-1}$  (Figure 4.10). The complete loss of this band is an indicator that the

reaction has reached completion. The other three bands only shift position slightly but the intensities change. As only one band is lost it indicates that the system changes from the *cis* four carbonyl system to a *mer* three carbonyl one, a *fac* geometry would show only two carbonyl bands due to degeneracy<sup>77</sup>.

### 4.3.3 Mass Spectrometry

An ESI-MS of the final product from the reaction of pyo-CORM and pyocyanin was recorded. In the positive mode, only the tetraethyl ammonium ion from pyo-CORM was observed. However when negative mode ESI was recorded a number of peaks were seen. These all showed the characteristic bromide isotope pattern, indicating one of the bromine atoms was still ligated to the manganese centre. The masses at 412.89 and 414.89  $m/z$  are consistent with the formation of the compound seen in **Figure 4.11**.

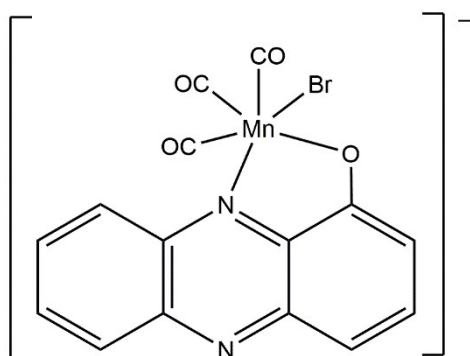


**Figure 4.11:** Product of pyo-CORM and pyocyanin

This is an unexpected compound due to the fact that the pyocyanin appears to have lost its N-methyl group. A search of the literature gave a possible mechanism for this<sup>79,80</sup>. Stone and Vukomanovic stated that when the metal centre interacts with the zwitterionic form of pyocyanin it removes electron density from the methyl nitrogen. The methyl can then be lost as a radical. The bonds between the manganese and the nitrogen and oxygen are then strengthened by the extra charge that becomes delocalised across the structure. An NMR study to confirm this structure was inconclusive as the paramagnetic properties of the central manganese makes basic NMR impossible to interoperate.

## 4.4 Analogues

The use of chemical analogues is a good way of probing the mechanism of a reaction. Using molecules with only one of the properties of a reactant can provide insight into how compounds interact with each other.

### 4.4.1 Pyo-CORM analogue

The structure of pyo-CORM means that the bromide ligands are labile and could be driving the reaction. The loss of a halide ligand occurs in compounds with the structure  $[MX(CO)_5]^-$  and could also occur in pyo-CORM<sup>67</sup>. There is a possibility that the changes observed in the pyocyanin UV/vis spectra during the reaction are due to the direct action of these bromide ions with pyocyanin rather than a direct interaction with the metal. Tetraethyl ammonium bromide (TEAB), was used as a bromide source to probe this possible mechanism of action.

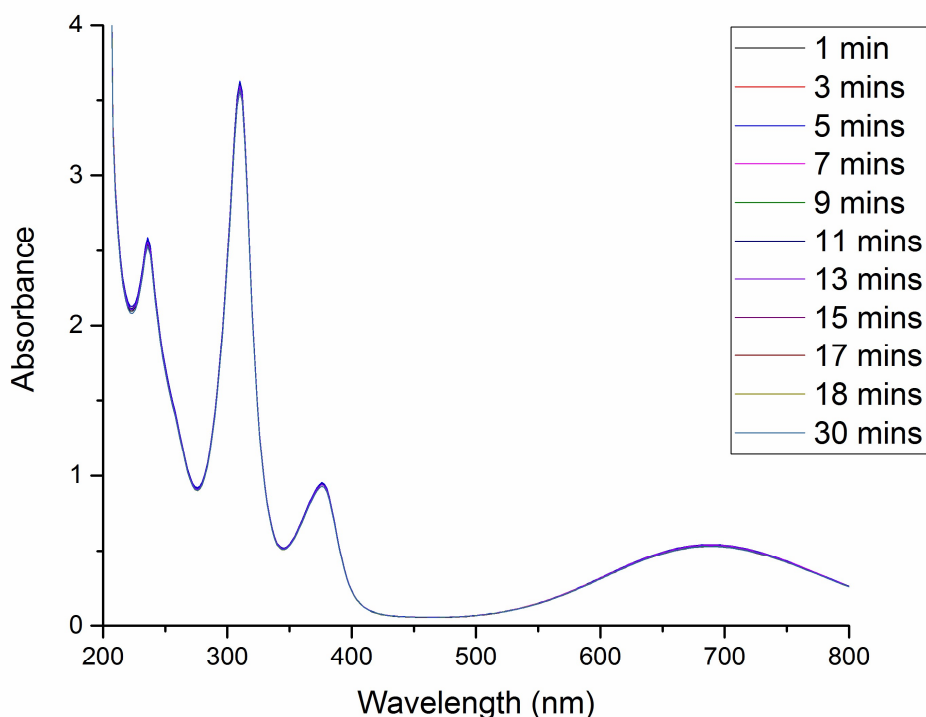


**Figure 4.12:** UV/vis spectra over 30 minutes of 24  $\mu\text{M}$  pyocyanin and 48  $\mu\text{M}$  tetraethyl ammonium bromide in DI water

Over 30 minutes no change was observed in the UV/vis spectra of pyocyanin and TEAB meaning that no reaction occurred (**Figure 4.12**). The colour of the solution also remained constant for three hours. Therefore it was determined that there was no reaction with free bromide and hence no reaction with the labile bromide ligands from pyo-CORM therefore a different mechanism was taking place.

#### 4.4.2 Pyocyanin analogues

##### 4.4.2.1 2-keto-N-methyl phenazine, 'Pink fraction'

During the synthesis of pyocyanin, a red/pink fraction was eluted just prior to pyocyanin, this is believed to be 2-keto-N-methyl phenazine<sup>81</sup> (2KMP, **Figure 4.13**), also known as N-methyl- $\beta$ -oxyphenazine. When analysed by ESI mass spectrometry the major peak was at 211.0829  $m/z$  the same mass seen for pyocyanin (this is one

mass unit above the expected mass indicating that the compound is protonated during analysis). 2KMP can be considered an electrical analogue because it has a reduction potential of  $-0.17$  V vs Ref at pH 6<sup>82</sup> which is similar to that of pyocyanin which is quoted as  $-0.045$  V vs Ref in the same paper (reference electrode unknown). The reduction also causes a colour change from red/pink to light yellow or colourless.

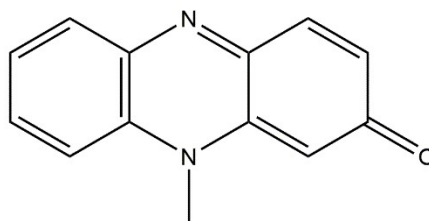


**Figure 4.13:** 2-keto-N-methyl phenazine

The UV/vis spectrum of 2KMP in **Figure 4.14** was similar to that of pyocyanin but with the peak in the visible region at 520 nm rather than 698 nm, as expected for the colour difference. The similarity of the UV/vis spectra to that of pyocyanin confirms that it is a closely related compound. The extinction coefficient at 518 nm is  $8130 \pm 60$  M<sup>-1</sup> cm<sup>-1</sup>.

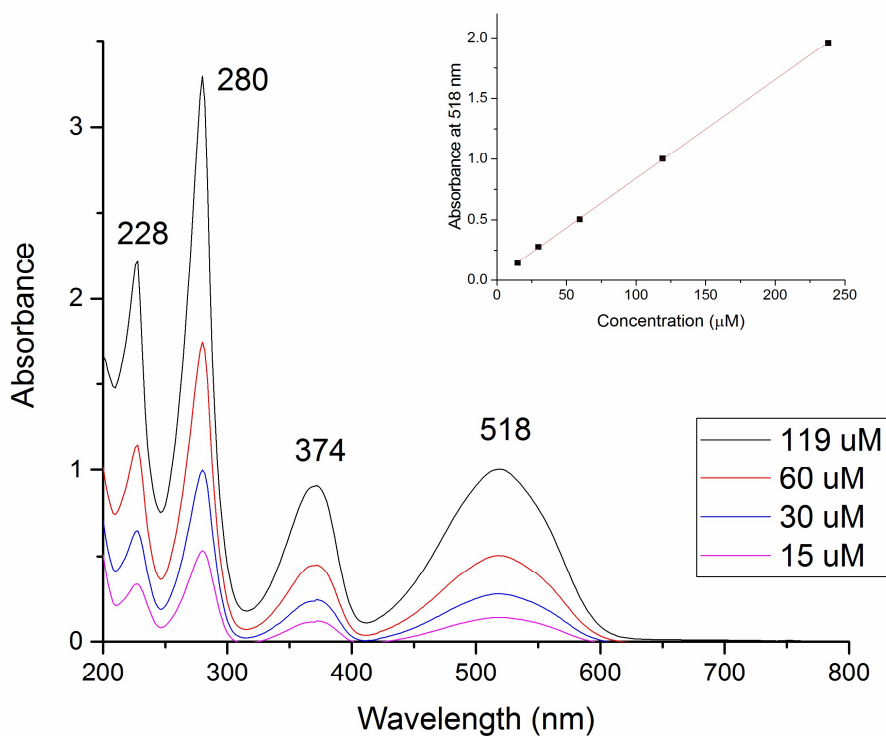


**Figure 4.14:** UV/vis absorbance spectra of pyocyanin synthesis pink fraction (2-keto-N-methyl phenazine) at different the concentrations indicated and the molar extinction plot

The reaction of 2KMP with pyo-CORM was monitored by infrared spectroscopy. The carbonyl region of the IR spectra is shown in **Figure 4.15**, with the two carbonyl bands as seen previously for pyo-CORM in water (**Figure 4.3B**). After 40 minutes there was no change in the carbonyl bands indicating that pyo-CORM has not lost any CO. Therefore, the electrochemical properties of 2-KMP, and by extension pyocyanin, are having no effect on the reactivity of pyo-CORM.

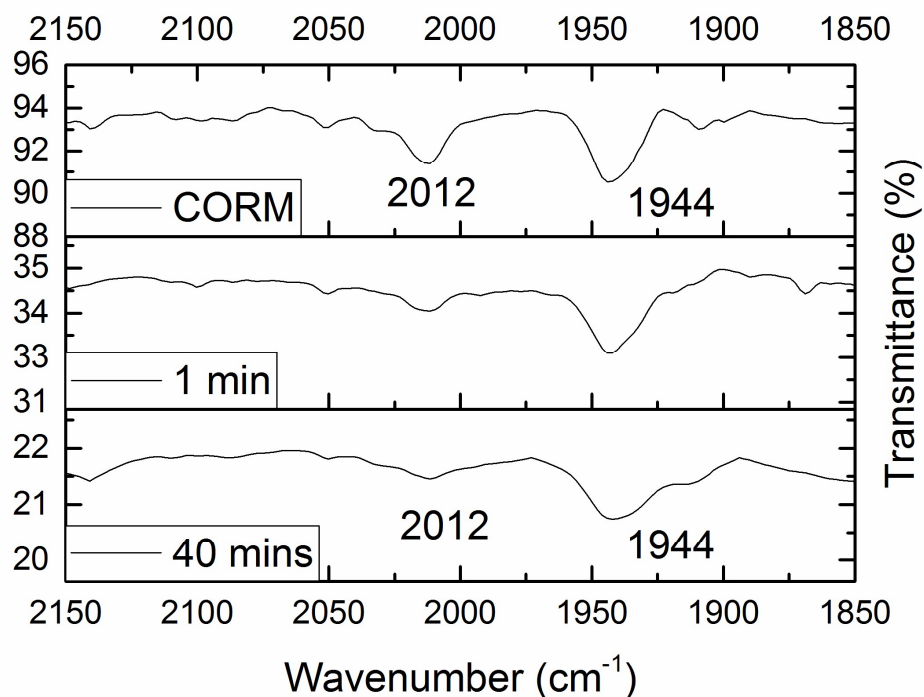


**Figure 4.15:** IR spectra of CO region for pyo-CORM and pyo-CORM with 2-keto-N-methyl phenazine over time in DI water

#### 4.4.2.2 8-hydroxyquinoline

8-hydroxyquinoline (8-HOQ, **Figure 4.16**) is a small heterocyclic molecule that has some antiseptic properties<sup>83</sup> attributed to its ability to chelate to metal ions. This was chosen as a suitable analogue for pyocyanin as the oxygen and nitrogen atoms are in the same positions and are also constrained. Another advantage as an analogue is purely a structural analogue as it has no known electrochemical properties.

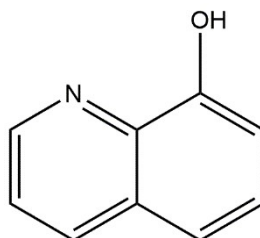


**Figure 4.16:** 8-hydroxyquinoline

IR spectroscopy was used to follow the reaction of pyo-CORM and 8-HOQ as neither compound has a very distinctive UV/vis spectra, making it difficult to follow with UV/vis spectroscopy. The reactions were carried out in chloroform because 8-HOQ is insoluble in water.

A stoichiometric mixture of pyo-CORM and 8-HOQ was reacted for 20 minutes in chloroform, and an IR spectrum recorded after this time (**Figure 4.17**). This spectrum shows significant changes when compared to the spectrum for pyo-CORM only. The change from four to three bands is indicative of the loss of a single carbonyl group; this is consistent with the loss seen with the reaction of pyo-CORM with pyocyanin (**Figure 4.10**).

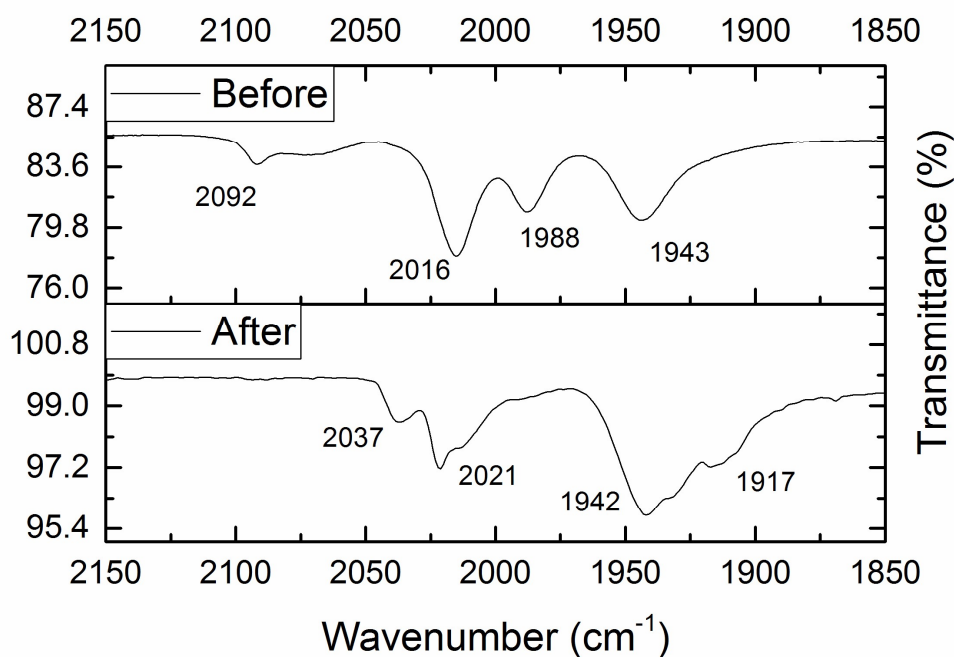


**Figure 4.17:** IR spectra of 8 mM of pyo-CORM before the addition of 8 mM of 8-HOQ and after 20 mins reaction.

The resulting solid from this reaction, obtained by removing the solvent under vacuum, was analysed by negative mode ESI mass spectrometry and this confirmed that 8-HOQ was binding to the manganese from pyo-CORM. The main peaks were at 363.88 and 361.9  $m/z$ , the isotope pattern confirms that there is still a bromine

in the molecule. The mass is consistent with the compound in **Figure 4.18**, which has a similar structure to the product of the reaction of pyo-CORM and pyocyanin (**Figure 4.11**). Other peaks in the mass spectra at 279.90 and 277.90  $m/z$  show the same compound with the loss of all CO ligands. These could have been lost during the analytical process. This product has three carbonyl ligands so is consistent with the three main bands seen in the IR spectra.

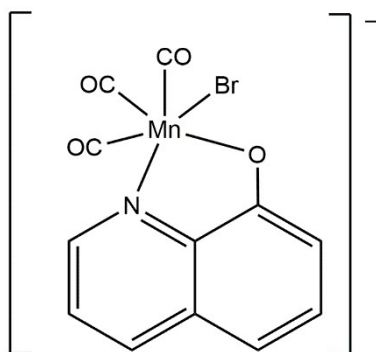


**Figure 4.18:** Product of pyo-CORM and 8-HOQ

#### 4.5 Aqueous IR reactions

Water activation is a possible mechanism for the release of CO from pyo-CORM. The CO-releasing properties of pyo-CORM were therefore tested in water both with and without pyocyanin. A water activated mechanism is seen in previous studies of  $[MX(CO)_5]^-$  species where water causes the loss of a halide and a dimer species is formed<sup>67</sup>.

The reaction of pyo-CORM with pyocyanin in water was monitored by IR spectroscopy for 30 mins (**Figure 4.19**). This showed an increase in the intensity of the band around  $2040\text{ cm}^{-1}$  and the growth of a band at  $1974\text{ cm}^{-1}$ . Although it is difficult to determine how many carbonyls the product of this reaction has due to the compression of the three bands between  $2016$  and  $1943\text{ cm}^{-1}$  in water, there is a change in the bands in this region, it can be assumed that some reaction is taking place.

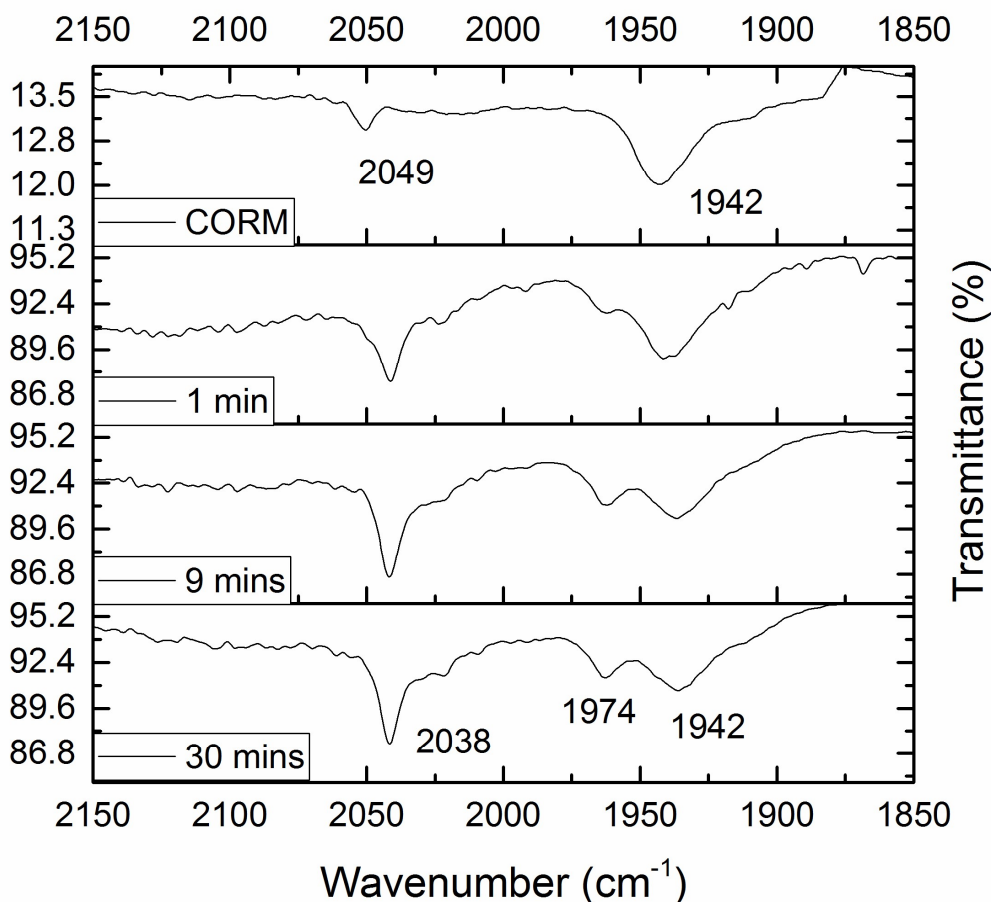


**Figure 4.19:** IR spectra of 10 mM of pyo-CORM and 5 mM of pyocyanin in DI water.

As shown in **Figure 4.4**, pyo-CORM is stable over short time periods in water. At longer time periods, however, a loss of carbonyl groups is observed between 60 and 90 minutes and no bands are observed in the carbonyl region of the spectrum (**Figure 4.20B**). This indicates that after an hour no metal carbonyl bands are observed consistent with the loss of all CO. This breakdown of pyo-CORM in water means that a secondary mechanism of pyo-CORM activation must also be taking place.

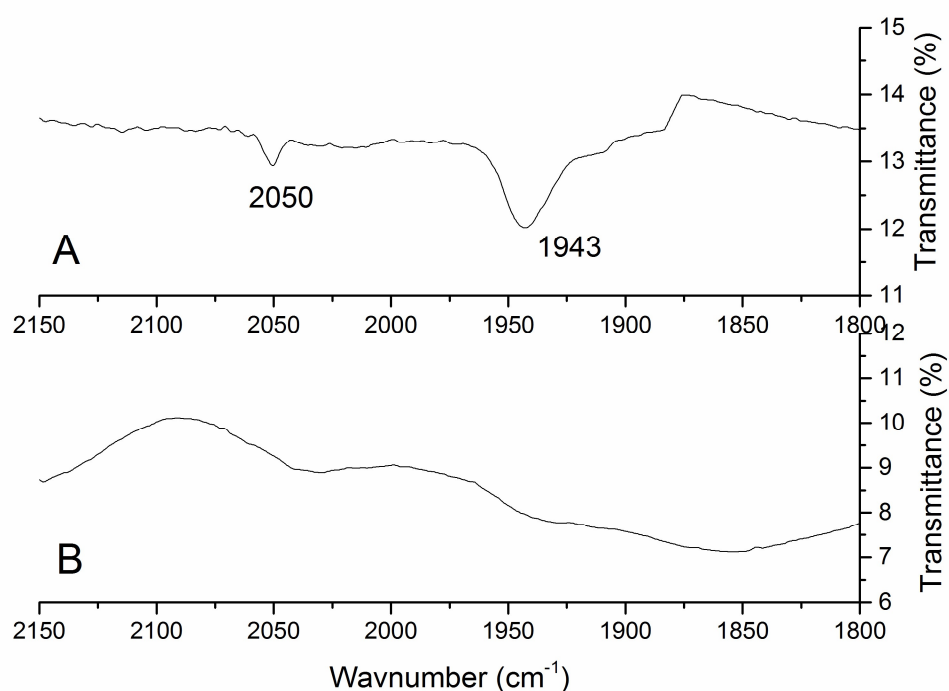


**Figure 4.20:** IR spectra of pyo-CORM only in DI water after A) 1 min and B) 90 mins.

#### 4.6 Evolved gas measurements

As the reaction of pyo-CORM and pyocyanin cannot be measured using the myoglobin assay a different method of detecting CO release was required. In an attempt to monitor the production of gas evolved from pyo-CORM the reaction mixture was attached to the closed vacuum line under vacuum, and the change in pressure on the line was recorded over time. The gas in the headspace of the flask increased the pressure in the line to over 1000 mbar, meaning that only very large changes in pressure could be observed. Therefore the flask was opened to vacuum till the pressure read 2 mbar. However, the amount of gas removed from the headspace varied for different reactions, making the results unquantifiable.

When using chlorobenzene as a solvent, because chloroform evaporates at the low pressure of the experiment, the chlorobenzene only control showed a steady decrease in pressure over a one hour time period (**Figure 4.21**). This trend was

reflected for pyo-CORM in chlorobenzene only. However, once a small amount of water was added, an increase in pressure was seen, indicating the release of gas.

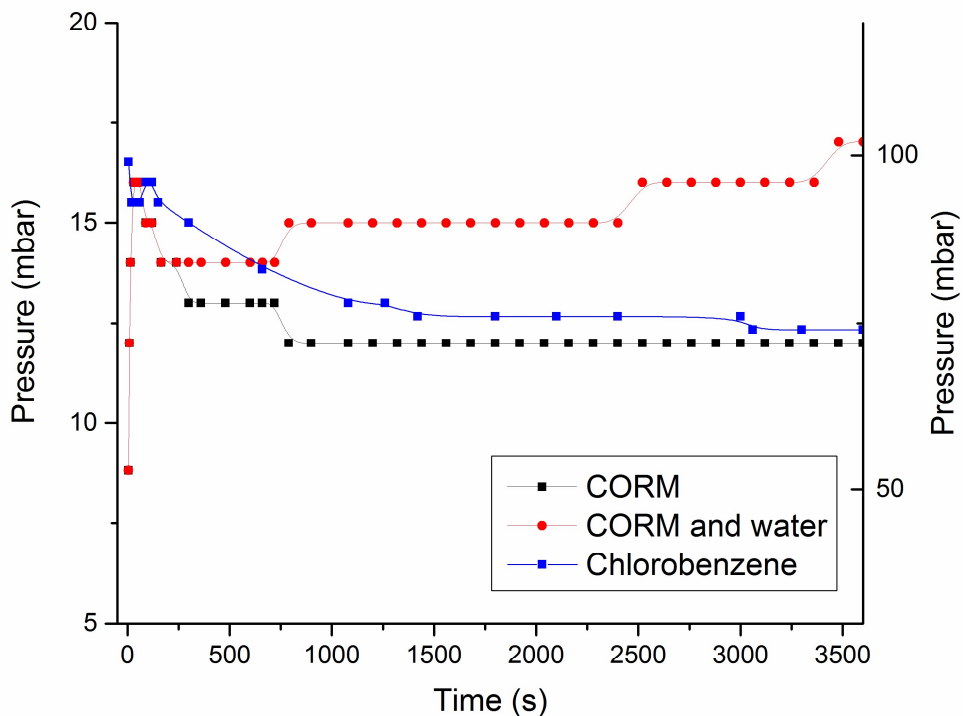


**Figure 4.21:** Change in pressure in the headspace of a flask containing pyo-CORM in chlorobenzene, pyo-CORM in chlorobenzene with water and chlorobenzene only (secondary axis).

When water only was put under the same conditions the pressure increased slowly over time, this could be due to small leaks in the system (**Figure 4.22**). The pressure increased significantly for the reaction of pyo-CORM with water, there was an initial fast increase in pressure followed by a levelling off after 1 minute. This shows that the largest amount of gas is given off soon after pyo-CORM is dissolved in water but continues for a time afterwards. The increase in pressure associated with the remaining headspace increases the pressure significantly between 0 and 5 seconds but has no impact after this.

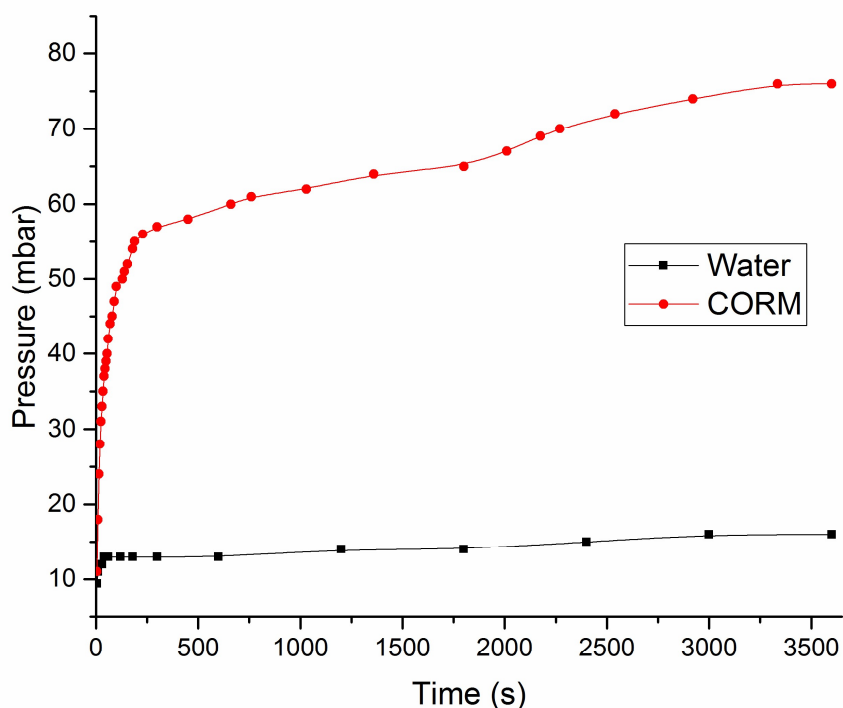


**Figure 4.22:** Change in pressure in the headspace of a flask containing only water and pyo-CORM in water.

Although this method shows that more gas is evolved by pyo-CORM when in the presence of water, it is unknown whether this gas is CO or not. So a method of identifying the evolved gas was required.

## 4.7 Gas phase IR

Carbon monoxide has a distinctive gaseous IR signature of a double band, with fine rotational splitting, centred at  $2150\text{ cm}^{-1}$ . Gas phase IR is, therefore, a way of directly observing the CO released from a reaction and the method used was based on a method developed by Klein et al. in 2014<sup>51</sup>. The method used here is not quantitative; however, the relative amount of CO released can be determined through comparison to the carbon dioxide band because this can be assumed to be constant in all cases and is therefore an internal standard.

When pyo-CORM alone was left to stir in chloroform a very small CO band was seen in the spectra (**Figure 4.23A**). However, this reduced significantly when dry DCM was used as the solvent (**Figure 4.23B**). Therefore it can be assumed that pyo-CORM is stable in chlorinated solvents but the residual water is causing the breakdown of a small amount of pyo-CORM and the release of CO. With the addition of a small amount of water to the solution of pyo-CORM in chloroform (**Figure 4.23C**) the amount of CO released increases significantly. All of the pyo-CORM, identified by its yellow colour, transferred from the chloroform layer to the water phase. When pyocyanin and pyo-CORM were reacted in chloroform (**Figure 4.23D**) a significantly higher proportion of CO was released than without pyocyanin. This proves that carbon monoxide released from pyo-CORM can be initiated via a reaction with pyocyanin.

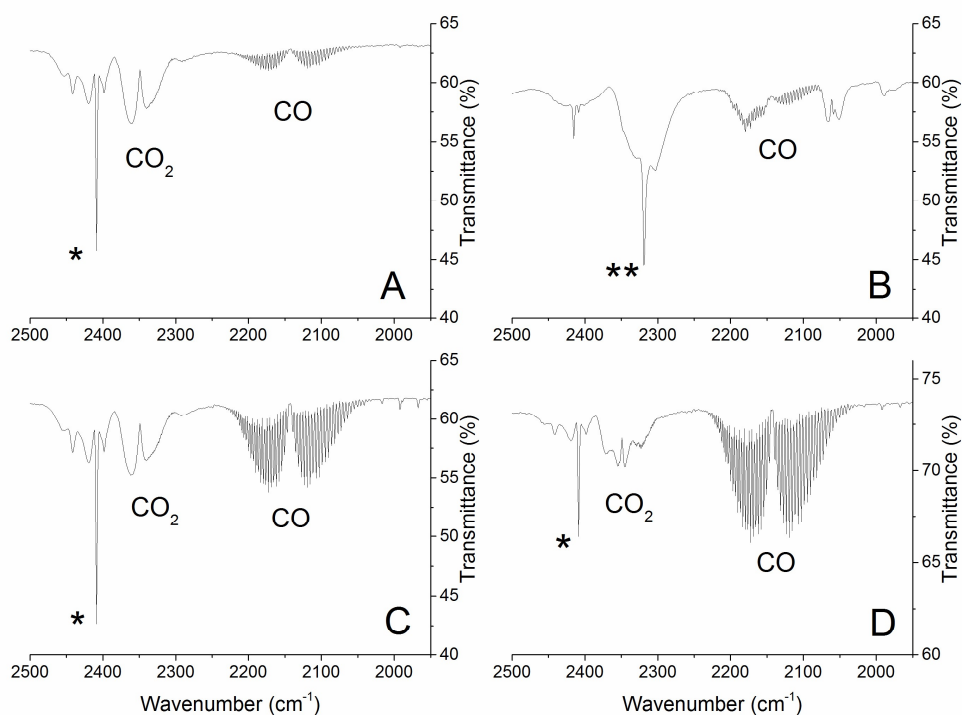


**Figure 4.23:** Gas phase IR spectra of 12 mg of pyo-CORM in 4 mL of chlorinated solvent after 1 hour A) chloroform, B) dry DCM, C) chloroform and 0.5 mL of water, D) chloroform with 12 mg of pyocyanin, \* chloroform band, \*\* DCM band.

In a PBS solution pyo-CORM appeared to evolve a similar amount of CO regardless of the presence of pyocyanin (**Figure 4.24**). Therefore there must be a water

activation mechanism for CO release from pyo-CORM, as we know that bromide (**Figure 4.12**) and probably other salts will not influence the reaction. This could involve the initial loss of a bromide and the dimerization of the metal species and the release of CO<sup>67</sup>, or the complete breakdown of the compound with the dissociation of all of the CO ligands.

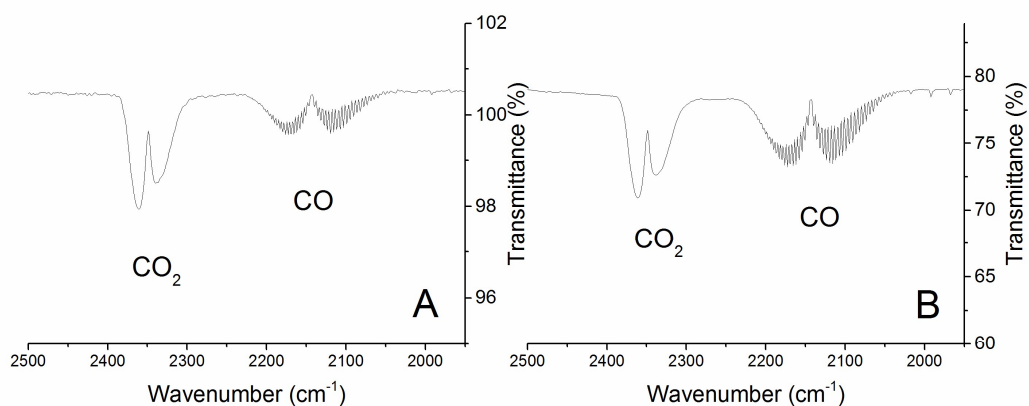


**Figure 4.24:** Gas phase IR spectra after 1 hour of A) 12 mg of Pyo-CORM with 12 mg of pyocyanin in PBS solution and B) 12 mg of pyo-CORM only in PBS solution.

Further to these tests in water, pyo-CORM was dissolved in other relevant aqueous solutions. This was to determine if the rate of activation changed with the solvent. In pure water, the greatest quantity of CO appears to have been released (**Figure 4.25A**). The amount of CO released when pyo-CORM is dissolved in DMSO or 100 vol% LB (**Figure 4.25B** and **C**) seems to be less than when it is dissolved in pure water (**Figure 4.25A**). These solvents have a smaller percentage of water due to the presence of other compounds which could influence the stability of pyo-CORM or indicate that . It is difficult to tell the relative amount of CO released from pyo-CORM in 2 molar salt solution (**Figure 4.25D**) because there was less carbon dioxide in the sample than the background, giving an inverse peak. However, it is likely to also be similar to the amount evolved when in DMSO and 100 vol% LB.

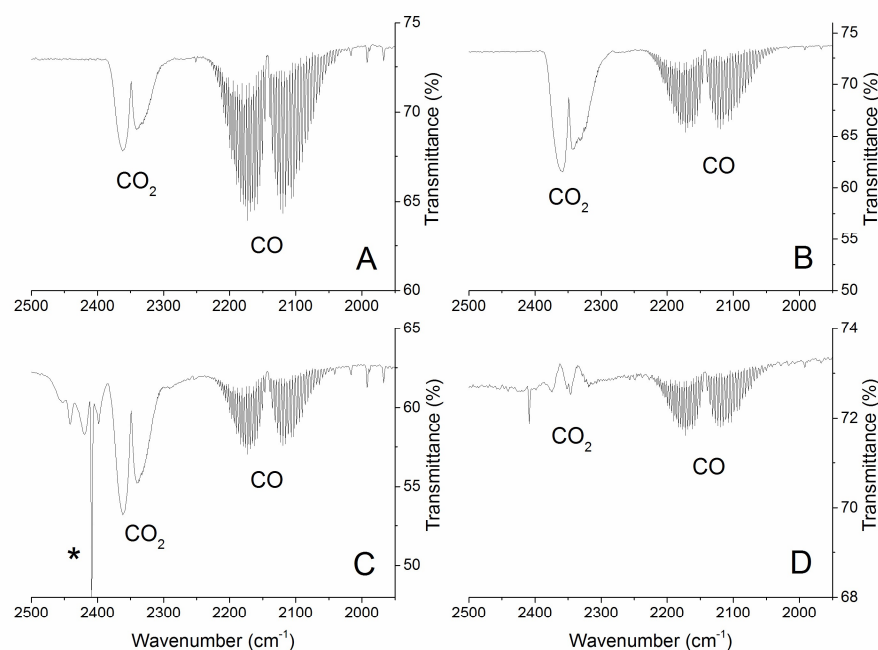


**Figure 4.25:** Gas phase IR spectra of 12 mg of pyo-CORM in 4 mL of aqueous solvent after 1 hour A) water, B) DMSO, C) 100 vol% LB, D) 2 molar NaCl, \*unknown band

## 4.8 Biological testing of pyo-CORM

Biological testing of pyo-CORM was carried out by Karinna Saxby and Dr Lindsey Flanagan in the Department of Biology at the University of York.

Although the mechanism of CO release from pyo-CORM is understood, the antimicrobial properties are still unknown. The affect of pyo-CORM on the growth of bacteria and the formation of biofilms are shown below. The number of bacteria in a sample is estimated using the optical density (OD) of a solution at 600 nm. The bacterial cells scatter the light of this wavelength meaning the higher the cell density the less light reaches the detector and the lower the absorbance value. To determine the biofilm in a culture the crystal violet absorbance is utilised. It uses the absorbance at 590 nm which is proportional to the biomass of the biofilm present<sup>84</sup>.

When *P. aeruginosa* PA01 strain was incubated in a media of 100% LB with varying concentrations of pyo-CORM very little difference was seen in the amount of bacteria present in the media after 24 hours (**Figure 4.26**). However in 10% LB by volume (10 vol%) and M9 glucose minimal media, large changes were observed. The population of bacteria is reduced significantly at high levels of pyo-CORM compared to the control. At lower percentages of LB and in minimal media, the bacteria grow slower as under these conditions fewer nutrients are available. This means that the pyo-CORM can have more of an impact on the number of bacteria in the culture. The restrictive media are closer to the environments the bacteria grow in clinically, as the immune system makes conditions less optimal for growth, and 10 vol% LB media and minimal M9 glucose media were used for subsequent reactions.

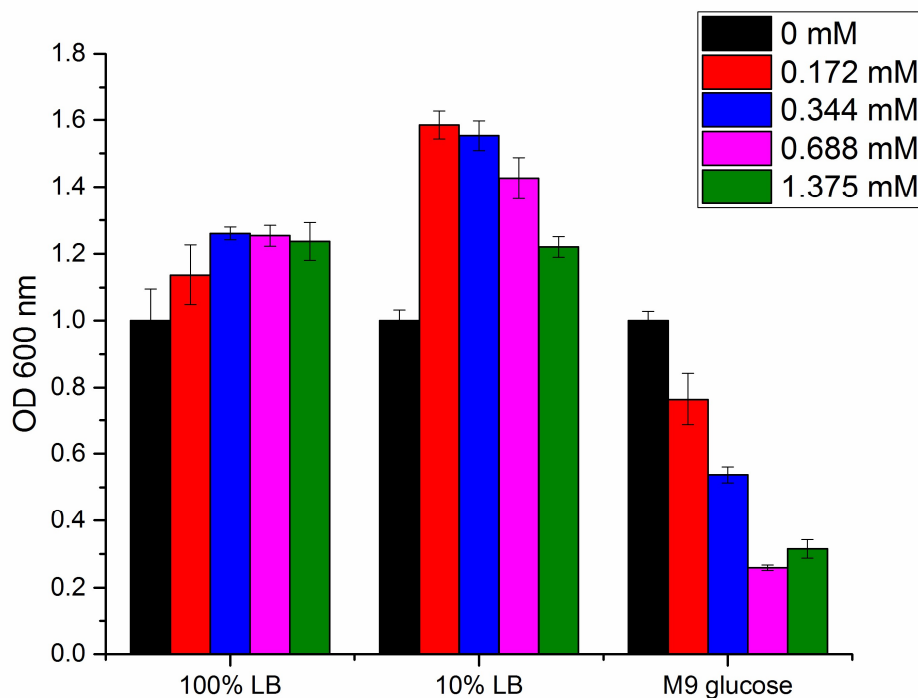


**Figure 4.26:** Corrected optical density at 600 nm of PA01 *P. aeruginosa* strain when grown with different concentrations of pyo-CORM for 24 hours at 37 °C in media as indicated.

The slight increase in bacterial growth at low concentrations of pyo-CORM compared to the control with no pyo-CORM is a known phenomenon for most

antibiotics. This is seen in **Figure 4.26** when comparing the growth of *P. aeruginosa* with 0 and 0.172 mM of pyo-CORM in 10% LB. This is when the antimicrobial compound is at a concentration below the effective dose, known as the sub-inhibitory concentration. The presence of the antimicrobial can cause the bacteria to produce a biofilm or increase its natural response to the compound<sup>85</sup>. When the conditions for growth were limited further by using the minimal media M9 glucose, pyo-CORM showed greater antimicrobial properties (**Figure 4.26**). In M9 glucose media, there is no evidence of the increase in bacterial growth associated with a sub-inhibitory concentration of pyo-CORM.

By following the optical density of the culture every half an hour over a 24 hour period the way pyo-CORM affects the growth of *P. aeruginosa* can be seen clearly (**Figure 4.27**). When no pyo-CORM is present in the media a steady increase in the number of bacteria in solution is observed. With the addition of 0.172 mM and 0.344 mM of pyo-CORM, the concentration of bacteria was steady for a period of time before there was an increase in the number of bacteria by the same amount as without pyo-CORM. This indicates that the antimicrobial effect of pyo-CORM wears off over time. Above a pyo-CORM concentration of 0.688 mM, no increase in the number of bacterial cells was observed, indicating total eradication of all the starting colonies (i.e. sterilisation was achieved).

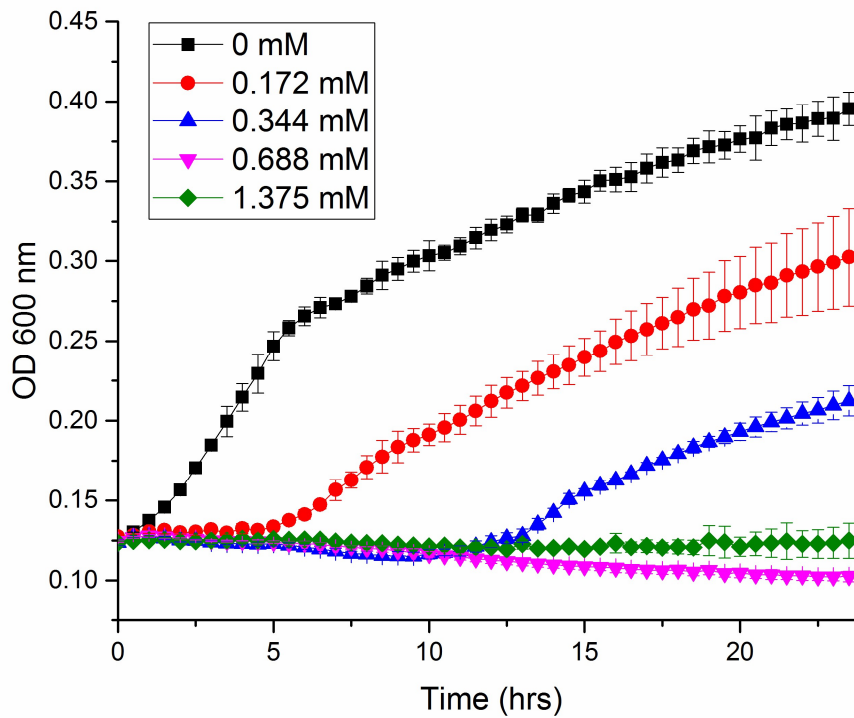


**Figure 4.27:** Optical density measurements at 600 nm of PA01 *P. aeruginosa* strain when grown with different concentrations of pyo-CORM for 24 hours at 37 °C in M9 glucose medium.

The bactericidal activity of pyo-CORM was then tested against a *P. aeruginosa* phenazine knockout strain (PCN), an engineered strain that produces no pyocyanin or other phenazine species. Because phenazines have such a wide range of functions in *P. aeruginosa* PCN doesn't grow at the same rate as the wild-type. Pyo-CORM appears to have a similar activity against both strains of *P. aeruginosa* (Figure 4.28).

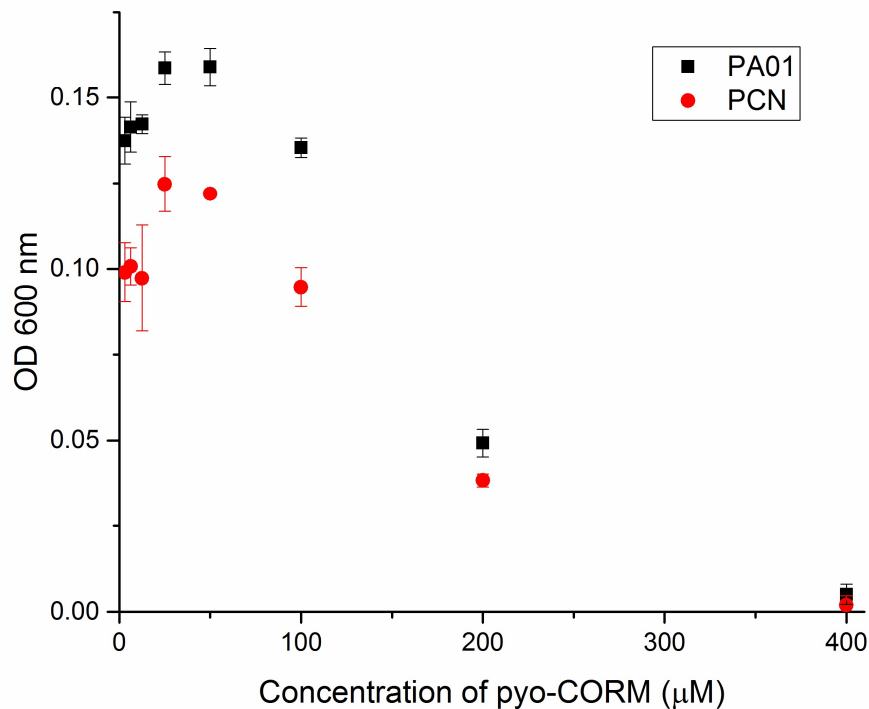


**Figure 4.28:** Optical density at 600 nm of PA01 *P. aeruginosa* strain and a phenazine knockout strain (PCN) when grown with different concentrations of pyo-CORM for 8 hours at 37 °C in 10 vol% LB.

When the lungs become infected with *P. aeruginosa* it is the mucoid phenotype that is the most difficult to remove with antibiotics<sup>19</sup>. The production of a biofilm is one of the reasons for this. Carbon monoxide from CORM-2 has been shown to reduce the production of *P. aeruginosa* biofilm<sup>39</sup> so tests were performed to ascertain if pyo-CORM has the same effect (**Figure 4.29**). The strains of *P. aeruginosa* in this experiment are different lab strains and mutants.

Control experiments without the addition of pyo-CORM all shows a significantly greater amount of biofilm than in the presence of pyo-CORM. The general trend is that at higher concentrations of pyo-CORM there is a reduction in the biomass of biofilm, however, this is not true for all strains. The incubation of pyo-CORM with the *P. aeruginosa* strains at the beginning of growth (**Figure 4.29A**) shows an overall reduction in the biofilm biomass, however, it is not strictly concentration dependant. With the addition of pyo-CORM to an established biofilm a thinning is also observed (**Figure 4.29B**). This is important because a therapeutic molecule is

almost always administered after an infection has reached the mucoid phase where biofilm is present.

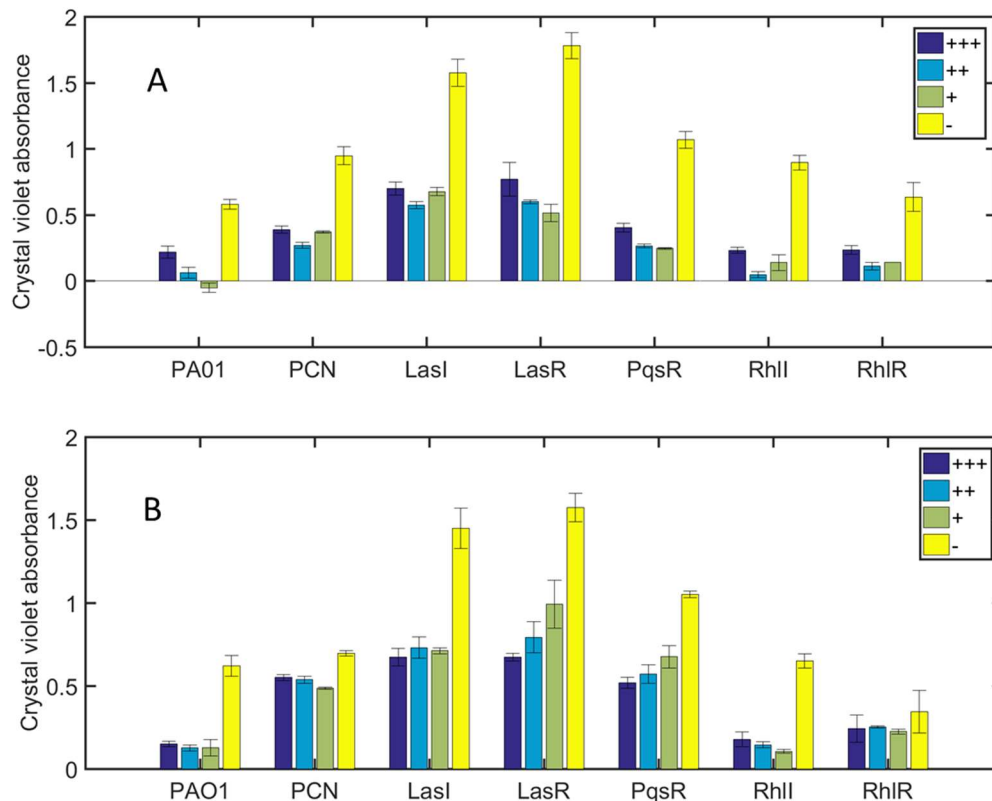


**Figure 4.29:** Crystal violet absorbance of different *P. aeruginosa* strains and mutants, grown at 37 °C in 10% LB media with the addition of pyo-CORM A) before 24 hours of biofilm formation and B) after 24 hours of biofilm formation. – to +++: no pyo-CORM and increasing pyo-CORM concentration, exact concentrations unknown.

Clinical bacterial strains are known to have slightly different properties to standard lab strains, so a selection were tested for their growth and biofilm production when incubated with pyo-CORM, and the biofilm reduction with pyo-CORM addition (**Figure 4.30**). These are the same batch of clinical strains used to quantify the *P. aeruginosa* pyocyanin production in **Chapter 2.2.7**.

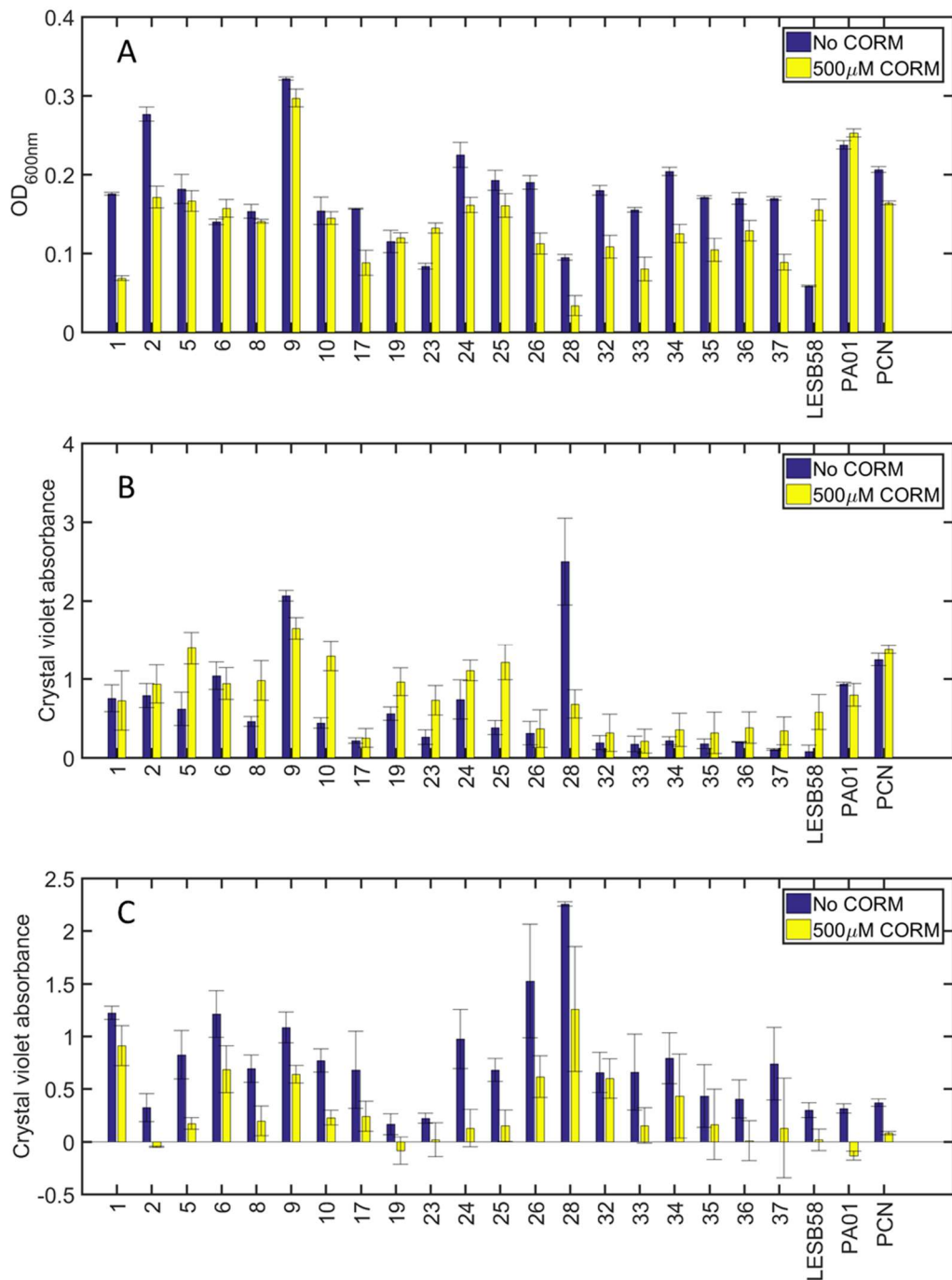


**Figure 4.30:** A) optical density at 600 nm, B) crystal violet absorbance of the addition of pyo-CORM before biofilm formation and C) crystal violet absorbance of the addition of pyo-CORM after biofilm formation, for different clinical and lab *P. aeruginosa* strains grown at 37 °C in 10% LB media

For the growth of clinical strains the addition of pyo-CORM generally causes a decrease in the number of bacteria present in the culture (**Figure 4.30A**). There are

a couple of isolates that show no significant or a slight increase in growth when pyo-CORM is present. This is possibly due to sub-inhibitory concentrations for those strains. The biomass of biofilm when pyo-CORM was incubated with clinical *P. aeruginosa* isolates tended to increase or stay constant when compared to the control (**Figure 4.30B**). The notable exception to this was isolate number 28, which has a high pyocyanin concentration in its supernatant (0.1312 mM). When pyo-CORM is introduced to the culture after biofilm has already been formed there is a universal decrease in the biofilm biomass (**Figure 4.30C**).

Because of the unexpected antimicrobial activity of pyo-CORM against PCN and clinical strains that produce very little pyocyanin, further tests were carried out using a larger range of bacterial species. These were used to test the specificity of pyo-CORM. The bacterial species tested included: PA01 *P. aeruginosa* wild-type strain, PCN knockout strain, *Ralstonia spp.*, *S. aureus* and *Stenotrophomonas maltophilia* (*S. maltophilia*). Pyo-CORM showed antimicrobial properties against all bacterial species (**Figure 4.31**). The bacterial species *Ralstonia spp* and *S. aureus* also have implications in CF and lung infections. Gram-negative bacteria are more susceptible to developing antibiotic resistance and can be difficult to treat, *Ralstonia spp.* are the only gram-positive bacteria in this set.

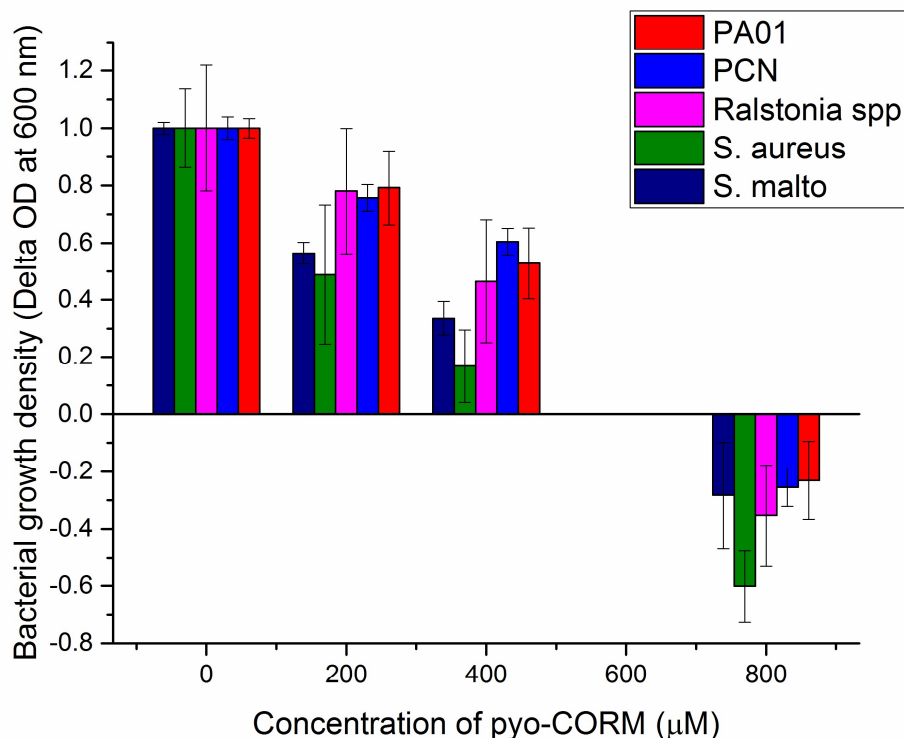


**Figure 4.31:** Corrected optical density at 600 nm of PA01 *P. aeruginosa* strain, PA01-phenazine knockout strain (PCN), *Ralstonia spp*, *S. aureus* and *S. maltophilia* when grown with different concentrations of pyo-CORM for 8 hours at 37 °C in 10 vol% LB

This series of biological tests confirmed that pyo-CORM has antimicrobial properties against both lab and clinical *P. aeruginosa* strains and reduces its established biofilm. It also demonstrated broad range antibiotic activity in the absence of pyocyanin, so therefore a different mechanism of activation must be occurring.

#### 4.9 Summary and conclusions

The reaction of pyocyanin and pyo-CORM is well defined in chloroform and other chlorinated solvents. Under these conditions pyocyanin appears to act as a bidentate ligand for the manganese with the loss of a bromide ion and a carbonyl group, and the loss of the N-methyl group from pyocyanin. The same reaction occurs with 8-hydroxyquinoline, a structural analogue of pyocyanin. Carbon

monoxide is known to be produced under these conditions through gas phase IR measurements. The reaction rate as measured in PBS is dependent on the water activation mechanism, with the amount of pyocyanin only contributing at high concentrations, therefore it can be assumed that even in the presence of pyocyanin water activation of pyo-CORM is dominant.

Although the exact water activation mechanism is unknown for pyo-CORM, previous studies in the group on compounds with a similar structure has shown a possible mechanism. The paper published in 2009<sup>67</sup> shows that when  $[\text{NEt}_4][\text{MoBr}(\text{CO})_5]$  and  $[\text{NEt}_4][\text{WBr}(\text{CO})_5]$  are dissolved in water CO is released via the initial formation of a dimer. The dimer is formed through the loss of bromide from one metal species and the bridging of the remaining one. It is possible that this same mechanism is taking place for pyo-CORM.

Biological tests indicate that pyo-CORM is capable of antimicrobial action against the wild type, PA01, *Pseudomonas aeruginosa* bacteria as well as other lab strains and clinical isolates. It is also an antimicrobial for several other bacterial species that do not produce phenazine compounds. The mechanism of action here is believed to be water activated, with the loss of all CO from pyo-CORM. This mechanism was proved through gas phase IR measurements, where CO is evolved from a solution of pyo-CORM in multiple aqueous solutions in the absence of pyocyanin.

# Summary, Conclusions and Future work

Chapter 5

## 5 Summary, conclusions and future work

### 5.1 Conclusions

The aims of this project were the synthesis and characterisation of pyocyanin and the discovery of a CO-RM that is activated by it. Once a suitable CO-RM was found, a study on the mechanism of CO release and its biological applications was to be carried out.

The complete characterisation of chemically synthesised pyocyanin has been performed and reported for the first time. This confirmed that naturally derived and chemically synthesised pyocyanin have identical properties<sup>86</sup> as the results matched the literature values which, in most cases, used biosynthesised pyocyanin.

The discovery that  $[\text{NEt}_4][\text{MnBr}_2(\text{CO})_4]$ , now known as pyo-CORM, reacts with pyocyanin and releases CO means that it can be characterised as a pyocyanin-triggered CO-RM. However, it appears that CO is also released when pyo-CORM is dissolved in water, even in the absence of pyocyanin.

This water-activation mechanism of CO release makes pyo-CORM an effective antimicrobial against many bacterial species not just *P. aeruginosa* or phenazine-producing species. Of the bacteria that were tested for an antimicrobial response to pyo-CORM, three are species that are associated with lung infections. The discovery that pyo-CORM can also reduce the biomass of biofilm is important for clinical use, as it means it could be used in conjunction with conventional antibiotics which are less effective with the barrier of biofilm. Therefore, pyo-CORM could still be a useful addition to the therapeutic toolkit for eradicating chronic lung infection in CF patients.

The direct observation of CO released into the headspace of the reaction vessel for a CO-release reaction has been seen for the first time in the University of York with the development of a gas phase IR technique. This technique can be used to show

that other CO-RMs can release CO even in the absence of sodium dithionite which is thought to, in some cases, contribute to the release of CO in a myoglobin assay<sup>51</sup>.

Because the reactivity of pyocyanin is related to its chemical structure rather than its redox properties, this makes it difficult to be a completely selective activator of a CO-RM. Any compound with a similar structure, e.g. 8-HOQ and 1-hydroxyphenazine, will also induce CO-release.

[NEt<sub>4</sub>][Mn(CO)<sub>4</sub>Br<sub>2</sub>], pyo-CORM, is a metal carbonyl which can be activated by pyocyanin or by water. Pyocyanin acts as a bidentate manganese ligand and releasing one CO molecule. Pyo-CORM is capable of reducing the growth and biofilm formation of *P. aeruginosa* as well as a range of different bacterial species. This is therefore a new antimicrobial which could become part of the treatment for patients with chronic lung infections.

## 5.2 Future work

There is still a lot of additional work, both chemical and biological, that needs to take place to optimise the reactivity of pyo-CORM and possibly improve its selectivity for activation by pyocyanin.

Other CO-RMs with similar structures to pyo-CORM could be used to try and increase the specificity of pyo-CORM to pyocyanin or slow the release of CO in aqueous solutions, for example [NEt<sub>4</sub>][MnI<sub>2</sub>(CO)<sub>4</sub>]. According to literature data the change in halogen to iodine makes for a more stable compound than pyo-CORM<sup>73</sup> and could, therefore, make it less susceptible to degradation and activation in water. So far the reaction between [NEt<sub>4</sub>][MnI<sub>2</sub>(CO)<sub>4</sub>] and pyocyanin has not been performed but is expected to involve the same activation mechanism.

Because other phenazine-derived compounds are produced by both *P. aeruginosa* and other bacterial species, they could also be contributing to the activity of pyo-CORM in bacterial studies. The synthesis of 1-hydroxyquinoline is outlined in the

literature<sup>55</sup> and its structure indicates that it would have similar reactivity to pyocyanin and 8-HOQ.

The biological work with pyo-CORM is ongoing. So far these studies have concentrated on the effect that pyo-CORM has on bacterial cultures. The next step towards developing pyo-CORM as an antimicrobial agent is to test its effect on eukaryotic and human cell lines. It can only be a viable therapeutic if the concentrations required to reduce the number of bacteria in a culture has little or no impact on the health of human cells. Wax moth larvae can also be used as an animal model, infecting them with *P. aeruginosa* and a known dosage of pyo-CORM would enable predictions to be made about the possible dosages required to clear the infection.

Further development of both the evolved gas and gas phase IR techniques is required in order to quantify the amount of CO gas released during the reaction. The evolved gas measurements requires a smaller headspace or more sensitive pressure gauge. To improve the gas phase IR measurements a CO standard is required and the uncertainty regarding the amount of gas that makes it into the IR cell needs to be removed. Indirect quantification of the amount of CO released from pyo-CORM during water activation can be measured using a myoglobin assay. As this required an aqueous solvent and the reducing agent sodium dithionite it is impractical to measure the release of CO when triggered by the presence of pyocyanin in this way, however, it could be used to quantify the amount of CO released from the water activated mechanism.

In summary, we have identified a CO-RM which has broad ranging antimicrobial and biofilm disruptive properties. Although not specific to pyocyanin, "pyo-CORM" could still be a useful compound in the fight against *Pseudomonas aeruginosa* chronic lung infections.

# Experimental

## Chapter 6

## 6 Experimental

### 6.1 Methods

#### 6.1.1 Solvents and Reagents

Commercially available reagents were purchased from Sigma-Aldrich (PBS tablets, 8-HOQ and silica), Aldrich (TEAB), Acros Organics (phenazine methosulphate) and used as received unless otherwise noted.

All solvents were AR grade from VWR. DCM was dried over calcium hydride and stored under a nitrogen atmosphere in a glove box.

#### 6.1.2 NMR

$^1\text{H}$  NMR spectra were recorded on a Jeol ECS400 or Joel ECX400 spectrometer at 400 MHz. Chemical shifts are reported in parts per million (ppm) and were referenced to residual undeuterated solvent ( $^1\text{H}$ : MeOH – 3.34 ppm,  $^1\text{H}$ :  $\text{CHCl}_3$  – 7.90 ppm) Coupling constants (J) have been quoted to the nearest 0.1 Hz.  $^1\text{H}$  NMR chemical shift are reported to 2 decimal places. Multiplicities are described as singlet (s), doublet (d), triplet (t), quartet (q), quintet (quin), multiplet (m) and broad (br.). Spectra were typically recorded at 298 K, unless otherwise specified. Spectra were processed using TopSpin 3.2.

#### 6.1.3 ESI-MS

Electrospray ionization (ESI) mass spectrometry was performed using a Bruker daltronics microTOF spectrometer, with less than 5 ppm error for all HRMS.

#### 6.1.4 UV/Vis Spectroscopy

UV-visible spectroscopy was performed on a Jasco V-560 spectrometer, at room temperature, with a background taken in the appropriate solvent prior to recording spectra, using a quartz cell with a path length of 1 cm. The wavelength of maximum

absorption ( $\lambda_{\max}$ ) is reported in nm along with the molar absorption coefficient ( $\epsilon$ ) in  $M^{-1} \text{ cm}^{-1}$ .

### 6.1.5 Electrochemistry

Cyclic voltammetry experiments were carried out at room temperature in a 0.5 mL glass cell with a platinum disk working electrode, silver wire pseudo-reference electrode and a platinum wire counter electrode was used to run cyclic voltammograms over the range 2.0 to -0.7 V using a PalmSens EmStat3+ potentiostat. As PBS contains a high level of salts no supporting electrolyte was required (One tablet dissolved in 200 mL of deionised water yields 0.01 M phosphate buffer, 0.0027 M potassium chloride and 0.137 M sodium chloride, pH 7.4, at 25 °C (CAS: MFCD00131855<sup>87</sup>).

### 6.1.6 Spectroelectrochemistry

A specialist UV electrochemical cuvette was used for spectroelectrochemical measurements. It was equipped with a platinum gauze working electrode, a platinum wire counter electrode and a silver/silver chloride reference electrode. The potential was controlled using a PalmSens EmStat3+ potentiostat. The cuvette has a path length of 0.5 mm and the electrodes sat in this part of the cuvette. Scans were run at room temperature against air on a Hitachi U-1900 UV/vis spectrophotometer between 900 and 200 nm and corrected using a spectrum of the dry electrochemical cuvette.

### 6.1.7 IR Spectroscopy

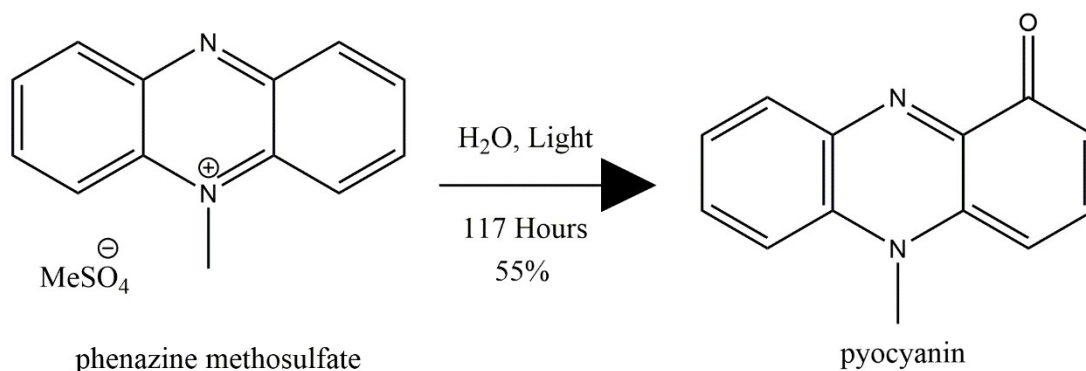
Solution phase and KBr disk IR measurements were carried out on a UNICAM Research series FTIR spectrometer. Other solid phase IR spectroscopy was performed using a Bruker Alpha with an ATR attachment. All solid state IR Spectroscopy was carried out using vacuum dried samples however residual solvents may be present. The gas phase IR measurements were run on an AVATAR

370 FT-IR spectrometer. All spectra were run between 400 and 4000  $\text{cm}^{-1}$  at room temperature. Absorption maxima ( $\nu_{max}$ ) are reported in wavenumbers ( $\text{cm}^{-1}$ ) to the nearest whole number.

### 6.1.8 DFT

Initial optimisations were performed at the (RI-)BP86/SV(P) level, followed by frequency calculations at the same level. All minima were confirmed as such by the absence of an imaginary frequency. Single-point calculations on the (RI-)BP86/SV(P) optimised geometries were performed using the hybrid PBE0 functional and the flexible def2-TZVPP basis set. No symmetry constraints were applied during optimisations. Vertical excitation energies were calculated using the ESCF module of TURBOMOLE (full TDDFT) on the (RI-)PBE0/def2-TZVPP optimised structures at the same level of theory. Tight SCF convergence criteria were used in these calculations. 50 singlet excitations were calculated for each state. All calculations were performed using the TURBOMOLE V6.40 package using the resolution of identity (RI) approximation<sup>88-96</sup>. The calculations were performed by Dr Jason Lynam.

## 6.2 Pyocyanin synthesis



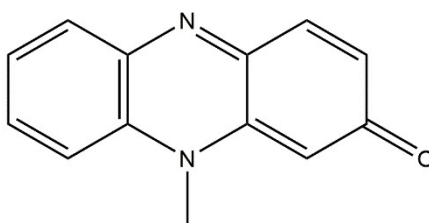
Phenazine methosulfate (204 mg, 0.667 mmol) was added to a flask of 200 mL deionised water and subjected to broad wavelength artificial light for 117 hours,

during which time the solution turned from green to dark red. The reaction was then quenched with 50 mL of 10% aqueous sodium carbonate. The deep blue solution was extracted exhaustively with portions of chloroform until it ran colourless. The organic layers were collected and dried over magnesium sulfate, filtered and concentrated under vacuum. The crude reaction was then purified by column chromatography on silica (9:1 ethyl acetate: methanol, **Figure 2.3**) to give 77 mg (55% yield) of pyocyanin as a blue solid. NOTE: Pyocyanin was synthesized using a known procedure<sup>55</sup>.

**<sup>1</sup>H NMR:** (400 MHz, CD<sub>3</sub>OD):  $\delta$  8.27 (br., 1H), 8.00 (m, 2H), 7.86 (br., 1H), 7.67 (d, J= 7.4 Hz, 1H), 6.49-6.57 (dd, J= 24.9 Hz, 2H), 4.17 (s, 3H, CH<sub>3</sub>)

**ESI-MS** positive ion  $m/z$ : 211.0872 ([M+H]<sup>+</sup>, calc. for C<sub>13</sub>H<sub>11</sub>N<sub>2</sub>O: 211.0866, error -0.6 mDa)

During the column chromatography purification of pyocyanin (above), a pink coloured fraction was eluted prior to pyocyanin. This is believed to be **2-keto-N-methyl phenazine**.

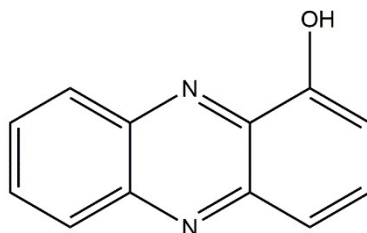


**<sup>1</sup>H NMR:** (400 MHz, CDCl<sub>3</sub>):  $\delta$  7.98 (dd, J= 8.0 Hz, 1H), 7.68 (t, J= 8.0 Hz, 1H), 7.61 (d, J= 10.2 Hz, 1H), 7.52 (d, J= 8.8 Hz, 1H), 7.43 (t, J= 7.3 Hz, 1H), 7.07 (d, J= 9.5 Hz, 1H), 6.81, (s, 1H), 3.77 (s, 3H, CH<sub>3</sub>)

**ESI-MS** positive ion  $m/z$ : 211.0869, ([M+H]<sup>+</sup>, calc. for C<sub>13</sub>H<sub>11</sub>N<sub>2</sub>O: 211.0866, error -0.3 mDa)

When pyocyanin was stored at room temperature in solid form a degradation product was formed. This product was seen as a yellow solid and was removed by

column chromatography. It is believed to be **1-hydroxyphenazine** primarily due to the loss of the distinctive CH<sub>3</sub> peak for pyocyanin at 4.17 ppm.



**<sup>1</sup>H NMR:** (400 MHz, CD<sub>3</sub>OD): δ 8.30 (d, J= 8.0 Hz, 1H), 8.17 (d, J= 9.0 Hz, 1H), 7.89 (qui, J= 7.8 Hz, 2H), 7.76 (d, J= 7.3 Hz, 1H), 7.68 (d, J= 8.9 Hz, 1H), 7.42 (m, 1H), 7.17 (d, J= 7.8 Hz, 1H).

**ESI-MS** positive ion *m/z*: 197.0707 ([M+H]<sup>+</sup>, calc. for C<sub>12</sub>H<sub>8</sub>N<sub>2</sub>O: 197.0709, error -0.3 mDa)

### 6.3 Pyo-CORM synthesis

Pyo-CORM synthesis carried out by James Pitt following the literature procedure outlined by Angelici<sup>73</sup> and shown below.

Mn(CO)<sub>5</sub>Br (200 mg, 0.73 mmol) and 140 mg (0.68 mmol) of [(C<sub>2</sub>H<sub>6</sub>)<sub>4</sub>N]Br were heated in 7 ml of absolute methanol under a nitrogen atmosphere at 45-50 °C for 1 hr. The methanol was then evaporated from the orange solution at the above temperature with a water aspirator. The remaining yellow solid was dissolved in 20 ml of chloroform, and the solution was filtered under nitrogen. After adding 100 ml of hexane to the filtrate, the cloudy solution was allowed to stand for 2 hr. The yellow crystals were separated by filtration, washed with hexane, and dried under vacuum giving a yield of 69% (230 mg).

### 6.4 CF sputum isolates preparation

The samples were prepared and provided by Dr Siobhan O'Brien (Brockhurst lab, Department of Biology, York).

These were prepared by growing up natural samples from a lung in LB broth overnight with shaking at 37 °C in 5 mL media in a 50 mL falcon tube. In the morning the tubes were centrifuged in swing buckets in an eppendorf centrifuge at 4000 rpm for 15 minutes to pellet the cells. 500  $\mu$ L of the supernatant was removed and 200  $\mu$ L of this was transferred to a 96 well plate. The absorbance at 691 nm was measured on a Tecan Sunrise Spectrophotometer with sterile media as a blank.

The supernatant was stored at -20 °C before the measurements were run on a Jasco V-560 spectrometer.

## 6.5 CO-RM screening

The screening of CO-RMs for activity with pyocyanin was carried out using a Jasco V-560 UV/Vis spectrometer. Solutions of CO-RM were made up new just before the experiment began at concentrations of either 24  $\mu$ M, 30  $\mu$ M or 48  $\mu$ M. A single stock solution of pyocyanin was used and diluted to 24  $\mu$ M or 48  $\mu$ M as the experiment required. Leukopyocyanin was reduced using 2eq. of sodium dithionite at a concentration of 30  $\mu$ M. Scans were run between 900 and 200 nm. The measurement of two cuvettes was taken in quick succession at each time point, a solution of CO-RM and pyocyanin or leukopyocyanin in PBS and a solution of CO-RM only in PBS. PBS was used to ensure that pyocyanin was in the same protonation state throughout the experiment and therefore keep the pH constant.

## 6.6 UV/vis concentration studies

Solutions of pyo-CORM were made up fresh before each experiment at concentrations between 24  $\mu$ M and 144  $\mu$ M. While solutions of pyocyanin were diluted from a single stock solution to between 12  $\mu$ M and 60  $\mu$ M. Scans were run from 900 to 200 nm at 4 minute intervals. The percentage change in the peak

intensity was calculated using the equation,  $(A_{\text{start}} - A_{\text{end}}) / A_{\text{start}}$ , which enabled comparison over different pyocyanin concentration experiments.

The rate of each reaction from these studies (**Chapter 4.3.1**) were extracted from the gradient of the straight line from corrected absorbance measurements every 4 minutes between 0 and 24 minutes during the reaction of pyo-CORM and pyocyanin. Each absorbance was corrected to the final absorbance in each run,  $t-t(28 \text{ minutes})$ . The natural log of these absorbance values were then plotted and the gradient recorded as the rate of reaction.

## 6.7 Gas Phase IR

The experimental set up for gas phase IR is shown in **Figure 6.1**.

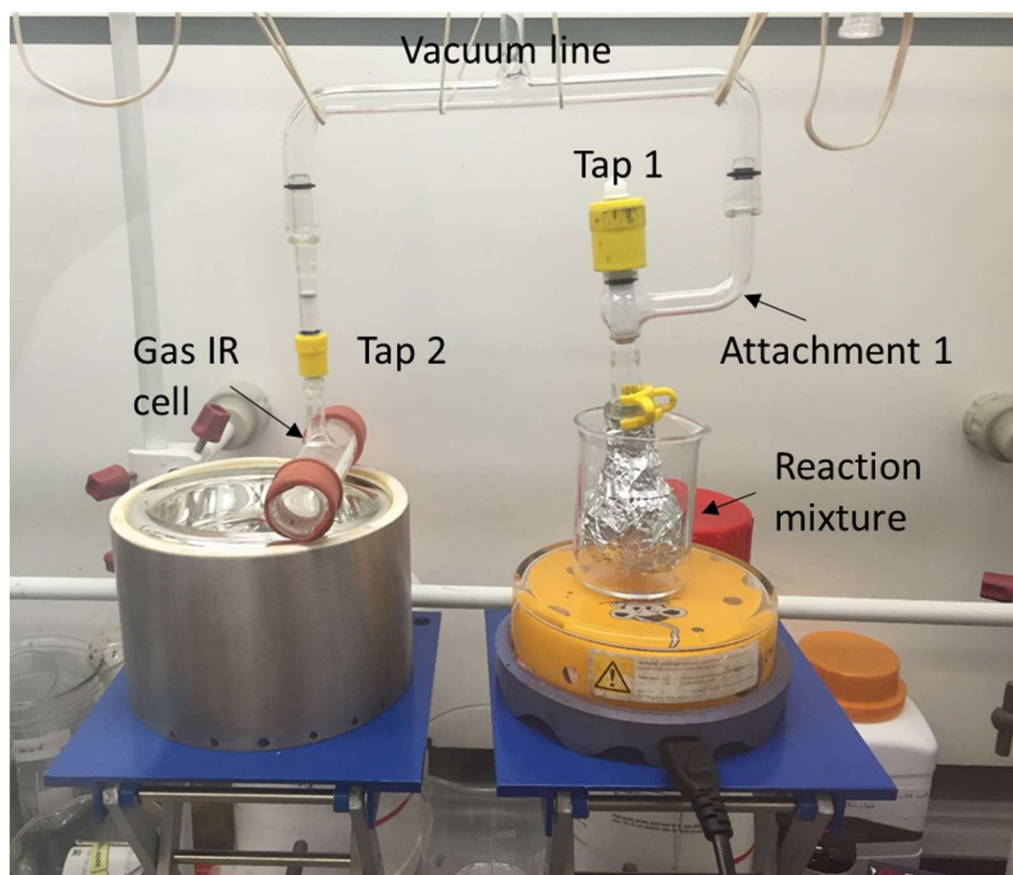


**Figure 6.1:** Gas phase IR experimental set up

12 mg of CORM (+ 10 mg of PYO) was added to 4 mL of solvent in a 25 mL round bottomed flask. The round bottomed flask was attached to the vacuum line via Attachment 1. Tap 1 was shut ensuring that any gas evolved from the reaction was maintained in the headspace. The T-piece and attached gas IR cell were kept under vacuum. After 1 hour of stirring the T-piece was closed to vacuum and the flask opened. Some of the gas from the headspace of the flask is then drawn into the gas IR cell. The IR cell is closed (Tap 2), removed from the line and an IR spectrum run (either against air or the evacuated IR cell).

## 6.8 Evolved gas measurements

The pressure gauge on the vacuum line was used to measure the volume of gas given off by pyo-CORM in different solvent systems. The vacuum line was initially left to equilibrate to  $1.1^{-1}$  mbar. 1 mg of CORM was added to 4 mL of solvent in a 25 mL round bottomed flask. The flask was attached to the vacuum line and opened up to vacuum till the pressure reached 2.0 mbar before being shut off again, leaving only a small amount of gas in the headspace of the flask. The line left to equilibrate back down to  $1.1^{-1}$  mbar before being closed off to vacuum. The flask was opened up to the line and the pressure recorded from a VAP5 vaccubrand pressure gauge over the course of an hour.

## 6.1 Biological testing of pyo-CORM

All strains were grown overnight with shaking at 37 °C in 5 mL media in a 50 mL falcon tube. In the morning the tubes were centrifuged in swing buckets in an eppendorf centrifuge at 4000 rpm for 15 minutes to pellet the cells. Supernatant was discarded and the cells were re-suspended in 5 mL sterile media. 200  $\mu$ L of this was transferred to a 96 well plate and the OD 600 was measured on a Tecan Sunrise Spectrophotometer with sterile media as a blank. 5 mL cultures were made up to an OD of 0.066 using fresh media. 150  $\mu$ L of each culture was aliquoted into 96 well plates, with a minimum of 3 repeats for each.

Where CORM was added at the start the CORM was made up in fresh media and syringe filtered to sterilise immediately before adding 50  $\mu\text{l}$  to each well (or 50  $\mu\text{l}$  sterile media to each control well).

For the growth curves, the plate was placed in a Tecan Infinite Spectrophotometer at 37 °C and the OD 600nm was measured every 30 minutes.

Crystal violet staining was carried out by adding at 10% v/v, shaking for 100s on the Tecan Sunrise spectrophotometer and leaving for 15 minutes. The biofilms were de-stained by dunking into successive buckets of deionised water and dried by tapping onto blue roll. 228  $\mu\text{L}$  of ethanol was then added to each well and the absorbance was taken at 600 nm on the teach sunrise spectrometer after 100s of shaking.

For the established biofilm, the 150  $\mu\text{l}$  of culture was left in an incubator at 37 °C for 24 hours (first few slides) or 48 hr (clinical strains) before 50  $\mu\text{l}$  fresh CORM solution or sterile media was added and left for 4 hours at 37 °C. At this point the crystal violet staining was performed as above.

Lineages of clinical strains were established in the paper by Williams et al<sup>97</sup>. The morphology was established by streaking the strains out onto LB agar plates and observing. For the clinical strains, starter cultures were composed of 100% LB, before centrifuging and re-suspending in 10% LB in the morning.

Biological testing was carried out by Miss Karinna Saxby and Dr Lindsey Flanagan.

# Abbreviations

## Abbreviations

%age or %	percentage
±	plus or minus
°C	degrees Celsius
2KMP	2-keto-N-methyl phenazine
8-HOQ	8-hydroxyquinoline
ATR IR	Attenuated total reflectance infra-red
br.	broad
CAS	Chemical Abstracts Service number
CF	Cystic Fibrosis
CFTR	Cystic Fibrosis transmembrane conductance regulator
cm <sup>-1</sup>	wavenumber
CO	carbon monoxide
conc.	concentration
CO-RM	carbon monoxide-releasing molecule
CV	cyclic voltammetry
cyclic-AMP	cyclic adenosine monophosphate
d	doublet
DCM	dichloromethane
dd	doublet of doublets
DFT	density functional theory
DI	de-ionised
DMSO	dimethyl sulfoxide
E <sub>avg</sub>	average potential
<i>E. coli</i>	<i>Escherichia coli</i>
E <sub>ox</sub>	oxidation potential
E <sub>red</sub>	reduction potential
ESI	Electrospray ionization
Et	ethyl
eV	electron Volts
FT-IR	Fourier transform infra-red

<i>H. influenzae</i>	<i>Haemophilus influenzae</i>
HOMO	highest occupied molecular orbital
hr	hour(s)
HRMS	high resolution mass spectrometry
Hz	Hertz
<i>in vivo</i>	in a living organism
IR	infra-red
J	coupling constant
K	Kelvin
$k_{\text{obs}} \text{ s}^{-1}$	observed rate constant
LB	Lysogeny broth
LESB58	<i>P. aeruginosa</i> Liverpool epidemic strain B58
ln	natural log
LPYO	leukopyocyanin
LUMO	lowest unoccupied molecular orbital
M	molar
m	multiplet
<i>m/z</i>	mass/charge
$\text{M}^{-1} \text{ cm}^{-1}$	molarity per cm
mbar	millibar
MDa	milliDalton
<i>mer</i>	meridional isomer geometry
mg	milligram
MHz	mega Hertz
min(s)	minute(s)
mL	millilitres
mM	milimolar
mmol	milimoles
MS	mass spectrometry
mV	millivolts
<i>n</i>	number of electrons
NAD(P)H	Nicotinamide adenine dinucleotide phosphate

nm	nanometre
NMR	nuclear magnetic resonance
OD	optical density
<i>P. aeruginosa</i>	<i>Pseudomonas aeruginosa</i>
PA01	<i>P. aeruginosa</i> wild type strain
PBS	phosphate buffered saline
PCN	<i>P. aeruginosa</i> phenazine knockout strain
pH	molar concentration of hydrogen ions
pKa	negative base-10 logarithm of the acid dissociation constant
ppm	parts per million
PYO	pyocyanin
pyo-CORM	pyocyanin triggered CO-RM, [NEt <sub>4</sub> ][MnBr <sub>2</sub> (CO) <sub>4</sub> ]
q	quartet
quin	quintet
s	singlet
<i>S. aureus</i>	<i>Staphylococcus aureus</i>
<i>S. maltophilia</i>	<i>Stenotrophomonas maltophilia</i>
<i>Spp.</i>	species
t	triplet
TEAB	tetraethyl ammonium bromide
UV	ultra violet
V	Volts
V/s	Volts per second
vis	visible
vol%	percentage by volume
vs Ag/AgCl	vs silver/silver chloride reference electrode
vs Ref	vs reference electrode
vs SHE	vs standard hydrogen electrode
wt	wild type
δ	chemical shift
λ	wavelength
ΔE	voltage separation

$\mu\text{A}$	microamps
$\mu\text{M}$	micromolar
$\mu\text{L}$	microliter

# References

## References

- 1 S. J. Bourke and G. P. Burns, *Lecture notes. Respiratory medicine*, John Wiley & Sons/Wiley-Blackwell, Chichester, 8th edn., 2011.
- 2 P. B. Davis, M. Drumm and M. W. Konstan, *Am. J. Respir. Crit. Care Med.*, 1996, **154**, 1229–1256.
- 3 J. M. Rommens, M. C. Iannuzzi, B. Kerem, M. L. Drumm, G. Melmer, M. Dean, R. Rozmahel, J. L. Cole, D. Kennedy and N. Hidaka, *Science*, 1989, **245**, 1059–65.
- 4 J. R. Riordan, J. M. Rommens, B. Kerem, N. Alon, R. Rozmahel, Z. Grzelczak, J. Zielenski, S. Lok, N. Plavsic and J. L. Chou, *Science*, 1989, **245**, 1066–73.
- 5 B. Kerem, J. M. Rommens, J. A. Buchanan, D. Markiewicz, T. K. Cox, A. Chakravarti, M. Buchwald and L. C. Tsui, *Science*, 1989, **245**, 1073–80.
- 6 E. F. Tizzano, M. M. Silver, D. Chitayat, J. C. Benichou and M. Buchwald, *Am. J. Pathol.*, 1994, **144**, 906–14.
- 7 M. Lopes-Pacheco, *Front. Pharmacol.*, 2016, **7**, 275.
- 8 P. R. Sosnay, K. R. Siklosi, F. Van Goor, K. Kaniecki, H. Yu, N. Sharma, A. S. Ramalho, M. D. Amaral, R. Dorfman, J. Zielenski, D. L. Masica, R. Karchin, L. Millen, P. J. Thomas, G. P. Patrinos, M. Corey, M. H. Lewis, J. M. Rommens, C. Castellani, C. M. Penland and G. R. Cutting, *Nat. Genet.*, 2013, **45**, 1160–1167.
- 9 J. F. Engelhardt, S. S. Smith, E. Allen, J. R. Yankaskas, D. C. Dawson and J. M. Wilson, *Am. J. Physiol.*, 1994, **267**, C491-500.
- 10 J. B. Lyczak, C. L. Cannon and G. B. Pier, *Clin. Microbiol. Rev.*, 2002, **15**, 194–222.
- 11 D. H. Anderson, *Am. J. Dis. Child.*, 1938, **56**, 344.
- 12 J. R. Govan and J. W. Nelson, *Br. Med. Bull.*, 1992, **48**, 912–30.
- 13 N. N. Huang, D. V. Schidlow, T. H. Szatrowski, J. Palmer, L. R. Laraya-Cuasay, W. Yeung, K. Hardy, L. Quitell and S. Fiel, *Am. J. Med.*, 1987, **82**, 871–9.
- 14 C. Gessard, *Fac. Médecine Paris*, 1882.
- 15 C. Gessard, *Clin. Infect. Dis.*, 1984, **6**, S775–S776.

- 16 R. Serra, R. Grande, L. Butrico, A. Rossi, U. F. Settimio, B. Caroleo, B. Amato, L. Gallelli and S. de Franciscis, *Expert Rev. Anti. Infect. Ther.*, 2015, **13**, 605–13.
- 17 K. Grimwood, J. M. Kyd, S. J. Owen, H. M. Massa and A. W. Cripps, *Hum. Vaccin. Immunother.*, 2015, **11**, 14–20.
- 18 M. R. Villarreal, [https://en.wikipedia.org/wiki/Cell\\_\(biology\)#/media/File:Average\\_prokaryote\\_cell-en.svg](https://en.wikipedia.org/wiki/Cell_(biology)#/media/File:Average_prokaryote_cell-en.svg), (accessed November 2016).
- 19 G. Doring, S. Conway, H. Heijerman, M. Hodson, N. Hoiby, A. Smyth and D. Touw, *Eur. Respir. J.*, 2000, **16**, 749–767.
- 20 T. L. Pitt, M. Sparrow, M. Warner and M. Stefanidou, *Thorax*, 2003, **58**, 794–6.
- 21 D. M. Livermore, *Clin. Infect. Dis.*, 2002, **34**, 634–40.
- 22 T.-F. Mah, B. Pitts, B. Pellock, G. C. Walker, P. S. Stewart and G. A. O’Toole, *Nature*, 2003, **426**, 306–310.
- 23 S. Jayaseelan, D. Ramaswamy and S. Dharmaraj, *World J. Microbiol. Biotechnol.*, 2014, **30**, 1159–68.
- 24 M. Fordos, *Rec. Trav. Soc. d’Émul. Sci. Pharm*, 1859, **3**.
- 25 W. Blankenfeldt and J. F. Parsons, *Curr. Opin. Struct. Biol.*, 2014, **29**, 26–33.
- 26 M. Mentel, E. G. Ahuja, D. V Mavrodi, R. Breinbauer, L. S. Thomashow and W. Blankenfeldt, *Chembiochem*, 2009, **10**, 2295–304.
- 27 S. A. Waksman and H. B. Woodruff, *J. Bacteriol.*, 1940, **40**, 581–600.
- 28 G. W. Lau, H. Ran, F. Kong, D. J. Hasset and D. Mavrodi, *Infect. Immun.*, 2004, **72**, 4275–8.
- 29 L. E. P. Dietrich, A. Price-Whelan, A. Petersen, M. Whiteley and D. K. Newman, *Mol. Microbiol.*, 2006, **61**, 1308–1321.
- 30 M. R. Parsek and E. P. Greenberg, *Trends Microbiol.*, 2005, **13**, 27–33.
- 31 C. Jacob, V. Jamier and L. A. Ba, *Curr. Opin. Chem. Biol.*, 2011, **15**, 149–55.
- 32 C. D. Cox, *Infect. Immun.*, 1986, **52**, 263–270.
- 33 T. Sjöstrand, *Acta Physiol. Scand.*, 1951, **22**, 137–141.
- 34 S. W. Ryter and L. E. Otterbein, *Bioessays*, 2004, **26**, 270–80.
- 35 R. Wang, *Trends Biochem. Sci.*, 2014, **39**, 227–32.

- 36 R. Motterlini and L. E. Otterbein, *Nat. Rev. Drug Discov.*, 2010, **9**, 728–43.
- 37 A. Nakao, A. M. K. Choi and N. Murase, *J. Cell. Mol. Med.*, 2006, **10**, 650–71.
- 38 R. Motterlini, *Circ. Res.*, 2002, **90**, 17e–24.
- 39 T. S. Murray, C. Okegbe, Y. Gao, B. I. Kazmierczak, R. Motterlini, L. E. P. Dietrich and E. M. Bruscia, *PLoS One*, 2012, **7**, e35499.
- 40 M. Desmard, K. S. Davidge, O. Bouvet, D. Morin, D. Roux, R. Foresti, J. D. Ricard, E. Denamur, R. K. Poole, P. Montravers, R. Motterlini and J. Boczowski, *FASEB J.*, 2009, **23**, 1023–31.
- 41 Sigma-Aldrich,  
<http://www.sigmaaldrich.com/catalog/product/aldrich/288144?lang=en&region=GB>, (accessed November 2016).
- 42 R. Motterlini, B. E. Mann and R. Foresti, *Expert Opin. Investig. Drugs*, 2005, **14**, 1305–18.
- 43 T. S. Pitchumony, B. Spingler, R. Motterlini, R. Alberto, C. Giacobazzo, A. Guagliardi, A. G. G. Moliterni, G. Polidori and R. Spagna, *Org. Biomol. Chem.*, 2010, **8**, 4849.
- 44 M. Desmard, R. Foresti, D. Morin, M. Dagouassat, M. Dagoussat, A. Berdeaux, E. Denamur, S. H. Crook, B. E. Mann, D. Scapens, P. Montravers, J. Boczowski and R. Motterlini, *Antioxid. Redox Signal.*, 2012, **16**, 153–63.
- 45 L. S. Nobre, J. D. Seixas, C. C. Romão and L. M. Saraiva, *Antimicrob. Agents Chemother.*, 2007, **51**, 4303–7.
- 46 J. S. Ward, J. M. Lynam, J. Moir and I. J. S. Fairlamb, *Chem. a Eur. J.*, 2014, **20**, 15061–8.
- 47 L. K. Wareham, R. K. Poole and M. Tinajero-Trejo, *J. Biol. Chem.*, 2015, **290**, 18999–19007.
- 48 U. Schatzschneider, *Br. J. Pharmacol.*, 2015, **172**, 1638–50.
- 49 M. A. Wright and J. A. Wright, *Dalt. Trans.*, 2016, **45**, 6801–6811.
- 50 S. Romanski, B. Kraus, U. Schatzschneider, J.-M. Neudörfl, S. Amslinger and H.-G. Schmalz, *Angew. Chem. Int. Ed. Engl.*, 2011, **50**, 2392–6.
- 51 M. Klein, U. Neugebauer, A. Gheisari, A. Malassa, T. M. A. Jazzazi, F. Froehlich, M. Westerhausen, M. Schmitt and J. Popp, *J. Phys. Chem. A*, 2014, **118**, 5381–90.

- 52 Sigma-Aldrich,  
<http://www.sigmaaldrich.com/catalog/product/sigma/p0046?lang=en&region=GB>, (accessed November 2016).
- 53 M. Z. El-Fouly, A. M. Sharaf, A. A. M. Shahin, H. A. El-Bialy and A. M. A. Omara, *J. Radiat. Res. Appl. Sci.*, 2015, **8**, 36–48.
- 54 H. McIlwain, *J. Chem. Soc.*, 1937, 1704.
- 55 N. V. Borrero, F. Bai, C. Perez, B. Q. Duong, J. R. Rocca, S. Jin and R. W. Huigens III, *Org. Biomol. Chem.*, 2014, **12**, 881.
- 56 A. Price-Whelan, L. E. P. Dietrich and D. K. Newman, *J. Bacteriol.*, 2007, **189**, 6372–6381.
- 57 G. Y. Liu and V. Nizet, *Trends Microbiol.*, 2009, **17**, 406–413.
- 58 K. Saosoong, W. Wongphathanakul, C. Poasiri and C. Ruangviriyachai, *KKU Sci. J*, 2552, **3737**, 163–172.
- 59 B. Elema, *Recl. des Trav. Chim. des Pays-Bas*, 2010, **50**, 807–826.
- 60 G. W. Lau, D. J. Hassett, H. Ran and F. Kong, *Trends Mol. Med.*, 2004, **10**, 599–606.
- 61 M. Muller, *Free Radic. Biol. Med.*, 2011, **50**, 971–7.
- 62 Y. Wang and D. K. Newman, *Environ. Sci. Technol.*, 2008, **42**, 2380–2386.
- 63 R. Barakat, I. Goubet, S. Manon, T. Berges and E. Rosenfeld, *Microbiologyopen*, 2014, **3**, 1–14.
- 64 R. Adams, *Electrochemistry at Solid Electrodes*, Marcel Dekker Inc., New York, 1968.
- 65 A. Burrows, J. Holman, A. Parsons, G. Pilling and G. Price, *Chemistry3*, Oxford University Press, Oxford, 2009.
- 66 K. J. Reszka, Y. O'Malley, M. L. McCormick, G. M. Denning and B. E. Britigan, *Free Radic. Biol. Med.*, 2004, **36**, 1448–59.
- 67 W.-Q. Zhang, A. J. Atkin, R. J. Thatcher, A. C. Whitwood, I. J. S. Fairlamb and J. M. Lynam, *Dalt. Trans.*, 2009, 4351–8.
- 68 A. J. Atkin, S. Williams, P. Sawle, R. Motterlini, J. M. Lynam and I. J. S. Fairlamb, *Dalt. Trans.*, 2009, 3653–6.
- 69 W.-Q. Zhang, A. C. Whitwood, I. J. S. Fairlamb and J. M. Lynam, *Inorg. Chem.*, 2010, **49**, 8941–52.

- 70 P. Sawle, J. Hammad, I. J. S. Fairlamb, B. Moulton, C. T. O'Brien, J. M. Lynam, A. K. Duhme-Klair, R. Foresti and R. Motterlini, *J. Pharmacol. Exp. Ther.*, 2006, **318**, 403–10.
- 71 J. S. Ward, J. M. Lynam, J. W. B. Moir, D. E. Sanin, A. P. Mountford and I. J. S. Fairlamb, *Dalt. Trans.*, 2012, **41**, 10514–7.
- 72 Sigma-Aldrich,  
<http://www.sigmaaldrich.com/catalog/product/aldrich/341622?lang=en&region=GB>, (Accessed December 2016).
- 73 R. J. Angelici, *Inorg. Chem.*, 1964, **3**, 1099–11021.
- 74 F. Mohr, J. Niesel, U. Schatzschneider and C. W. Lehmann, *Zeitschrift für Anorg. und Allg. Chemie*, 2012, **638**, 543–546.
- 75 M. Dixon, *Biochim. Biophys. Acta - Bioenerg.*, 1971, **226**, 241–258.
- 76 E. W. Abel and I. S. Butler, *J. Chem. Soc.*, 1964, 434.
- 77 D. Shriver, P. Atkins, T. L. Overton, J. P. Rourke, M. T. Weller and F. A. Armstrong, *Inorganic Chemistry*, Oxford University Press, 4th edn., 2006.
- 78 A. J. Atkin, J. M. Lynam, B. E. Moulton, P. Sawle, R. Motterlini, N. M. Boyle, M. T. Pryce and I. J. S. Fairlamb, *Dalt. Trans.*, 2011, **40**, 5755–61.
- 79 J. A. Stone and D. Vukomanovic, *Int. J. Mass Spectrom.*, 2001, **210**, 341–359.
- 80 K. C. Costa, N. R. Glasser, S. J. Conway and D. K. Newman, *Science (80-. )*, 2016.
- 81 F. Dickens and H. Mcilwain, *Biochem. J.*, 1938, **32**, 1615–1625.
- 82 P. W. Preisler and L. H. Hempelmann, *J. Am. Chem. Soc.*, 1937, **59**, 141–144.
- 83 J. P. Phillips, *Chem. Rev.*, 1956, **56**, 271–297.
- 84 E. Peeters, H. J. Nelis and T. Coenye, *J. Microbiol. Methods*, 2008, **72**, 157–165.
- 85 J. F. Linares, I. Gustafsson, F. Baquero and J. L. Martinez, *Proc. Natl. Acad. Sci.*, 2006, **103**, 19484–19489.
- 86 D. V Vukomanovic, D. E. Zoutman, J. A. Stone, G. S. Marks, J. F. Brien and K. Nakatsu, *Biochem. J.*, 1997, **29**, 25–29.
- 87 Sigma-Aldrich,  
<http://www.sigmaaldrich.com/catalog/product/sigma/p4417?lang=en&region=GB>, (accessed December 2016).

- 88 P. Császár and P. Pulay, *J. Mol. Struct.*, 1984, **114**, 31–34.
- 89 R. Ahlrichs, M. Bär, M. Häser, H. Horn and C. Kölmel, *Chem. Phys. Lett.*, 1989, **162**, 165–169.
- 90 K. Eichkorn, O. Treutler, H. Öhm, M. Häser and R. Ahlrichs, *Chem. Phys. Lett.*, 1995, **240**, 283–290.
- 91 O. Treutler and R. Ahlrichs, *J. Chem. Phys.*, 1995, **102**, 346.
- 92 K. Eichkorn, F. Weigend, O. Treutler and R. Ahlrichs, *Theor. Chem. Accounts Theory, Comput. Model. (Theoretica Chim. Acta)*, 1997, **97**, 119–124.
- 93 M. von Arnim and R. Ahlrichs, *J. Chem. Phys.*, 1999, **111**, 9183.
- 94 P. Deglmann and F. Furche, *J. Chem. Phys.*, 2002, **117**, 9535.
- 95 P. Deglmann, F. Furche and R. Ahlrichs, *An efficient implementation of second analytical derivatives for density functional methods*, 2002, vol. 362.
- 96 P. Deglmann, K. May, F. Furche and R. Ahlrichs, *Nuclear second analytical derivative calculations using auxiliary basis set expansions*, 2004, vol. 384.
- 97 D. Williams, B. Evans, S. Haldenby, M. J. Walshaw, M. A. Brockhurst, C. Winstanley and S. Paterson, *Am. J. Respir. Crit. Care Med.*, 2015, **191**, 775–785.